Winter 1997

Myoglobin-facilitated oxygen diffusion in the heart: A mathematical assessment

Jason D. Gardner

INFORMATION TO USERS

This manuscript has been reproduced from the microfilm master. UMI films the text directly from the original or copy submitted. Thus, some thesis and dissertation copies are in typewriter face, while others may be from any type of computer printer.

The quality of this reproduction is dependent upon the quality of the copy submitted. Broken or indistinct print, colored or poor quality illustrations and photographs, print bleedthrough, substandard margins, and improper alignment can adversely affect reproduction.

In the unlikely event that the author did not send UMI a complete manuscript and there are missing pages, these will be noted. Also, if unauthorized copyright material had to be removed, a note will indicate the deletion.

Oversize materials (e.g., maps, drawings, charts) are reproduced by sectioning the original, beginning at the upper left-hand corner and continuing from left to right in equal sections with small overlaps. Each original is also photographed in one exposure and is included in reduced form at the back of the book.

Photographs included in the original manuscript have been reproduced xerographically in this copy. Higher quality 6" x 9" black and white photographic prints are available for any photographs or illustrations appearing in this copy for an additional charge. Contact UMI directly to order.

UMI

A Bell & Howell Information Company
300 North Zeeb Road, Ann Arbor MI 48106-1346 USA
313/761-4700 800/521-0600

MYOGLOBIN FACILITATED OXYGEN DIFFUSION IN THE HEART: A MATHEMATICAL ASSESSMENT

by

Jason D. Gardner, B.S.

A Dissertation Presented in Partial Fulfillment
of the Requirements for the Degree
Doctor of Philosophy

COLLEGE OF ENGINEERING AND SCIENCE
LOUISIANA TECH UNIVERSITY

February 1997

LOUISIANA TECH UNIVERSITY

THE GRADUATE SCHOOL

February 13, 1997
Date

We hereby recommend that the dissertation prepared under our supervision

by Jason D. Gardner

entitled Myoglobin Facilitated Oxygen Diffusion in the Heart:

A Mathematical Assessment

be accepted in partial fulfillment of the requirements for the Degree of

Doctor of Philosophy

Supervisor of Research R.W. Schubert

Head of Department S.A. Napper

Biomedical Engineering
Department

Recommendation concurred in:

P.N. Hale, Jr.

F.J. Jones

S.A. Napper

J.G. Spaulding, III

Advisory Committee

Approved:

Director of Graduate Studies

Dean of the College

Approved:

Dean of Graduate School

GS Form 13
8/96

ABSTRACT

Myoglobin facilitated oxygen diffusion and Michaelis-Menten kinetics are added to an experimentally-validated cardiac tissue model to determine the steady-state function of myoglobin in working heart tissue. Previous modeling of tissue oxygen partial pressure (pO_2) data suggests that the oxygen diffusion coefficient in working heart tissue is greater than expected. To fit the pO_2 data, the tissue oxygen diffusion coefficient in the model must be elevated to 8 to 12 times reported values. These elevated values of the tissue oxygen diffusion coefficient are not acceptable based upon the current understanding of cardiac muscle physiology. In this dissertation the effect of including myoglobin facilitated diffusion in the model is evaluated to determine if this phenomenon can explain the need for an elevated oxygen diffusion coefficient.

The Radially-Averaged, Axially-Distributed (RAAD) model considers axial diffusion of oxygen in tissue, myoglobin facilitation of oxygen transport, and pO_2-dependent oxygen consumption. Models are solved numerically using a variable-mesh finite-difference scheme. Parameters are optimized with Nelder-Mead simplexing and are chosen to minimize the sum-of-squares error between model pO_2 predictions and pO_2 data.

The addition of myoglobin to the RAAD model does not provide a better data fit. Simulations led to the conclusion that myoglobin facilitation is not responsible for the elevated oxygen diffusion found through modeling pO_2 data. Also, simulations indicate that myoglobin facilitated diffusive transport of oxygen can be disregarded in future steady-state oxygen transport models of the isolated perfused cat heart. Possible explanations for the elevated oxygen diffusion coefficient include tissue stirring by contractile elements, inter-capillary oxygen exchange, and preparation-specific transport conditions of the isolated heart.

TABLE OF CONTENTS

LIST OF TABLES

LIST OF FIGURES

ACKNOWLEDGEMENTS

I wish to express my most sincere appreciation to all those who have assisted me in completing this dissertation. First and foremost I must thank God for giving me the talent, patience, and tenacity needed to acquire this degree. I must also thank God for His benevolent gift of love, my wife-to-be, Hope. Without her, I am not sure I could have dealt with the stresses and uncertainties of the last year. With God's blessing I wish to have a long and fruitful life with my little Cajun sweetheart.

I thank Dr. Roy Schubert for all of his effort and guidance during my years at Louisiana Tech that led to this work. He has impressed me with his sincere concern for the students, desire for knowledge, and quest for understanding life's journey. Thanks are given to my committee members for their time and contribution to this effort. Special thanks go to Dr. Gene Callens, Dr. Frank Jones, and Dr. Jim Spaulding for inspiring in me much needed confidence. I would like to thank Celia Wall, Sherry Jones, and Bobbie Cupit for all of their assistance. I also want to thank Dr. Jim Barnes, Dr. John Grant, and Dr. Susan Nodurft for their positive influence early in my academic endeavor.

I owe much of my success to the influence of my family and friends. I thank my father, Dr. Joseph Gardner, and my mother, Marilyn, for their unwavering devotion and support through my college years. Many times I felt like quitting, but they never had a doubt. I thank my sister, Lisa, for making me laugh when I needed to laugh. I thank my

late grandmother, Janice Watson, for being my biggest fan and for always having those just-right sundaes and lemon icebox pies. Grandma, you left too soon, but I know you will always be there for me. I must express my gratitude to all of the family members who have no idea what I have been doing for the past five years but still managed to show interest and offer help. Lastly, I want to thank Maxwell for being my best friend during those lonely years on California Avenue.

Funding for this research was provided by the Louisiana Board of Regents and the American Heart Association.

CHAPTER 1

INTRODUCTION

1.1 Clinical Relevance

The heart is dependent on an uninterrupted supply of oxygen. Removal of oxygen supply quickly leads to cardiac cell death. Ischemic heart disease is the result of reduced oxygen supply to the cardiac tissue primarily from blockage of the coronary arteries. Blockage of the coronary arteries leads to loss of contractile function of heart muscle, cardiac arrhythmia, and cardiac cell death [Katz, 1992]. For the patient, this sequence of events usually results in heart failure. The human cost of ischemic heart disease is immense. Since 1918, cardiovascular disease has been the leading cause of death in the United States. In 1993, 954,138 lives were lost because of cardiovascular diseases; nearly 500,000 of these deaths were caused by coronary heart disease [American Heart Association, 1996]. The financial cost of cardiovascular disease is also substantial, burdening the health care system, with approximately $151.3 billion spent treating cardiovascular diseases in 1996 [American Heart Association, 1996]. Based upon these statistics the need for further understanding of cardiovascular disease and improved treatment is clear.

The further development of a mathematically accurate model describing oxygen transport can provide insight into physical phenomena which govern oxygen utilization and cardiac functions. An accurate model would be useful for predicting oxygen levels in tissues where direct measurement is unavailable. The results of this project will aid in determining if there exists another chemical transport pathway in contracting heart muscle that may elevate diffusion. The implications of discovering another transport pathway are quite relevant to the study of cardiovascular disease. The discovery of elevated diffusion in the working heart could lead to improved treatment methods for myocardial ischemia. The ischemic heart is in a state of oxygen supply and demand imbalance; sustained oxygen levels less than those required by the tissue lead to a buildup of harmful metabolites (e.g., H^+ and lactate) and eventually cell death. Treatments of artherosclerotic ischemia (blockage of the coronary arteries) attempt to restore oxygen balance by restoring oxygen levels to the afflicted area and by reducing adenosine triphosphate (ATP) utilization. Metabolite delivery to tissue involves both convective and diffusive processes. Enhanced diffusion in working heart tissue would represent another means of delivery. To treat the ischemic heart, increasing heart rate is felt to be detrimental because of the increased metabolic requirements of the tissue, while a reduced heart rate is clinically felt to be best. But, if diffusion is enhanced by stirring, then increased heart rate must be reevaluated as a treatment condition. Theoretically, the heart rate could be paced so that increased delivery by stirring exceeds increased metabolic demand. This increase could provide a new treatment strategy that has not been considered. The simulations described in this dissertation will not provide definite proof of another transport pathway in working heart

tissue, but determining the role of myoglobin in elevated oxygen diffusion is the next step towards such a goal.

1.2 Overview of Research

Oxygen partial pressure (pO_2) data obtained from an isolated perfused cat heart [Schubert, Whalen, Nair, 1978] has been modeled using the Krogh Cylinder model to simulate oxygen transport to tissue [Schubert, 1976]. The pO_2 histogram, an estimate of the probability distribution, predicted by the Krogh model did not match the experimental pO_2 histogram (Figure 1). Whereas the Krogh model [1919] predicts a flat, featureless pO_2 profile, the experimental data reflect a higher percentage of tissue at low pO_2. Attempting to provide better agreement between model prediction and experimental data, Schubert et al. proposed an alternative to the Krogh model [Schubert, 1976; Schubert, Whalen, 1976; Schubert, Fletcher, Reneau, 1985]. Instead of including only radial oxygen transport in tissue (Krogh model), the new model also included axial oxygen transport. Radial diffusion was replaced with a mass transfer coefficient through space averaging. The new model fit the pO_2 data better than the Krogh model. The pO_2 distribution predicted by the new model, Figure 1, showed the same leftward shift as the pO_2 data [Schubert, Fletcher, Reneau, 1985]. One major problem with the axial model is that the tissue oxygen diffusion coefficient ($D_{Z,TIS}$) had to be elevated to about ten times normal (1.65×10^{-4} cm^2/s) to predict the tissue data accurately.

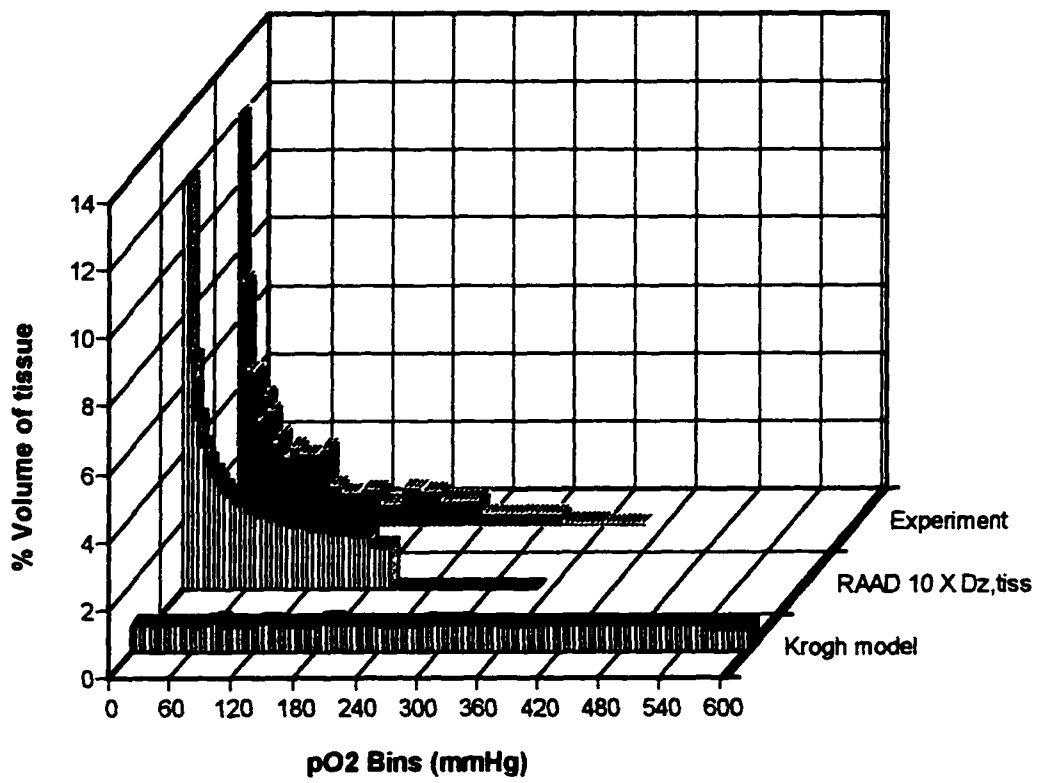

Figure 1: Comparison of model pO_2 histograms. Contrasting pO_2 histograms are shown: featureless Krogh model prediction, axial model (RAAD) prediction with 10 x $D_{Z,TIS}$ showing leftward shift towards low pO_2 bins, and experimental data from isolated heart microelectrode measurements (average of low and high perfusion pressure data from Schubert, Whalen, and Nair [1978]).

Several of the model assumptions were questioned. With the addition of Michaelis-Menten oxygen consumption kinetics, the need for an elevated diffusion coefficient is reduced by 20% to 1.32 x 10^{-4} cm^2/s [Napper, Schubert, 1988]. The assumption of radial averaging was also questioned by comparing the axial model to a fully distributed model (axial and radial oxygen diffusion). The comparison justified the use of radial averaging by showing that the model pO_2 distributions were highly insensitive to changes in radial parameters [Schubert, Zhang, 1992]. However, the need for an elevated axial diffusion coefficient was not explained. The current study will determine what effect the addition of myoglobin facilitated oxygen diffusion will have on the axial model. The axial model is now called the Radially-Averaged, Axially-Distributed (RAAD) model [Gardner, Schubert, 1995].

1.3 Research Need

Through comparison between physiological data and models predicting experimental pO_2 data, diffusion appears to be elevated in contracting cardiac tissue. Napper determined that some of this enhancement was apparent (as opposed to actual) and could be explained by adding Michaelis-Menten kinetics of oxygen consumption to the RAAD model [Napper, 1985]. Estimates of the tissue oxygen diffusion coefficient decreased from twelve to eight times normal with Michaelis-Menten in the model. However, his results show that the Michaelis-Menten "constant," K_m, varied from 4 to 5 mmHg. These values are considered somewhat high relative to experimental determinations [Whalen, 1971; Buerk,

Saidel, 1978; Duling, 1978] and very high compared to data from isolated mitochondria [Chance et al., 1974]. Although values in the range of Napper's numbers have been measured in intact tissues, the possibility exists that the elevated K_m values may mask the effects of another oxygen transport phenomenon in tissue such as myoglobin facilitated diffusion [Araki, Tamura, Yamazaki, 1983]. Therefore, both the independent and combined contributions of myoglobin facilitation and Michaelis-Menten kinetics should be assessed using the RAAD tissue model. The combined effect of adding myoglobin and Michaelis-Menten to the model can be compared to the individual effects of adding either myoglobin or Michaelis-Menten. Individual effects must be assessed to eliminate the possibility of Michaelis-Menten masking the effect of myoglobin facilitation.

At this time, the elevated oxygen diffusion has not been explained. A possible explanation is the stirring or sloshing of contracting tissue [Kreuzer, 1982; Jacquez, 1984; Schubert, Fletcher, 1993]. It is hypothesized that the shortening and expanding of muscle fibers during contraction causes movement of cytosol (intracellular fluid) back and forth between the myofibrils of the muscle [Jacquez, 1984]. Furthermore, Schubert and Fletcher [1993] suggest that the actual contractile elements may provide additional stirring during contraction; stirring may occur as the myosin filament ratchets along the actin filament. If this is true, the transport of many chemical species, including myoglobin, should be enhanced by the convective effects of the contractile stirring. Verification of these proposed mechanisms will require complicated experimental measurements and the development of instrumentation to measure the chemical species involved. Before justification can be given to these costly

experimental techniques, the exclusion of myoglobin facilitation of oxygen transport from the RAAD tissue model must be addressed.

This dissertation addresses the steady-state role of myoglobin facilitated diffusion in delivering oxygen to cardiac tissue. Facilitation of oxygen transport by myoglobin has been assessed by other modeling attempts, but there is no agreement on the magnitude of myoglobin's effect. Many researchers suggest that myoglobin does not diffuse significantly in tissue and therefore cannot provide oxygen transport [Fletcher, 1980; Gonzalez-Fernandez, Atta, 1982, 1986; Hoofd, 1995; Loiselle, 1987; Papadopoulas, Jurgens, Gros, 1995]. Yet, others conclude that myoglobin is a direct and significant source of extra oxygen transport for the tissue, especially during periods of low tissue pO_2 [Jacquez, 1984; Federspiel, 1986; Covell, Jacquez, 1987; Groebe, 1995]. As a group, they have all failed to verify modeling results with experimental data. Model-to-model comparisons are often made, conclusions from which may not hold true in living, working, or contracting tissue. In cases where experimental data are used, the data have been obtained at the whole organ level. The problem with many evaluations of myoglobin facilitation in tissue is that the basic model used does not mimic data measurements at the tissue level. Major exclusions in these models include 1. neglecting axial diffusion of oxygen in tissue, and 2. neglecting the possibility of stirring in working tissue. What makes this dissertation unique is that the tissue model that forms the basis of the analysis mimics experimental data at the tissue level [Schubert, Fletcher, 1993].

It must be determined if the effect of adding myoglobin facilitated diffusion to the RAAD tissue model is large enough to explain the elevated diffusion found through

modeling pO_2 data, or to what extent myoglobin can account for the elevated diffusion. This dissertation is basically the next step in determining why diffusion levels appear higher in living, working cardiac tissue than in dead tissue. Once the effects of myoglobin have been determined, then justification can be given to more complicated modeling and experimentation. The RAAD model results supplied by this dissertation should provide an answer to the question, "Is myoglobin facilitated diffusion of oxygen significant in the working heart?"

1.4 Objectives of Research

The goal of this dissertation is to determine the steady-state role of myoglobin in enhancing the diffusion of oxygen in tissue, and whether myoglobin facilitated oxygen diffusion can account for elevated oxygen diffusion observed in pO_2 data modeling.

Specific objectives are as follows:

1. add myoglobin facilitated oxygen diffusion and Michaelis-Menten kinetics to the existing validated cardiac tissue model (RAAD model);
2. solve the resulting cardiac tissue model equations using numerical techniques, and compare the modeling results to the experimental data;
3. optimize the solution to provide a best fit to the experimental data by searching for the diffusion coefficients of oxygen and myoglobin, Michaelis-Menten coefficient (K_m), and maximum oxygen consumption (V_{max});

4. determine the extent that myoglobin facilitation accounts for the apparent enhancement of oxygen diffusion in cardiac tissue; and
5. investigate the independent and combined contributions of myoglobin facilitation and Michaelis-Menten kinetics to the RAAD model by comparison of model results.

CHAPTER 2

RELATED RESEARCH

2.1 Models of Oxygen Transport in Tissue

Oxygen plays a vital role in cellular metabolism. In mammals, the transport of oxygen from blood to tissue occurs by the following pathway. Oxygen is taken up by red blood cell hemoglobin in intimate exchange with gases in the lungs. The oxygen-rich red blood cells are transported by convection through blood vessels to capillary beds within the tissue. Oxygen is released from the red blood cell hemoglobin and is transported by diffusion through the capillary wall and into the tissue where it is utilized for cellular function. Each step of this delivery system of oxygen to tissue has been studied and modeled by investigators. Popel provides an excellent review of methods for modeling oxygen transport to tissue [Popel, 1989]. Tissue models are useful for predicting oxygen levels in tissue where direct measurement is impossible or not feasible. Tissue models also provide the researcher with a means of investigating a broad range of oxygen delivery conditions that would be difficult to explore experimentally.

Krogh's original theories [1919] on oxygen transport to tissue laid the groundwork for future modeling efforts. Krogh observed that capillaries were somewhat uniformly distributed in a cross-section of striated muscle. Based upon this observation,

Krogh introduced a model (Figure 2) describing oxygen transport in tissue. Krogh's model consisted of non-interacting tissue cylinders perfused by a central capillary. Oxygen is introduced in the capillary and passively diffuses into the surrounding tissue cylinder. Diffusion is driven in the radial direction by radial concentration gradients. Axial tissue diffusion is neglected in Krogh's concept. Theoretically, a section of tissue could be represented by repeating the basic cylinder model several times [Krogh, 1919]. Given capillary pO_2, the Krogh model allows calculation of the radial pO_2 distribution in tissue. The capillary is not modeled as a separate region in Krogh's original model. Further research by Bloch led to the addition of a radially well-mixed capillary region represented as a central cylinder [Bloch, 1943]. This change allowed for additional modeling involving variable perfusate flow rates. This tissue-capillary cylindrical unit is known as the Krogh cylinder (Figure 2). The Krogh cylinder model predicts axial gradients in the tissue, but does not allow transport by these gradients.

The basic Krogh cylinder model of Krogh and Bloch has been extended by many researchers and is often used as a comparison tool when a new model is developed [Groebe, Thews, 1990a; Secomb et al., 1993]. Blum extended the Krogh cylinder model by adding axial diffusion in the tissue region [Blum, 1960], but his solution showed lack of continuity at the capillary-tissue interface. This error was finally resolved in later modeling [Fletcher, Schubert, 1982]. The details of the non-linear properties of blood have been added to the capillary region and applied to brain tissue [Reneau, Bruley, Knisely, 1969]. More recently, Fletcher and Schubert and others [Kreuzer, 1982] have questioned the ability of the Krogh model to predict accurately oxygen distributions in

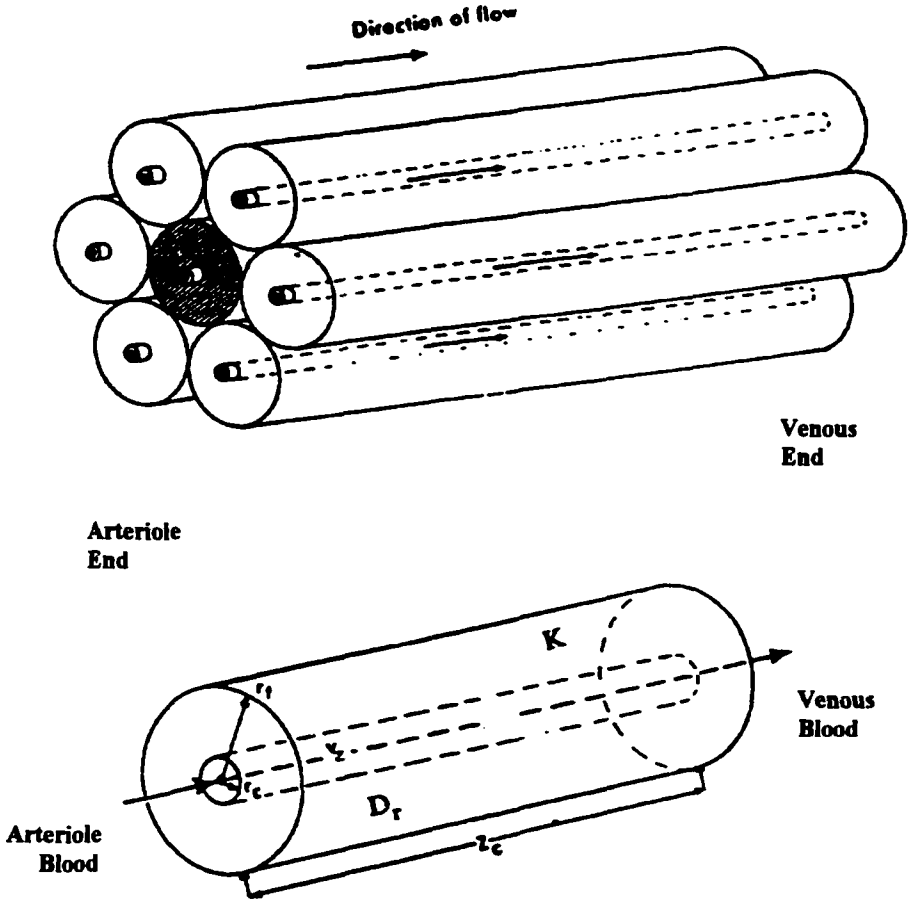

Figure 2: Sketch of the Krogh cylinder model. Top: The Krogh cylinder is repeated to represent a section of tissue. The individual tissue cylinders do not interact. Bottom: The model is comprised of a capillary surrounded by a cylindrical tissue region. There is radial diffusion of oxygen in the tissue region. Axially diffusion is neglected [Fletcher, Schubert, 1987].

tissue (Section 2.3) [Fletcher, Schubert, 1987]. Fletcher and Schubert suggest an alternative representation of tissue transport based on comparison to measurements of tissue pO_2 [Fletcher, Schubert, 1987; Schubert, Fletcher, 1993].

The Krogh model's repeating cylinder does not account for heterogeneity of tissue perfusion and assumes that capillaries are uniformly spaced in tissue. Pittman offers a review of research involving the influence of microvascular architecture on oxygen transport to tissue [Pittman, 1995]. For example, Levitt created a model which allows interaction between capillary-tissue units and found that tissue appears "well-stirred" [Levitt, 1971]. Secomb, and Hsu et al. have simulated oxygen delivery in complex geometrical capillary arrangements [Hsu, Secomb, 1989; Secomb, Hsu, Dewhirst, 1992; Secomb et al., 1993]. These highly ordered models of blood vessel networks are very situation specific and cannot generally predict tissue oxygen profiles other than for the specific arrangement that is modeled. The arrangement of vessels in tissue cannot be determined without disturbing the tissue.

When modeling oxygen transport, it is important to determine if the model is physiologically sound. That is, does the model reflect actual oxygen distributions in tissue? There are several techniques utilized in the measurement of tissue pO_2. The measurement technique should minimize damage to tissue and disturbance of the tissue pO_2 field. Available pO_2 measurement methods have been reviewed by Vanderkooi et al. [Vanderkooi, Ericinska, Silver, 1991]. Optical methods are limited by the depth of light penetration and can only be used on tissue surfaces or optically clear regions. This limitation requires that the sampled region be exposed such that tissue pO_2 may be

increased by oxygen diffusion into the exposed surface. Also, the axial sensitivity of optical probes is difficult to determine. Larger electrodes may cause tissue distortion through vascular compression. Also, large probes can span several capillaries for most of their length and do not provide the spatial resolution required for comparison to tissue models. Bare noble-metal electrode measurements are sensitive to the rate of oxygen consumption at the metal surface and are dependent on the transport properties of the tissue around the tip of the electrode. These electrodes measure an average convective-diffusive oxygen "availability". An electrode measuring average oxygen would predict high median pO_2 because the pO_2 sampled is not normally distributed (see Schubert, et al. [1978] for a complete discussion). The recessed tip microelectrodes of Whalen and Nair provide absolute tissue pO_2 and are the only technique to measure local pO_2 reliably [Whalen, Riley, Nair, 1967; Schneiderman, Goldstick, 1975]. The Whalen-Nair electrode exhibits minimal to no stir sensitivity; convection at the tip does not affect measurement. With a tip diameter of less than 1 μm, the electrode measures pO_2 from a tissue volume of approximately 1 μm^3 and does not significantly disturb the tissue [Whalen, Nair, Buerk, 1973]. Other techniques do not provide the spatial resolution necessary for model-to-data comparison; for example, the spectrophotometric measurement technique used by Gayeski and Honig [1991] has an estimated spatial resolution of 5x5x3 μm^3.

The problem with the prior evaluations of tissue models is that there is typically no comparison to tissue level data. As noted by Popel [1989] in his review of oxygen transport models,

> "At present none of the models of oxygen transport (including Krogh's model) has been carefully tested against experimental data. The main reason appears to be the lack of accurate measurements of oxygen tension...in vivo with the spatial resolution necessary for validation of distributed transport models."

While there may be comparisons to whole-organ data, a model that mimics whole-organ data may not and most likely will not predict tissue-level data accurately. In the worst case of attempted model validation, model-to-model comparisons are made [Groebe, Thews, 1990a; Secomb et al., 1993]. One model is evaluated on how well it compares to another model, neither of which has been validated with experimental data. The error committed is that the basic model used is faulty in that it does not mimic experimental data at the tissue level. The uniqueness of this dissertation is in using a mathematical model that has been validated through comparison with tissue level pO_2 data.

2.2 Microelectrode Measurement of Oxygen in Tissue

Schubert et al. obtained pO_2 measurements from an isolated perfused cat heart, Figure 3, using the Whalen-Nair oxygen microelectrode [Schubert, 1976; Schubert, Whalen, Nair, 1978]. The isolated cat heart preparation was used to reduce the number of independent variables that affect the oxygen consumption of the heart. Most obvious is the lack of nervous intervention caused by isolation of the organ. A small latex balloon was inserted into the left ventricle to keep contractions isovolumic. This procedure was supposed to eliminate length-dependent changes in left ventricular function. The balloon

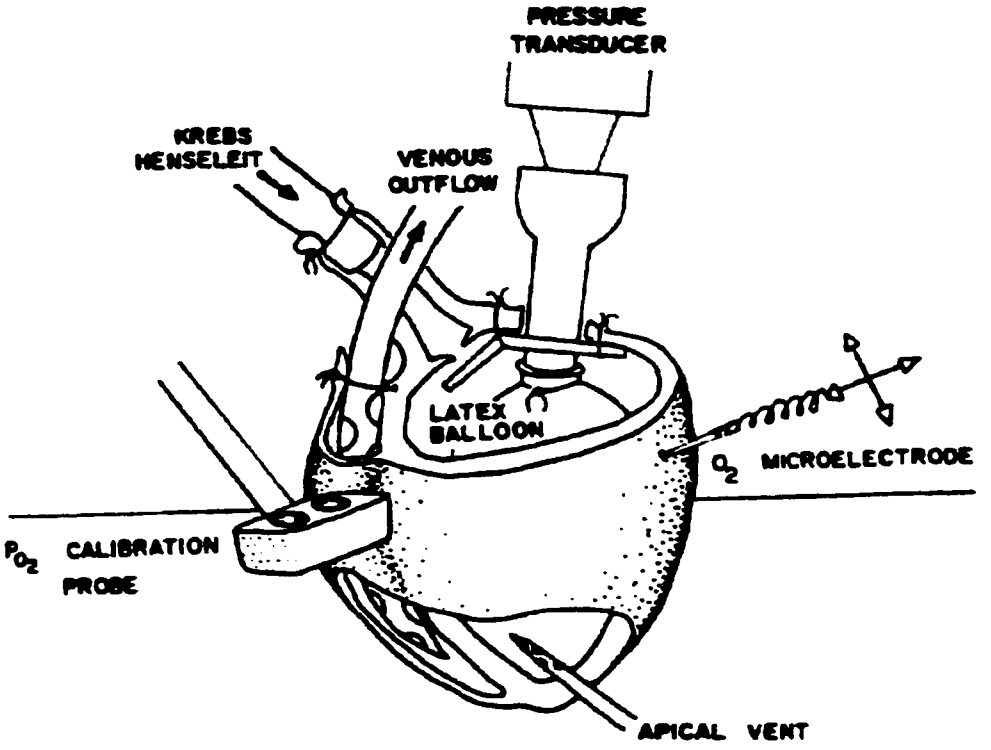

Figure 3: Isolated cat heart preparation. Temperature maintained at 32-33 °C [Schubert, Whalen, Nair, 1978].

also stabilizes the left ventricular wall allowing easier penetration of the wall with the Whalen-Nair microelectrode. A suction device utilized previously to stabilize the tissue surface [Whalen, Nair, Buerk, 1973] was not used in Schubert's measurements [Schubert, 1976; Schubert, Whalen, Nair, 1978]. The heart was paced to avoid time dependencies. A cell-free perfusate, Krebs-Henseleit solution, was used to perfuse the heart. All of these experimental considerations simplify the modeling of oxygen transport. Details about the data collection and microelectrode are reported in Schubert et al. [Schubert, 1976; Schubert, Whalen, Nair, 1978]. It is important to note that the isolated hearts exhibited flow autoregulation and were stable for several hours.

The pO_2 data were randomly sampled. Observations in hamster cheek-pouch tissue show that the electrode does not penetrate capillaries; rather, it deflects away from them [Whalen, Nair, Buerk, 1973]. Therefore, it was assumed that the electrode samples only tissue pO_2. There was no knowledge of microelectrode tip position relative to blood vessels. Tissue pO_2 was sampled at perfusion pressures of 78.2 mmHg (low) and 113.4 mmHg (high). Perfusion pressure is proportional to perfusate flow into the coronary arteries times the vascular resistance. Vascular resistance is intrinsically adjusted by the autoregulating heart. Increasing perfusion pressure increases the potential for flow, yet this pressure increase does not necessarily increase flow because of the dependence on resistance. In fact, Schubert showed that a 40% increase in perfusion pressure led to only a 9% increase in perfusate flow [Schubert, Whalen, Nair, 1978]. This result suggests that Schubert's isolated heart preparation is autoregulating, that is, the heart is intrinsically adjusting the resistance to flow (for further discussion see Schubert, 1976). There were

40 tissue penetrations with 894 samples at low and 898 samples at high perfusion pressure both with a coronary perfusate pO_2 of 722 mmHg. Statistical analysis performed on the data removed deviant heart preparations to ensure that the data set included measurements from viable heart preparations only [Schubert, Whalen, Nair, 1978].

2.3 Modeling of Microelectrode Tissue Data

2.3.1 Histogram Comparison of Model and Data

The randomly sampled raw pO_2 data cannot be compared directly to modeled pO_2. Typically, models have some set geometric arrangement. Knowledge of the exact positioning of the electrode tip would be needed to make a direct comparison. A statistical comparison can be made through the formation of a pO_2 histogram. Basically, this formation involves determining the volume of tissue that falls within a pO_2 range or bin. The resulting histogram is percent volume of tissue versus bins of pO_2 (see Schubert, Fletcher, 1993, for details). Figures 4 and 5 show the experimental pO_2 histograms for low and high perfusion pressure, respectively. Differences between the two data sets are small; the only significant difference occurs in the 0 to 5 mmHg bin (95% confidence level) [Schubert, Whalen, Nair, 1978]. One consequence of using this statistical means of data comparison is that any number of models may successfully predict the randomly sampled pO_2 distribution. There is no uniqueness associated with a model that matches a data set of this sort [Schubert, Fletcher, 1993].

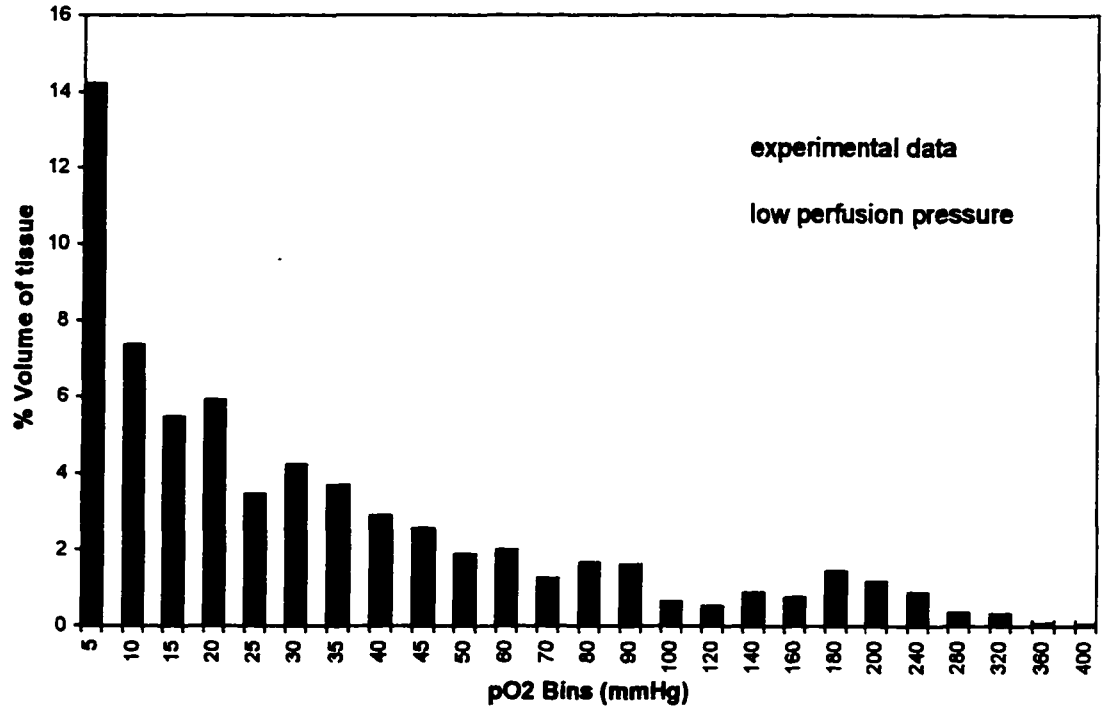

Figure 4: Low perfusion pressure pO_2 histogram. Experimental data taken from the isolated perfused cat heart preparation [Schubert, Whalen, Nair, 1978]. Note the change in bin size at higher pO_2. For data compression bins start at 5 mmHg wide and double at 50, 100, and 200 mmHg. Data compression was not used in Figure 1. In Schubert's original work, data compression was used to maintain equal variance in bin values (for details see Schubert, et al., [1978]).

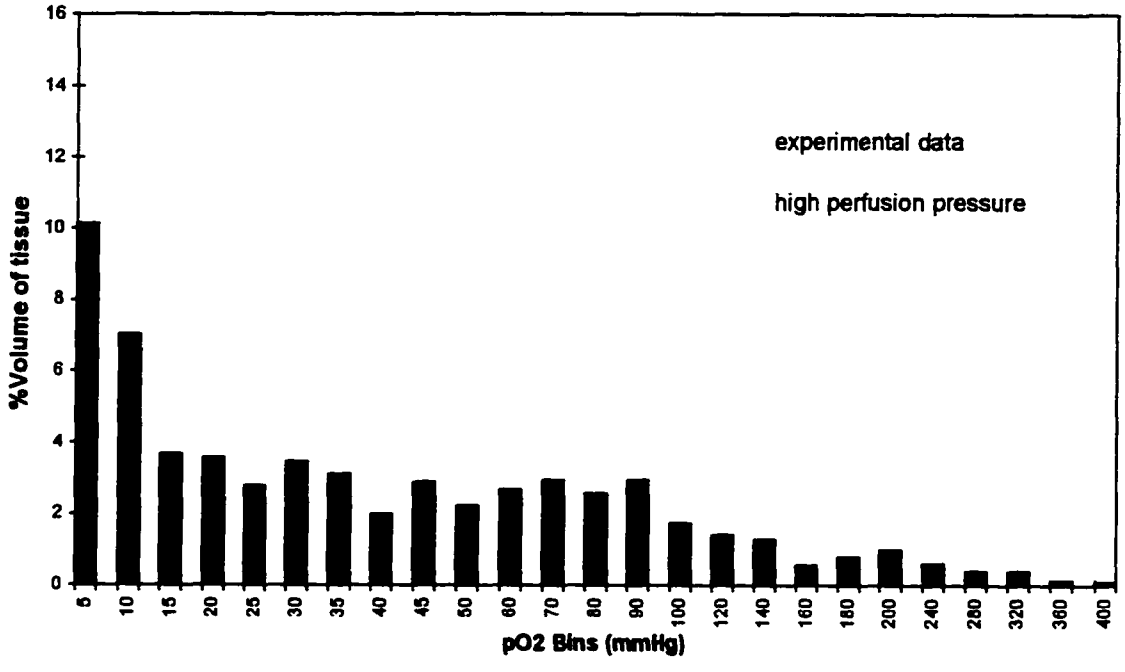

Figure 5: High perfusion pressure pO_2 histogram. Experimental data taken from isolated perfused cat heart preparation. The only statistically significant difference between the high and low (Figure 4) data sets occurs in the 0 to 5 mmHg bin (95% confidence level) [Schubert, Whalen, Nair, 1978].

2.3.2 Inadequacy of Krogh Model

Schubert used pO_2 distributions predicted by the Krogh cylinder model to compare with his data [Schubert, 1976]. He discovered that the pO_2 predictions of the Krogh model did not match the pO_2 tissue data (Figure 1). While the experimental data showed a distinct leftward shift, the Krogh model predicted a featureless histogram. Trying to explain this, Schubert proposed an alternative to the Krogh model which included axial oxygen diffusion in tissue [Schubert, Whalen, 1976; Schubert, Fletcher, Reneau, 1985; Schubert, Fletcher, 1993]. This model will be referred to as the Radially-Averaged, Axially-Distributed (RAAD) model [Gardner, Schubert, 1995].

2.3.3 Radially-Averaged, Axially-Distributed (RAAD) Model

The RAAD model suggested by Schubert retained the same geometry as the original Krogh model (Figure 2), but replaced the radial gradients with a mass transfer coefficient (radially space-averaged) and added axial transport by diffusion in the tissue region [Schubert, 1976; Schubert, Fletcher, Reneau, 1985]. The cylinder model is not meant to represent an actual capillary. Rather, the model is used to represent some "equivalent" capillary that describes the average transport characteristics of the heart. The model is thought to be equivalent in the sense that randomly sampling the tissue region of the model will result in a pO_2 distribution that is similar to an experimentally determined distribution. The RAAD model is therefore called the "equivalent" Krogh cylinder model [Schubert, Fletcher, 1993]. The RAAD model pO_2 histogram distribution exhibits the

leftward shift similar to the pO_2 data (Figure 1). Schubert found that, to have the RAAD model adequately predict the experimental pO_2 distributions, the tissue axial diffusion coefficient for oxygen ($D_{Z,TIS}$) had to be increased to ten times what was presently accepted as normal. This value was by most standards unacceptably large. The most probable explanation for this increased diffusion in the tissue region was a model oversimplification. The model assumptions have been inspected and evaluated as summarized in the following review.

2.4 Evaluation of RAAD Model Assumptions

2.4.1 Exclusion of Hemoglobin in the Capillary

The RAAD model does not consider hemoglobin in the capillary. Since the model is compared to experimental data, the model assumptions should match the experimental conditions. The isolated cat heart was perfused with a cell-free, hemoglobin-free perfusate. Therefore, the RAAD model excludes hemoglobin in the capillary, using instead a perfusate whose oxygen content is related linearly to the solubility of oxygen in Krebs-Henseleit solution. Some models of oxygen transport to tissue do account for Hemoglobin and red blood cell distribution in the capillary. These models are compared to whole organ data that are obtained from blood perfused tissues. For example, Groebe presents a Krogh cylinder type model that accounts for red cell spacing and Hemoglobin unloading of oxygen in the capillary [Groebe, 1995]. He is not able to validate his model

with experimental data because no tissue level data are available for the blood-perfused tissue that his model describes.

2.4.2 Exclusion of Michaelis-Menten Kinetics

The original RAAD model, like the Krogh model, included the assumption that tissue consumption of oxygen is homogeneous and zero order which does not allow the consumption to vary with the pO_2 as occurs in living tissue [Guyton, Hall, 1994]. Oxygen consumption in tissue decreases with decreasing pO_2 in a non-linear manner; the effects are significant at low pO_2. Through modeling of pO_2 data from brain and liver slices, Buerk and Saidel [1978] determined that a better model of oxygen consumption in tissue is the Michaelis-Menten kinetic model. Based upon this finding, Napper replaced the homogeneous consumption in the RAAD model tissue region with Michaelis-Menten kinetics, and found that including Michaelis-Menten kinetics in the RAAD model reduced the need for a high value of axial oxygen diffusion coefficient, $D_{Z,TIS}$, by 20% [Napper, Schubert, 1988]. Clearly the inclusion of Michaelis-Menten kinetics did not entirely explain the elevated diffusion coefficient needed to match Schubert's experimental data.

Through his simulations, Napper determined Michaelis-Menten coefficients (K_m) ranging from 4 to 5 mmHg. These values are higher than experimentally determined values in brain and liver tissues which range from 1.5 to 3.5 mmHg [Buerk, Saidel, 1978; Duling, 1978; Whalen, 1971], and much higher than Kreutzer and Jue [1995] determined for heart tissue (K_m = 2.1 mmHg). Higher values for K_m (3 to 4 mmHg) have been measured in intact rat heart

tissue [Araki, Tamura, Yamazaki, 1983]. Since Napper's predicted K_m values are higher than experimental values, it seems reasonable to ask if elevated K_m is masking the effect of myoglobin facilitated diffusion or other pO_2-dependent phenomena in tissue.

2.4.3 Radial Averaging

The original Krogh model described transport of oxygen in tissue as radial diffusion only and entirely neglected axial diffusion. The RAAD model considers both axial and radial transport of oxygen. Axial, or lengthwise, transport of oxygen is modeled as simple diffusion. Radially, the RAAD model is space averaged, meaning that there is no variation in the radial direction in either the capillary or the tissue; but, an oxygen gradient is present because a finite permeability "barrier" is placed at the capillary-tissue interface. Oxygen in the capillary moves radially through the capillary wall into the tissue. Instead of describing the radial transport as distributed diffusion, transport radially is represented by a lumped mass transfer coefficient, such that the radial flux from the capillary is equal to the product of the mass transfer coefficient times the concentration gradient between the capillary and tissue.

Once it was recognized that the Krogh model was inadequate and that the capillary and tissue region had large axial gradients, neglect of axial transport was suspect. Blum added axial diffusion to the Krogh cylinder model [Blum, 1960], but continuity at the capillary-tissue interface was not maintained [Schubert, personal communication]. Blum revealed that he was aware of the problem and that the correct solution had not been found [Schubert, personal communication]. Schubert was unable to find the solution, so

he proposed lumping the radial diffusion into a permeability between two radially space-averaged regions and maintaining distributed axial diffusion [Schubert, 1976; Schubert, Whalen, 1976; Schubert, Fletcher, Reneau, 1985]. This solution produced histograms that show a leftward shift similar to experimental pO_2 data [Schubert, Whalen, Nair, 1978]. However, in order to produce histograms resembling the experimental measurements, Schubert had to use an artificially high value of axial diffusion coefficient of oxygen in tissue. The reasons for this elevated coefficient were unknown, but modeling assumptions were questioned.

Lenhoff and Lightfoot [1982] used a space-averaging concept, similar to Schubert and Whalen [1976], and constructed a time-dependent Krogh cylinder model. Fletcher and Schubert [1982] derived and solved a steady-state two-dimensional tissue model (axial and radial oxygen diffusion in the tissue region). Oscillations (ringing) in the solution at the inlet of the model forced them to utilize a Fejer summation technique to smooth the solution. This technique required extensive computation time, but, for the first time, a useful solution to combined radial and axial diffusion in tissue was obtained. They later added axial diffusion in the capillary and a permeability barrier at the capillary wall [Fletcher, Schubert, 1987]. Maintaining diffusion in the capillary region added little to oxygen transport, but led to smoothing of the model solution and eliminated the need for a smoothing technique. Zhang performed a mathematical comparison between the original Krogh model, the RAAD model, and the mathematically difficult two-dimensional model of Fletcher and Schubert, 1987 [Zhang, 1992]. He concluded that the Krogh model was inadequate for predicting pO_2 distributions in the Krebs-Henseleit perfused heart, but that

the RAAD model could be used instead of the two-dimensional model to predict accurately pO_2 distributions for 95% of the model domain. The inlet pO_2 fields were not predicted well by the RAAD model, but make up a small percentage of the total pO_2 distribution. Recall that, for accurate predictions, the $D_{Z,TIS}$ must still be elevated to eight to ten times normal. Zhang found that the RAAD model was relatively insensitive to large changes of the radial oxygen diffusion coefficient ($D_{R,TIS}$), suggesting that oxygen diffusion was not anisotropic as earlier results suggested [Fletcher, Schubert, 1982, 1987], but was probably elevated isotropic diffusion [Schubert, Fletcher, 1993]. Through his model comparisons, Zhang showed that use of the RAAD (radially averaged) model instead of the mathematically difficult two-dimensional model was justified unless entrance conditions were of interest. The explanation for the elevated diffusion suggested by Schubert's data clearly did not reside within the replacement of radial diffusion by a mass transfer coefficient.

2.4.4 Exclusion of Myoglobin

Another RAAD model simplification was the exclusion of myoglobin kinetics in the tissue region. In addition to acting as a buffer for oxygen in tissue, myoglobin facilitates oxygen transport, but the extent of this facilitation is limited by myoglobin's ability to diffuse in tissue.

2.5 Myoglobin Facilitation of Oxygen Diffusion

Myoglobin (Mb) binds reversibly with oxygen in a 1:1 reaction to form oxymyoglobin (MbO_2). No information is available on alteration of myoglobin's affinity for oxygen due to pH or carbon dioxide level changes; however, variation of hemoglobin's affinity for oxygen are well documented [Guyton, Hall, 1994]. Myoglobin is believed to facilitate oxygen diffusion in tissue by binding to oxygen in areas of high oxygen concentration, diffusing as MbO_2 to areas of lower MbO_2 concentration (which correspond to low pO_2), and then releasing the bound oxygen. Key to myoglobin facilitation of oxygen transport is the ability of MbO_2 to diffuse in tissue. Myoglobin was initially excluded from the RAAD model because the then current literature suggested that myoglobin did not diffuse in tissue and therefore could not facilitate oxygen transport [Kreuzer, 1970; Leninger-Follert, Lubbers, 1973]. However, recent measurements in skeletal muscle determined that myoglobin does diffuse in tissue. Therefore, facilitated diffusion may significantly contribute to oxygen transport [Baylor, Pape, 1988; Jurgens, Peters, Gros, 1994; Papadopoulos, Jurgens, Gros, 1995]. In this study, myoglobin's role in contracting heart tissue is evaluated using the RAAD model. A comparison to tissue level pO_2 measurements is used to validate the model.

2.5.1 Experimental Determination of Factors Affecting Myoglobin Diffusion

The primary factors that determine the extent of myoglobin diffusion are the concentration (C_{Mb}) and diffusion coefficient (D_{Mb}) of myoglobin in tissue. The concentration of myoglobin varies by species and by tissue type. Concentration of myoglobin is greater in red muscles such as heart and skeletal muscle. The highly oxidative muscle cells of the heart contain the greatest concentration of myoglobin. Schuder et al. have determined the myoglobin content of skeletal and cardiac muscle through subunit-exchange chromatography [Schuder et al., 1979]. They found that the myoglobin concentration in cat ventricle tissue was 177 μmol/kg. This value was not used in modeling of the isolated cat heart because the sample size was too small to rule out variation among animals [Wittenberg, personal communication]. Wittenberg and Wittenberg have compiled values for C_{Mb} in various tissues [Wittenberg, Wittenberg, 1990]. Mammalian skeletal and heart muscle was found to contain an average 225 and 250 μmol/kg of myoglobin, respectively.

There is no consensus on the value for diffusion coefficient of myoglobin in tissue. The absolute maximum value can be determined using the Stokes-Einstein formula, $D_{Mb} = 2.97 \times 10^{-6}$ cm^2/s [Fletcher, 1980]. Experimentally measured values are an order of magnitude lower. Measurements in dilute myoglobin solutions (18% solution by weight thought to represent tissue) result in $D_{Mb} = 0.7 \times 10^{-6}$ cm^2/s [Fletcher, 1980]. Baylor and Pape introduced a met-myoglobin pulse into frog skeletal muscle and optically measured its distribution over time. They assumed that the diffusive properties of met-myoglobin

were identical to those of myoglobin and found, $D_{Mb} = 0.16 \times 10^{-6}$ cm^2/s at 20 °C [Baylor, Pape, 1988]. Jurgens et al. determined through photooxidation of myoglobin to met-myoglobin a diffusivity of 0.12×10^{-6} cm^2/s in rat skeletal muscle [Jurgens, Peters, Gros, 1994]. Using a technique similar to Baylor and Pape, Papadopoulos et al. determined the diffusivity of met-myoglobin in rat skeletal muscles of varying muscle types. The diffusivity in red soleus and white extensor digitorum longus muscles was determined to be 0.13×10^{-6} and 0.19×10^{-6} cm^2/s, respectively at 22 °C [Papadopoulos, Jurgens, Gros, 1995]. The highest value of diffusivity, 0.22×10^{-6} cm^2/s, was found in red soleus muscle at 37 °C. Each of these experiments determined values of diffusivity utilizing a spectrophotometric technique that measures the absorbance of met-myoglobin. The met-myoglobin is either injected [Baylor, Pape, 1988] or produced from native myoglobin with a high-energy pulse of UV-irradiation [Jurgens, Peters, Gros, 1994; Papadopoulos, Jurgens, Gros, 1995]. These methods are under scrutiny for various reasons. One problem is that these techniques measure the diffusion of met-myoglobin and not native myoglobin; it is not known if the diffusive properties of these molecules are identical. Furthermore, met-myoglobin has a net positive charge versus the close to zero or slightly negative charge of myoglobin [Baylor, Pape, 1988]. Met-myoglobin may interact with the negatively charged muscle fiber proteins giving a lower diffusivity versus myoglobin; although, Baylor suggests that this effect is negligible [Baylor, Pape, 1988]. The techniques involving UV-irradiation of a region of tissue experience difficulty in quantifying a baseline value for met-myoglobin produced after the UV pulse. This problem is due to enzymes that act to

reduce the newly formed met-myoglobin and oxidants created by the UV pulse that act to produce more met-myoglobin. The tissue damage caused by UV exposure and the subsequent effects on the apparent diffusion coefficient are difficult to quantify. A change in absorbance occurs after the UV pulse that is not saturation dependent; this change is related to tissue damage caused by the pulse. The damage may affect transport proteins in membranes and causes water uptake by the tissue [Jurgens, Peters, Gros, 1994; Papadopoulos, Jurgens, Gros, 1995]. In this study, a $D_{Mb} = 0.22 \times 10^{-6}$ cm^2/s is considered "normal." This value corresponds to that measured by Papadopoulos et al. [1995], in the rat soleus muscle at 37 °C.

2.5.2 Experimental Evaluations of Myoglobin Facilitated Diffusion

Myoglobin has been shown to facilitate oxygen diffusion in 18% (by weight) protein solutions [Kreuzer, Hoofd, 1987]. Myoglobin facilitation has been evaluated experimentally through oxygen uptake measurements in fish hearts and in cardiac myocytes (muscle cells). Wittenberg and Wittenberg concluded that, in isolated rat cardiac myocytes, approximately 1/3 of the oxygen uptake is due to myoglobin. This finding suggests that the function of myoglobin in cardiac myocytes is direct myoglobin-mediated oxygen delivery even under conditions of high extracellular oxygen [Wittenberg, Wittenberg, 1987]. Unlike myoglobin facilitated diffusion, myoglobin-mediated oxygen delivery does not require that myoglobin diffuse in tissue. A comparable measurement by Jones and Kennedy using similar myocytes (isolated rat cardiac muscle) led to the conclusion that myoglobin was not a significant

facilitator of oxygen transport [Jones, Kennedy, 1986]. This preparation is questionable since the myocytes changed shape during the measurements and therefore were considered structurally abnormal and not representative of natural heart cells. Gayeski and Honig measured intracellular pO_2 in cardiac myocytes by cryospectroscopy [Gayeski, Honig, 1991]. Observed intracellular oxygen gradients were shallow, and median pO_2 was 2.5 mmHg. Gayeski and Honig's results suggest that myoglobin exists near its 50% saturation level in cardiac tissue. They concluded that myoglobin acts to minimize spatial and temporal heterogeneities of pO_2 and that myoglobin facilitation is significant in cardiac tissue. Caution is advised because pO_2 measurements and determination of myoglobin facilitation in isolated cells may not be representative of intact tissue. Because of the lack of pO_2 gradients in their tissue measurements, Gayeski and Honig [1991] argue that myoglobin facilitation of oxygen diffusion is significant. Their conclusion is based on a comparison to pO_2 gradients predicted by the Krogh cylinder model, i.e., radial transport only. An alternate explanation of shallow pO_2 gradients in tissue is axial diffusion. Fletcher and Schubert [1987] show that axial diffusion in tissue effectively reduces radial pO_2 gradients in tissue.

Gayeski et. al. also applied their cryospectroscopy technique to dog gracilis muscle to measure intracellular pO_2. This technique uses fast freezing of tissue to "lock" the myoglobin in muscle at its saturation level prior to freezing. The myoglobin saturation of the frozen tissue is then measured with a spectrophotometer and pO_2 is determined. Based upon this measurement, Gayeski suggests that myoglobin plays a critical role in preventing tissue from becoming too hypoxic, and therefore avoiding cellular damage [Gayeski, Connett, Honig, 1987]. Furthermore, during myocardial ischemia, myoglobin

may provide the low pO_2 areas of heart tissue with more oxygen than would be available in a myoglobin-transport absent tissue. A problem with the fast-freezing technique is that the post-freezing values of myoglobin saturation may not be entirely representative of pre-freezing saturation values. Also, the technique has a large tissue sampling volume, 45 μm^3, relative to the Whalen-Nair electrode, 1 μm^3 [Gayeski, Connett, Honig, 1987].

Bailey et al. determined oxygen uptake of isolated perfused fish hearts for species with varying myoglobin concentrations [Bailey, Sephton, Driedzic, 1990]. They found that myoglobin-rich hearts were able to attain half-maximal oxygen consumption at lower oxygen concentrations than myoglobin-poor hearts. Myoglobin-poor hearts could not utilize oxygen at input pO_2's of less than 40 mmHg. This result suggests that myoglobin plays a role even at higher pO_2. Also, myoglobin-poor hearts were unable to recover from periods of hypoxia whereas myoglobin-rich hearts recover fully, implying that myoglobin-rich hearts can maintain oxidative metabolism over a wider range of hypoxic conditions than myoglobin-poor hearts. Bailey et al. suggest that the fundamental role of myoglobin in heart is maintenance of adequate oxygen flow to the mitochondria [1990]. To evaluate myoglobin function, Bailey et al. used nitrite to block myoglobin function. Nitrate oxidizes myoglobin to a non-functional state. Bailey et al. acknowledged that nitrate may affect the metabolism of the tissue, although their isolated heart preparations showed no statistical evidence of reduced metabolism after treatment with nitrate.

2.5.3 Theoretical Evaluations of Myoglobin Facilitated Diffusion

Myoglobin facilitated oxygen transport has been assessed by many researchers through modeling, but conclusions vary. Arguments against the effectiveness of myoglobin as a facilitator of oxygen transport typically suggest that the D_{Mb} or C_{Mb} of myoglobin is too low for substantial facilitation. The measurements of Jurgens et al. and Papadopoulos et al. found that D_{Mb} was very low, and subsequent modeling showed that myoglobin did little to increase intracellular oxygen [Jurgens, Peters, Gros, 1994; Papadopoulos, Jurgens, Gros, 1995]. Both of these studies used the Krogh model (no axial diffusion) to evaluate myoglobin facilitation. Baylor and Pape, although determining D_{Mb} to be essentially the same as Jurgens et al. and Papadopoulos et al., concluded that myoglobin could still double the transport of oxygen even at this low value of diffusivity [Baylor, Pape, 1988]. Baylor's evaluation of myoglobin facilitation is suspect since it does not consider consumption in the tissue. Each of these studies utilized a spectrophotometric technique to measure the diffusivity of met-myoglobin; problems associated with this technique are discussed in Section 2.5.1.

Fletcher utilizes a Krogh cylinder model (radial only) to evaluate myoglobin effectiveness as a facilitator of oxygen transport. Fletcher concludes that myoglobin facilitation does not add significantly to total oxygen pressure, but that facilitation does become significant near the venous end of the tissue cylinder. Fletcher states that this result suggests a possible safety mechanism against local hypoxia in muscle tissue [Fletcher, 1980]. Fletcher's conclusions were based on relatively high values of D_{Mb} (0.3 to 2.7 x 10^{-6} cm^2/s), although he does acknowledge that D_{Mb} in living tissue may be much smaller.

A model describing the diffusion of myoglobin in the presence of membranes representing diffusive barriers was developed by Gonzalez-Fernandez and Atta. Their findings suggest that membranes in the diffusive path reduce myoglobin's facilitative effects by decreasing D_{Mb} [Gonzalez-Fernandez, Atta, 1982]. Loiselle concluded that myoglobin facilitated oxygen diffusion was insignificant in the in vitro papillary muscle preparation model [Loiselle, 1987]. Loiselle's results cannot be extended to in vivo situations because the in vitro papillary muscle preparation is bathed in high pO_2 possibly causing myoglobin in the muscle to remain fully saturated with oxygen.

Myoglobin facilitation was determined to be significant when evaluated with slab models of skeletal muscle [Jacquez, 1984; Covell, Jacquez, 1987]. The models by Jaquez and Covell considered myoglobin kinetics and Michaelis-Menten kinetics but were not compared to experimental data. A two-dimensional model of skeletal muscle (r and θ, no axial diffusion) was developed by Federspiel. The model consists of a cylindrical tissue fiber with capillaries on the outer surface of the cylinder. Federspiel found that myoglobin acts to reduce pO_2 gradients in tissue [Federspiel, 1986]. Salathe and Chen utilize a space-averaged (multi-capillary), time-dependent slab model to evaluate myoglobin facilitation. They conclude that myoglobin is only effective at very low pO_2 [Salathe, Chen, 1993].

Groebe has presented extensive modeling of oxygen transport to tissue [Groebe, 1990, 1995; Groebe, Thews, 1990a, b]. His models include Krogh-type models and non-Kroghian models. Groebe's most recent paper utilizes a radial-diffusion-only, Krogh-like arrangement which considers hemoglobin and red blood cells in the capillary and myoglobin facilitation in the tissue region. Groebe linearizes the oxygen-myoglobin dissociation curve and estimates

Michaelis-Menten kinetics of oxygen consumption with a tissue region that switches consumption on or off depending on the local pO_2. Groebe attempts to include axial diffusion of oxygen, but admittedly cannot obtain the precise Bessel's function solution. Groebe concludes that myoglobin facilitation of oxygen transport is significant. He does suggest that changes in myoglobin parameters, such as D_{Mb} and C_{Mb}, do not affect the pO_2 distributions but may drastically change the extent of tissue anoxia (no oxygen) [Groebe, 1995].

Both from an experimental and a theoretical viewpoint, there is no universal agreement on the role of myoglobin in muscle. Those who believe that myoglobin is a significant facilitator of oxygen transport tend to see the muscle, especially cardiac muscle, as operating on the edge of hypoxia. Near hypoxia low tissue pO_2 leads to oxymyoglobin unloading of oxygen. Because the isolated heart preparation of Schubert appears to operate near hypoxia (10-14% of the tissue volume is below pO_2 = 5mmHg), myoglobin facilitation may be significant in the working heart and should be evaluated. Those who do not believe that myoglobin facilitates oxygen transport significantly tend to view the tissue as being well oxygenated and far from hypoxic. Higher levels of tissue pO_2 do not allow oxymyoglobin to unload bound oxygen. Although researchers cannot agree on a role for myoglobin, they cannot deny the possibility that myoglobin may act as a facilitator of oxygen transport. This possibility exists because oxymyoglobin concentrations in cardiac cells have been estimated to be approximately 30 times that of free oxygen, providing a ready source of oxygen if pO_2 levels drop [Wittenberg, Wittenberg, 1989].

CHAPTER 3

METHODOLOGY

3.1 Derivation of RAAD Model with Myoglobin

To include myoglobin facilitation in the Radially-Averaged, Axially-Distributed (RAAD) model, a reaction term is added which will represent the myoglobin-oxygen reaction. Recall that myoglobin (Mb) binds reversibly to oxygen (O_2) in a 1:1 fashion to form oxymyoglobin (MbO_2) as shown in Equation (1).

$$Mb + O_2 \underset{k2}{\overset{k1}{\rightleftarrows}} MbO_2 \tag{1}$$

Following Fletcher's development, the myoglobin reaction term as rate/volume is

$$\rho = C_{Mb,TOT}\left[k_1 C_{O2,TISS}(1-Y) - k_2 Y\right] \tag{2}$$

where Y is the fraction of myoglobin saturated with oxygen [Fletcher, 1980]. For a full parameter list see Appendix A. The RAAD model is shown in Figure 6. Although the model appears very similar to the Krogh cylinder model, the assumptions are quite different, notably the inclusion of myoglobin diffusion, axial diffusion of oxygen, and radial averaging.

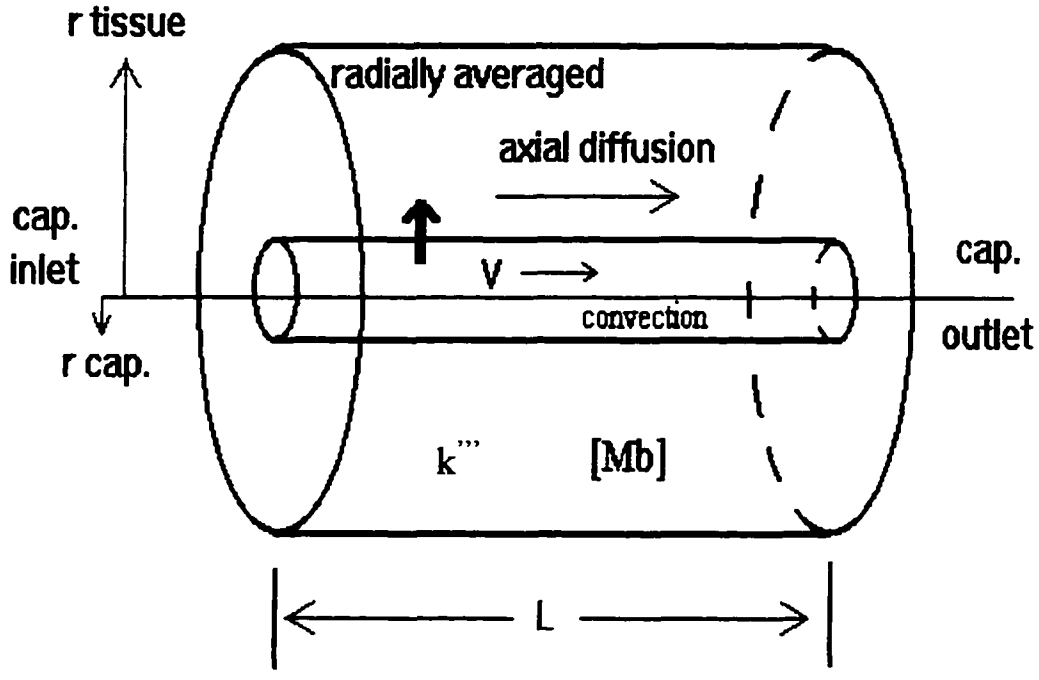

Figure 6: The RAAD model. The model consists of a central capillary which perfuses a surrounding tissue cylinder. Oxygen is transported in tissue via axial diffusion. Flux of oxygen from the capillary to the tissue is represented by a mass transfer coefficient times a concentration difference (equal solubilities). The tissue and capillary are radially space averaged. No oxygen leaves the outer surfaces except through the inlet and outlet of the capillary.

3.1.1 Equations Describing Tissue Region

In the tissue region, there is axial diffusion of oxygen ($D_{Z,TIS}$), zero-order consumption (k'''), and myoglobin facilitation of oxygen diffusion (MbO_2 diffusion). Modifications to the model for including Michaelis-Menten kinetics of oxygen consumption are shown in Section 3.1.4. Radial oxygen flux entering the tissue from the capillary is represented by a concentration difference times a mass transport coefficient (P); the tissue is space-averaged radially. Equal solubility of oxygen in the tissue and perfusate is assumed (see Schubert and Zhang, 1995, for RAAD model with unequal solubilities). With the appropriate mass balances on oxygen, the following equations result, describing the Radially-Averaged, Axially-Distributed (RAAD) model tissue region (an overbar on variables indicates normalization; see Appendix B for a complete derivation of the model, and Appendix A for a list of parameters, assumptions, and nominal values):

Transport of oxygen,

$$\frac{d^2\overline{C}_{O2,TIS}}{d\overline{Z}^2} + \alpha \cdot \left[\overline{C}_{O2,CAP} - \overline{C}_{O2,TIS}\right] - \mathrm{K} - \Omega_1 = 0 \qquad (3)$$

Transport of oxymyoglobin,

$$D_{MbO2,TIS}\frac{d^2C_{MbO2,TIS}}{dZ^2} + \rho = 0 \qquad (4)$$

where,

$$\alpha = \frac{2\, r_{CAP}\, Z_O^{\,2}\, P}{\left(r^2_{TIS} - r^2_{CAP}\right) \cdot D_{Z,TIS}} \tag{5}$$

$$\mathrm{K} = \frac{k'''\, Z_O^{\,2}}{D_{Z,TIS}\, C_O} \tag{6}$$

$$\Omega_1 = \frac{\rho\, Z_O^{\,2}}{D_{Z,TIS}\, C_O} \tag{7}$$

Equation (4) is normalized to

$$\frac{d^2Y}{d\bar{Z}^2} + \Omega_2 = 0 \tag{8}$$

where,

$$\Omega_2 = \frac{\rho\, Z_O^{\,2}}{D_{MbO2,TIS}\, C_{Mb,TOT}} \tag{9}$$

3.1.2 Equations Describing Capillary Region

Diffusion is omitted from the capillary region of the RAAD model because consistency between the model and experiment was impossible to achieve with axial diffusion in the capillary region; an explanation follows. In addition to choosing appropriate modeling assumptions describing the conditions of the isolated heart

preparation, the overall tissue oxygen consumption predicted by the model must match the experimentally-determined whole-organ consumption. For homogeneous consumption, the model consumption (k''') is set to the experimentally determined values; but, in the case of Michaelis-Menten kinetics, the overall consumption cannot be set in the model. For comparison, the predicted arterio-venous (A-V) difference from the model is used to calculate an overall consumption, which is then used to adjust the boundary condition describing capillary inlet pO_2 (see Appendix D). Adjustments are made until the model converges to an acceptable A-V difference (95% confidence, as described by Schubert, Whalen, Nair, 1978). This consumption-matching strategy becomes difficult to apply when there is diffusion in the capillary region of the model. Specifically, capillary diffusion requires another region in the model, a region that would represent a well-mixed segment of capillary at the entrance to the RAAD model capillary. This region would be needed to calculate the diffusive and convective portions of the flux into the RAAD capillary resulting from a set inlet convective capillary pO_2. A formula for the RAAD model inlet capillary pO_2 could be determined through an oxygen mass balance across the well-mixed segment of capillary. This formula for inlet pO_2 could then be used as a boundary condition. Numerically, this boundary condition is more difficult to use because a mixed boundary condition results. A mixed boundary condition specifies a dependent variable or combination of dependent variables at more than one of the system boundaries simultaneously. This method did not provide acceptable results because the concentration gradient in the capillary region was difficult to estimate numerically. With diffusion in the capillary, the RAAD model was not able to match the experimental A-V difference

[Schubert, Whalen, Nair, 1978] to within one standard deviation (see Appendix D). To avoid these complications, diffusion is omitted from the capillary.

In previous modeling, the transport of oxygen by diffusion was shown to contribute little to overall oxygen transport in the presence of convection within the capillary, yet the diffusive term was maintained because it reduced oscillations (ringing) in the analytical solution [Fletcher, Schubert, 1987]. As stated before, diffusion in the capillary region has been omitted because the experimental A-V difference could not be matched by the model. Prior studies did not discover this problem because Napper did not include diffusion in the capillary [Napper, Schubert, 1988] and Zhang dealt only with the homogeneous oxygen consumption model (no Michaelis-Menten) [Schubert, Zhang, 1992]. In this study, without capillary diffusion, oscillations of the capillary pO_2 solution at the capillary inlet were eliminated by increasing the number of nodal points.

In the capillary region, there is axial convection of oxygen caused by perfusate flow and radial flux into the tissue region. As stated before, oxygen flux leaving the capillary is represented by a concentration difference times a mass transport coefficient. With the appropriate oxygen mass balances, the following equations result, describing the RAAD model capillary region (see Appendix B for full derivation):

$$\frac{d\overline{C}_{O2,CAP}}{d\overline{Z}} + \beta \cdot \left[\overline{C}_{O2,CAP} - \overline{C}_{O2,TIS}\right] = 0 \qquad (10)$$

where,

$$\beta = \frac{2\, Z_O\, P}{v_{CAP}\, r_{CAP}} \tag{11}$$

3.1.3 Boundary Conditions for RAAD with Myoglobin Model

$$\left.\frac{d\,\overline{C}_{O2,TIS}}{d\,\overline{\overline{Z}}}\right|_{Z=0.0} = 0 \tag{12}$$

$$\left.\frac{d\,Y}{d\,\overline{\overline{Z}}}\right|_{Z=0.0} = 0 \tag{13}$$

$$\left.\frac{d\,\overline{C}_{O2,TIS}}{d\,\overline{\overline{Z}}}\right|_{Z=1.0} = 0 \tag{14}$$

$$\left.\frac{d\,Y}{d\,\overline{\overline{Z}}}\right|_{Z=1.0} = 0 \tag{15}$$

$$\left.\overline{C}_{O2,CAP}\right|_{Z=0.0} = set\ to\ match\ A-V\ diff \tag{16}$$

Equations (12), (13), (14), and (15) describe no oxygen or oxymyoglobin flux out of the ends of the tissue. These boundary conditions describe the Krogh cylinder repeating unit,

i.e., no interaction between adjacent cylinders. Equation (16) sets the inlet capillary concentration. This concentration is determined by matching the model's overall oxygen consumption to the experimentally determined consumption (see Appendix D).

3.1.4 Michaelis-Menten Kinetics

Michaelis-Menten kinetics is added to the RAAD+Mb model (RAAD model with myoglobin facilitation) to determine the synergistic effect that these kinetics have on myoglobin facilitation. Also, the combined effect of Michaelis-Menten kinetics and myoglobin facilitation on the elevated value of $D_{Z,TIS}$ is determined. Napper has shown that the oversimplification of tissue metabolism by using zero-order consumption in the RAAD model does account for some of the elevated diffusion needed in Schubert's modeling. Researchers have included both Michaelis-Menten kinetics and myoglobin facilitation in the same model, but the independent effects of these phenomena were not analyzed. Also, the possibility of elevated diffusion of either oxygen or myoglobin was not considered [Covell, Jacquez, 1987].

Inclusion of Michaelis-Menten kinetics requires that k''' in Equation (6) describing zero-order consumption be replaced with Equation (17) which describes Michaelis-Menten kinetics.

$$\frac{V_{MAX}\, C_{O2.TIS}}{\left[C_{O2,TIS} + K_m\right]} \tag{17}$$

resulting in the normalized expression:

$$K = \frac{V_{MAX}\,\bar{C}_{O2,TIS}\,Z_O^{\,2}}{\left[\bar{C}_{O2,TIS} + \frac{K_m}{C_O}\right] D_{Z,TIS}\,C_O} \tag{18}$$

As stated before, the high values of K_m predicted by Napper's modeling [Napper, Schubert, 1988] may mask the effects of myoglobin facilitated diffusion. With the assumption of oxygen-myoglobin reaction equilibrium, the equation describing myoglobin reaction, Equation (2), can be solved for Y, myoglobin saturation, providing Equation (19). The non-linear expressions for Michaelis-Menten kinetics, Equation (17), and myoglobin saturation, Equation (19), are very similar.

$$\frac{C_{Mb,TOT}\,C_{O2,TIS}}{\left[C_{O2,TIS} + P_{50}\right]} \tag{19}$$

Figure 7 shows the saturation vs. pO_2 curves of myoglobin and Michaelis-Menten oxygen consumption reactions. The 50% saturation level for each reaction is the substrate level (oxygen) required to cause 50% saturation of myoglobin (P_{50}) and 50% maximal oxygen consumption (K_m). Napper determined through numerical simulations a maximum K_m = 5.0 mmHg [Napper, Schubert, 1988]. Wittenberg [1970] determined a P_{50} = 2.1 mmHg for horse myoglobin at 37 °C. This value corresponds to $k_1 = 2.4 \times 10^{10}$ conc^{-1} s^{-1} and k_2 = 65 s^{-1}. From these values, it should be clear that the "active region" for

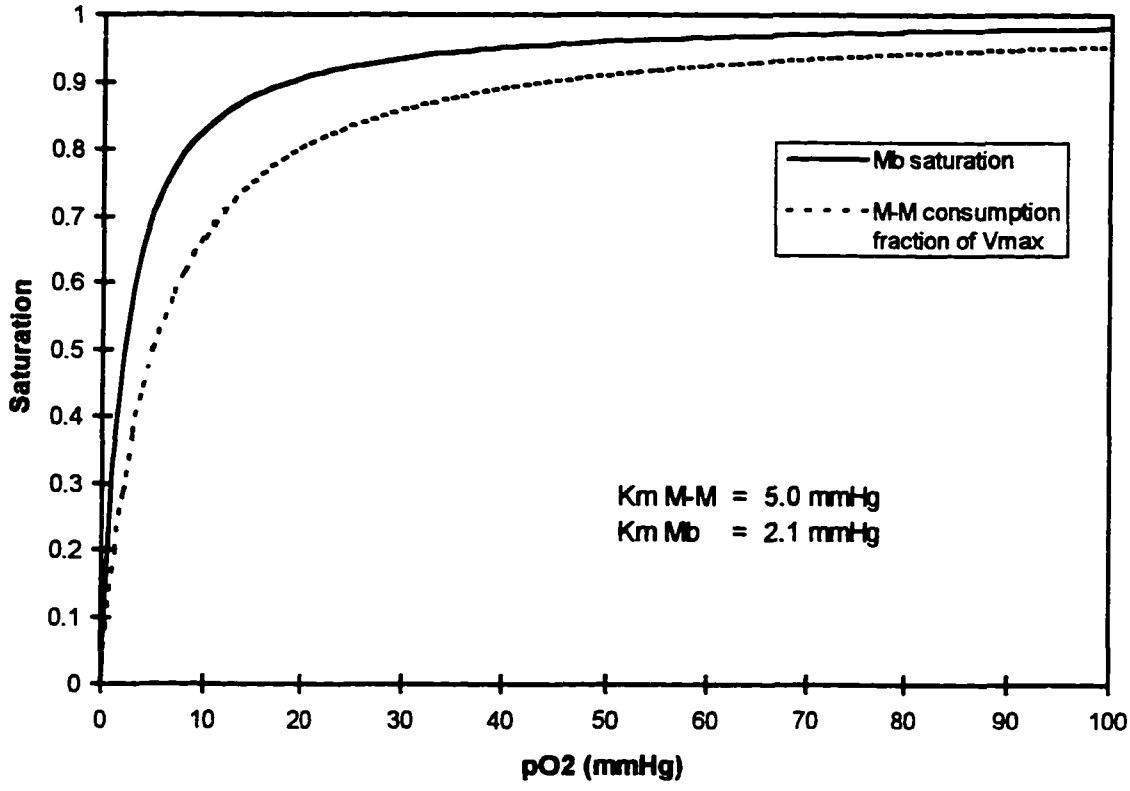

Figure 7 : Saturation curves. Shown are the saturation curves for the myoglobin and Michaelis-Menten consumption reactions. The substrate level (in this case oxygen) corresponding to 50% saturation is K_m. Shown are K_m = 5 mmHg for Michaelis-Menten [Napper, Schubert, 1988] and K_m = 2.1 mmHg (P_{50}) for myoglobin [Wittenberg, 1970].

Michaelis-Menten and myoglobin overlap. Because of this overlap, the relative effects of these phenomena may mask each other when included simultaneously in a tissue model.

3.2 Solution Technique and Optimization

Formulation of the mathematical problem describing the RAAD model yields a stiff, fourth-order, non-linear, ordinary differential equation, boundary-value problem. The non-linear reaction term from myoglobin transport or Michaelis-Menten kinetics makes an analytic solution impossible.

3.2.1 Numerical Methods for Stiff Boundary-value Problems

Standard techniques for solving initial-value problems, such as Runge-Kutta, can often be applied to boundary-value problems by using a "shooting" technique. The boundary-value problem is treated as an initial-value problem by guessing one or more values at one of the boundaries (i.e., the "initial" boundary), and is then solved stepwise from initial condition to final condition. The solution at the "final" boundary is then compared to the actual "final" boundary condition, and the difference is used to adjust the trial boundary variable [Hoffman, 1992]. Unfortunately, the Runge-Kutta algorithm applied with shooting technique is inadequate for stiff non-linear boundary-value problems. Stiff problems are difficult to solve using propagation (initial-value) techniques, such as Runge-Kutta, because the step-size necessary for stability is much smaller than the

step-size required for the desired solution accuracy [Press et al., 1992]. Typically for stiff problems, the eigenvalues (coefficients that characterize a solution) of the problem differ by an order of magnitude or more [Hoffman, 1992; Press et al., 1992]. Normalization is a must when dealing with stiff problems (see Appendix B). Most of the numerical analysis literature concerned with stiff equation sets is dedicated to solving initial-value problems.

Finite differencing, or relaxation, is more applicable to solving stiff non-linear boundary-value problems than shooting methods [Press et al., 1992]. Relaxation methods involve replacing the differential equations with approximating finite-difference equations on a mesh of points that spans the domain of interest. A set of differential equations is reduced to a set of coupled finite-difference, algebraic equations, which can then be solved using a matrix solution technique. One difficulty is the large number of equations that result when a high degree of spatial resolution is needed. For larger systems, mainframe performance and storage is required. Several public domain finite-difference packages are available. A package called PASVA was used to solve the RAAD model in this dissertation.

3.2.2 PASVA Routine

The PASVA finite-difference routine is based upon a numerical technique described by Lentini [Lentini, Pereyra, 1979]. A FORTRAN version of the routine was provided by Dr. John Fletcher (Applied Mathematics, NIH). PASVA is a variable-order, variable-mesh, finite-difference routine, designed specifically for solving stiff, non-linear, ordinary differential, two-point boundary-value problems. The routine uses the Jacobian

matrix of the differential equation set to automatically adjust step-size. Mesh points are allocated based upon local gradients. If there is little change from point-to-point, the routine will use fewer mesh points (larger step-size). If there are large gradients from point-to-point, the routine will use more mesh points (smaller step-size). A user-input tolerance determines the relative error for the solution. PASVA will attempt to meet this tolerance over the solution grid. The routine has built in checks to determine if the grid is converging to a solution that meets the user-input tolerance or diverging. PASVA will retract a diverging integration step and attempt to use a finer step-size. If this fails the user is alerted that the solution did not converge and/or tolerance was not met.

The PASVA routine allows the input of an initial guess matrix to aid solution. For the RAAD model simulations, the analytic solution to the basic RAAD model without myoglobin or Michaelis-Menten was used as an initial guess. The PASVA routine also has the capability of "continuation." The continuation method can be used to "ease" into a difficult (non-linear) portion of a solution. This process involves scaling a portion of the differential equation that is believed to be difficult by a factor, EPSNU. A solution to the ordinary differential equation set is obtained for EPSNU = 0. The value of EPSNU is advanced by one step, DELEPS, which can be input by the user, but the PASVA routine will make adjustments as needed. The solution for a previous step can be input as the initial guess for the next step of EPSNU. EPSNU is advanced by the PASVA routine from 0 to 1. EPSNU factors were included in the myoglobin and Michaelis-Menten terms of the equation set describing the RAAD model.

PASVA was successfully applied to the RAAD model excluding myoglobin, but including Michaelis-Menten kinetics [Napper, Schubert, 1988]. The reaction terms describing myoglobin facilitation and Michaelis-Menten kinetics, Equations (19) and (17), introduce non-linearity and stiffness to the RAAD model.

3.2.3 Optimization of Parameters

In addition to solving the RAAD model, it is desirable to fit the solution to a real tissue pO_2 data set. Parameters within the model are varied in an effort to match the tissue data as closely as possible. The parameter optimization technique used is the downhill simplex strategy of Nelder and Mead [Nicol, Smith, Raggatt, 1985; Press et al., 1992]. This technique requires function evaluations only; no derivatives are needed. The simplex routine used in this study should not be confused with the simplex method of linear programming. Although both methods make use of the geometrical concept of the simplex, Nelder and Mead's simplex technique is not restricted to linear equation sets. In fact, the simplex routine requires no a priori knowledge of the function being minimized.

Optimization techniques for single parameters can utilize bracketing strategies. In bracketing, the minimum of the function is known to be between two points. Optimization of more than one parameter cannot make use of bracketing. The simplex method involves the creation of a geometrical figure, a simplex. A problem involving N number of parameters requires N+1 trial points to begin. The function to be minimized, also called the cost function, is evaluated at the trial points. From this, a simplex is created; in the case of a two-parameter optimization the simplex is a triangle. Based upon the value

of the cost function for each trial point, the simplex is adjusted. The simplex can be reflected away from high error points, expanded, or contracted. Figure 8 shows the possible outcomes for a step of a three-parameter simplex optimization.

3.2.4 Optimization of RAAD Model

Optimized parameters. Parameter optimization is performed on the RAAD model solution to determine the value of the axial diffusion coefficient of oxygen ($D_{Z,TIS}$) and the axial diffusion coefficient of myoglobin (D_{Mb}) which will attain the best match to pO_2 measurements. The diffusion coefficients of oxygen and myoglobin are allowed to vary because of the possibility of elevated values for these coefficients in working cardiac tissue. The simplex optimization for the RAAD model with myoglobin (RAAD+Mb) requires that two parameters be optimized, $D_{Z,TIS}$ and D_{Mb}. The addition of Michaelis-Menten kinetics requires the optimization of six parameters: $D_{Z,TIS}$, D_{Mb}, V_{max}^{HI}, V_{max}^{LO}, K_m^{HI}, and K_m^{LO}, where HI and LO denote high and low perfusion pressure experimental measurement conditions. Although Napper has shown that K_m varies depending on perfusion pressure whereas V_{max} does not, V_{max} is still simplexed because of the unknown effects of adding myoglobin facilitation [Napper, Schubert, 1988]. The data set that is modeled includes data at high and low perfusion pressures. Therefore, to assist the minimization, instead of solving for a global K_m, K_m^{HI} and K_m^{LO} are determined, fitting the high and low perfusion data sets individually, thereby assigning a K_m to each set. Table 1 contains parameters for the low and high perfusion pressure measurements. These values

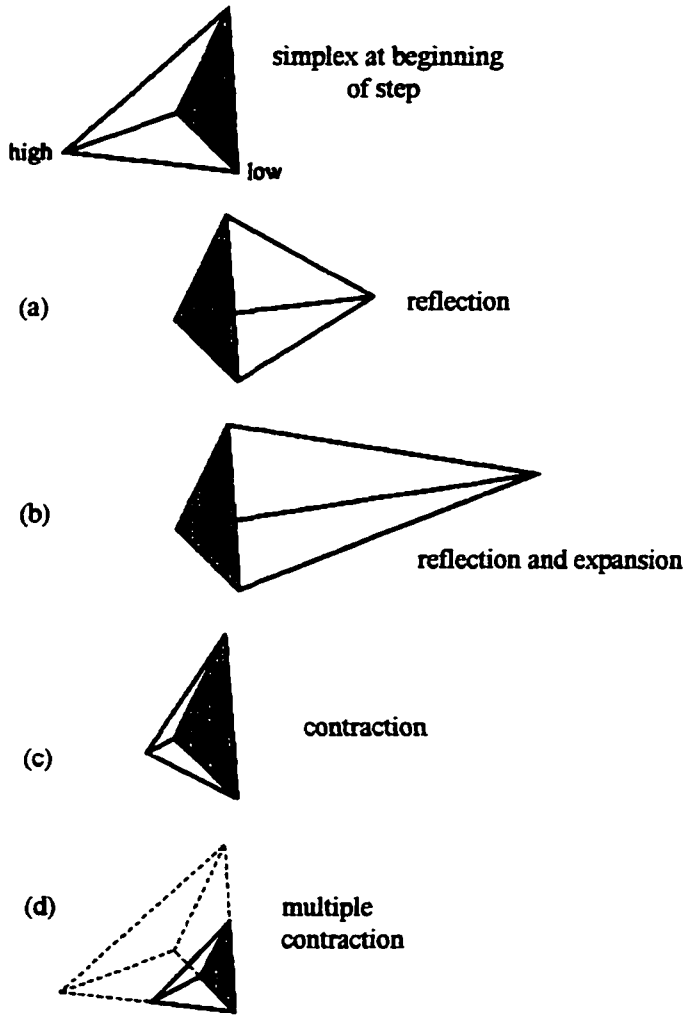

Figure 8: Geometric simplex. Simplex shown is for a three-parameter optimization. The initial simplex is shown, Top. The simplex at the end of a step can be (a) reflected away from high error, (b) reflected and expanded away from high error, (c) contracted away from high error, or (d) contracted along all dimensions towards low error [Press et al., 1992].

Table 1: Model parameter values. Parameter values for low and high perfusion pressures (PP) used in RAAD model simulations (see Appendix D for further description). Only those parameters dependent on perfusion pressure are listed. For a comprehensive list of parameters, see Appendix A.

Parameter	LOW	HIGH	units
PP	79.2	111.1	mmHg
A-V difference	620 ± 4	602 ± 5	mmHg
Consumption, k'''	5.4618×10^{-8}	5.7712×10^{-8}	mol O_2 / s · cm^3
Capillary density, μ_{CAP}	300 000	200 000	capillaries / cm^3
Flow rate	4.03033	4.38595	ml / min
Capillary velocity, v_{CAP}	0.0570	0.0931	cm / s
Capillary permeability, P	7.8546×10^{-2}	6.6037×10^{-2}	cm / s
Krogh tissue radius, r_{TIS}	1.0600×10^{-3}	1.2861×10^{-3}	cm

were used in the simulation in conjunction with the low and high perfusion pressure pO_2 data. The listed perfusion pressures (PP) and arterio-venous (A-V) differences are measurements from Schubert [Schubert, Whalen, Nair, 1978].

The optimized values for $D_{Z,TIS}$ and D_{Mb} along with the histogram error (see below) are used to determine if myoglobin facilitated diffusion accounts for the apparent elevated oxygen diffusion needed to match the experimental pO_2 distribution. If the RAAD+Mb solution provides a better fit to data than the RAAD model, myoglobin facilitation explains some of the requirement of elevated diffusion in the RAAD model. The possibility exists that phenomena elevating oxygen diffusion may also elevate myoglobin diffusion. If this is the case, then D_{Mb} and $D_{Z,TIS}$ would be simultaneously elevated, providing a better fit to the data. The RAAD solution with Michaelis-Menten and myoglobin (RAAD+M-M+Mb) will be compared to the RAAD+M-M model to determine if the combined addition of myoglobin and Michaelis-Menten provides a better data fit than myoglobin or Michaelis-Menten considered individually. Optimized values for diffusion coefficients in the normal range ($D_{Mb} = 2.2 \times 10^{-7}$ and $D_{Z,TIS} = 1.65 \times 10^{-5}$ cm^2/s), as accepted by current literature, reflect that passive diffusion, not enhanced diffusion, occurs in the tissue [Homer, et al., 1984; Baylor, Pape, 1988; Meng, Bentley, Pittman, 1993; Jurgens, Peters, Gros, 1994; Papadopoulos, Jurgens, Gros, 1995]. Elevated values reflect that enhanced diffusion may exist in working heart tissue.

Cost function. Equation (20) depicts the cost function, or error function, for the simplex routine. The simplex routine uses this as an error criterion, changing parameters in the model in an attempt to minimize the value of the cost function.

$$Cost = \omega_1 \cdot HISERR + \omega_2 \cdot HISDIF + \omega_3 \cdot CONSERR \qquad (20)$$

The function is assembled as a combination of factors that describe how well the model fits the experimental data. HISERR and HISDIF provide a measure of how well the model predicts the sampled pO_2 data, whereas CONSERR constrains the simplex to match the isolated heart whole-organ consumption. ω_1, ω_2, and ω_3 are the relative error weights. HISERR represents the error associated with the independent fits of the low and high perfusion histogram data. The first bin (0 to 5 mmHg) was not used in the data fit because it was determined by Schubert that the histogram distribution is insensitive to this value [Schubert, Zhang, 1992]. Only the 5 to 240 mmHg range is considered when fitting the experimental data because of the small sample size associated for tissue pO_2 above these values [Schubert, 1976]. Determining the HISERR for the RAAD model solution involves solving the model with both low and high perfusion pressure parameters (Table 1), and then calculating a sum-of-squares error (SSE) for the model prediction versus the pO_2 data set for that perfusion pressure. SSE represents a goodness-of-fit for the model prediction of the experimental data. The SSE is standardized by an estimate of the variance for each bin, as shown by Equations (21) and (22) for low perfusion [Snedecor, Cochran, 1989].

$$SSE_{LO} = \sum_{bins} \left[\frac{\left(HIST_{DATA,LO} - HIST_{MODEL,LO} \right)^2}{VAR_{LO}} \right] \tag{21}$$

where,

$$VAR_{LO} = \frac{HIST_{DATA,LO} \cdot \left(1 - HIST_{DATA,LO} \right)}{NData_{LO}} \tag{22}$$

$HIST_{DATA,LO}$ and $HIST_{MODEL,LO}$ represent the low perfusion experimental data and model prediction, respectively. NData is the number of experimental pO_2 observations, 894 for low and 898 for high perfusion pressure. The resulting SSE_{LO} and SSE_{HI} are then summed to obtain HISERR [Schubert, 1976].

To ensure that the model predicts both low and high perfusion pressure data equally well, the pO_2 experimental data sets for low and high perfusion are given equal significance with the cost function term HISDIFF, which is the square of the difference between the SSE_{LO} and SSE_{HI}, $(SSE_{LO} - SSE_{HI})^2$. The term CONSERR is used to match the RAAD model's A-V difference (extraction) to the experimentally determined A-V difference (see Appendix D). This term provides consistency between the tissue oxygen consumption in the heart preparation and the predicted consumption of the model. The procedure for simplex optimization follows that of Napper and Schubert [1988]. The relative error weights, ω_1, ω_2, and ω_3, were 1.0 for the RAAD model simulations. This weighting led to satisfactory values for A-V difference and maintained equal weighting of the high and low perfusion histogram errors.

Simplex procedure. The simplex routine used to optimize the model parameters required good initial values to converge to the absolute minimum of the cost function. Many trial points consisting of various combinations of model parameters were necessary to rule out local minima. If the simplex was started considerably far from the minimum, convergence was not guaranteed. Good initial guesses were determined by trying a broad range of parameter values, particularly for the diffusion coefficients of myoglobin and oxygen. The process of finding a global minimum became a combination of trial-and-error and simplex optimization. This process involved providing the simplex with a trial point, letting the simplex routine converge, and then using the solution as a starting point for the next simplex trial. The set of parameters resulting in the lowest cost function was considered to be the global minimum.

CHAPTER 4

RESULTS

The RAAD model was successfully solved numerically using the PASVA finite-difference routine. Double precision was used for all calculations. To ensure convergence, the error tolerance of the routine was decreased until there was no significant change in solution. A tolerance of 10^{-5} was used for all simulations. This tolerance has been shown to produce pO_2 values within 10^{-5} relative error of the analytical solution for the RAAD model with no myoglobin or Michaelis-Menten kinetics [Napper, 1985]. Computation time for the simulations varied from 10 to 60 minutes on an IBM VM mainframe, depending primarily on the goodness of simplex trial points and the number of parameters optimized. The various RAAD solutions required 115 to 458 nodes to solve. A program listing is available from the Biomedical Engineering Department at Louisiana Tech University.

4.1 Axial Profiles

Figure 9 shows the pO_2 axial profiles and myoglobin saturation predicted by the RAAD+Mb model at low perfusion pressure. Only the low perfusion pressure plot is shown because the plots for high and low perfusion are indistinguishable when plotted on the same axis. The axial profiles of oxygen consumption for the RAAD model tissue

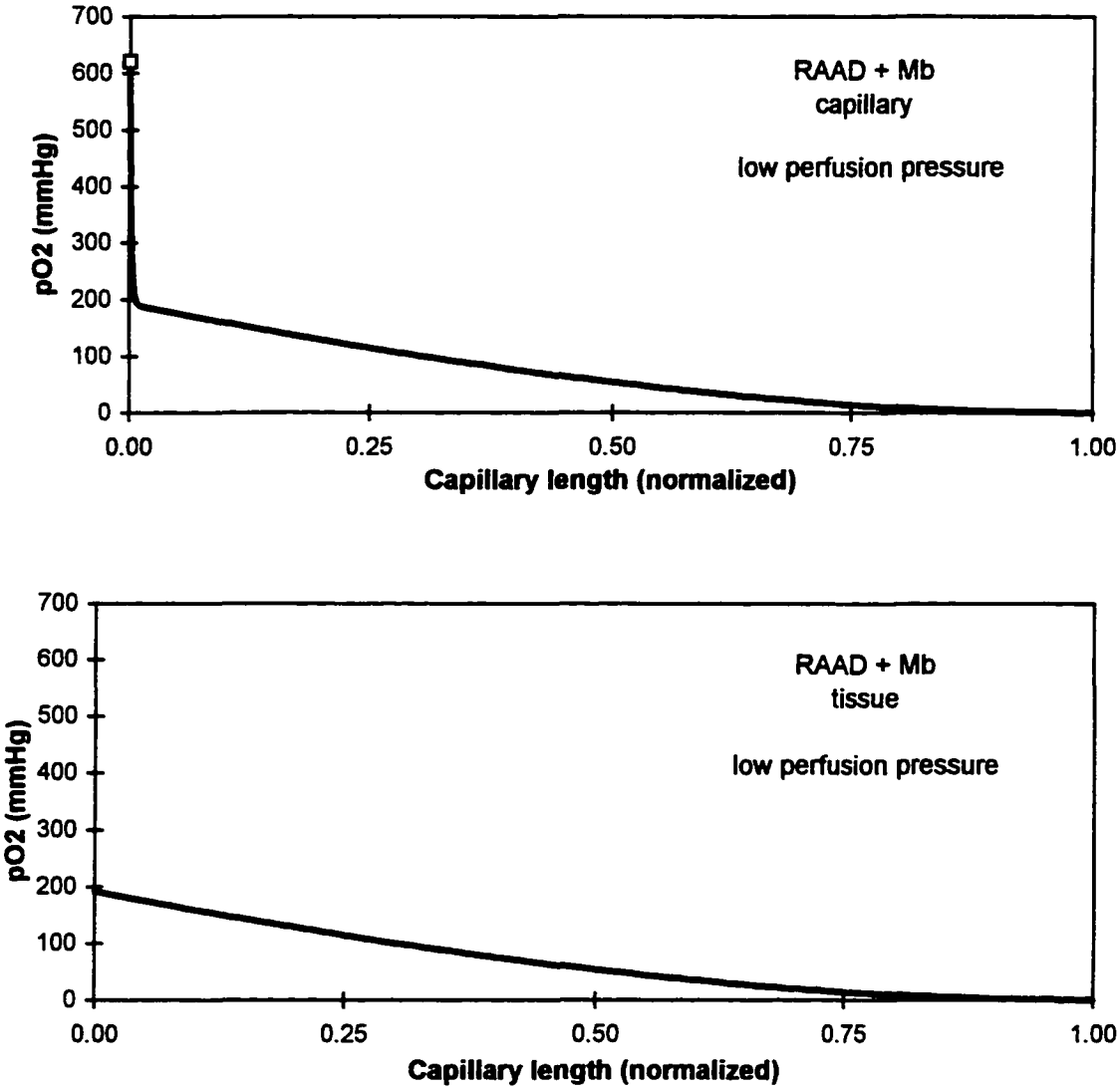

Figure 9: Axial pO_2 profiles. Top: axial profile of capillary pO_2, data point marks entrance pO_2 = 620.3 mmHg, and Bottom: axial profile of tissue pO_2 for the RAAD+Mb model at low perfusion pressure.

region with and without Michaelis-Menten (M-M) kinetics are plotted (Figure 10). Saturation profiles predicted by the RAAD+Mb+M-M model for myoglobin and Michaelis-Menten consumption are displayed in Figure 11. Michaelis-Menten saturation was calculated as a fraction of V_{max}, that is $M\text{-}M_{sat}$ = consumption / V_{max}.

4.2 Optimized Solution and Parameters

Simplex parameter optimizations were performed on the RAAD, RAAD+Mb, RAAD+M-M, and RAAD+Mb+M-M models. Starting points for the simplex were calculated by the simplex routine which modified, by ± 30%, a user-supplied trial set of parameters to be optimized. Once the simplex reached a minimum, the solution was then introduced as a starting point and simplex was restarted to ensure that the solution was not merely a local minimum [Zitko, 1986].

The optimized histogram fit for the RAAD+M-M model and experimental pO_2 data are plotted for low and high perfusion pressures in Figure 12. Histogram error, HISERR + HISDIF, is reported rather than the value of the cost function because the cost function is determined by the histogram error and another term, CONSERR, that is not representative of histogram fit (see Section 3.2.4). Cost function relative error weights (ω_1, ω_2, and ω_3,) of 1.0 were used in all simulations. Table 2 contains the simplex parameter optimization results for the RAAD+M-M model along with the modeling results of Napper's Michaelis-Menten model [Napper, Schubert, 1988]. Table 3 summarizes the simplex parameter optimization results for each of the RAAD model

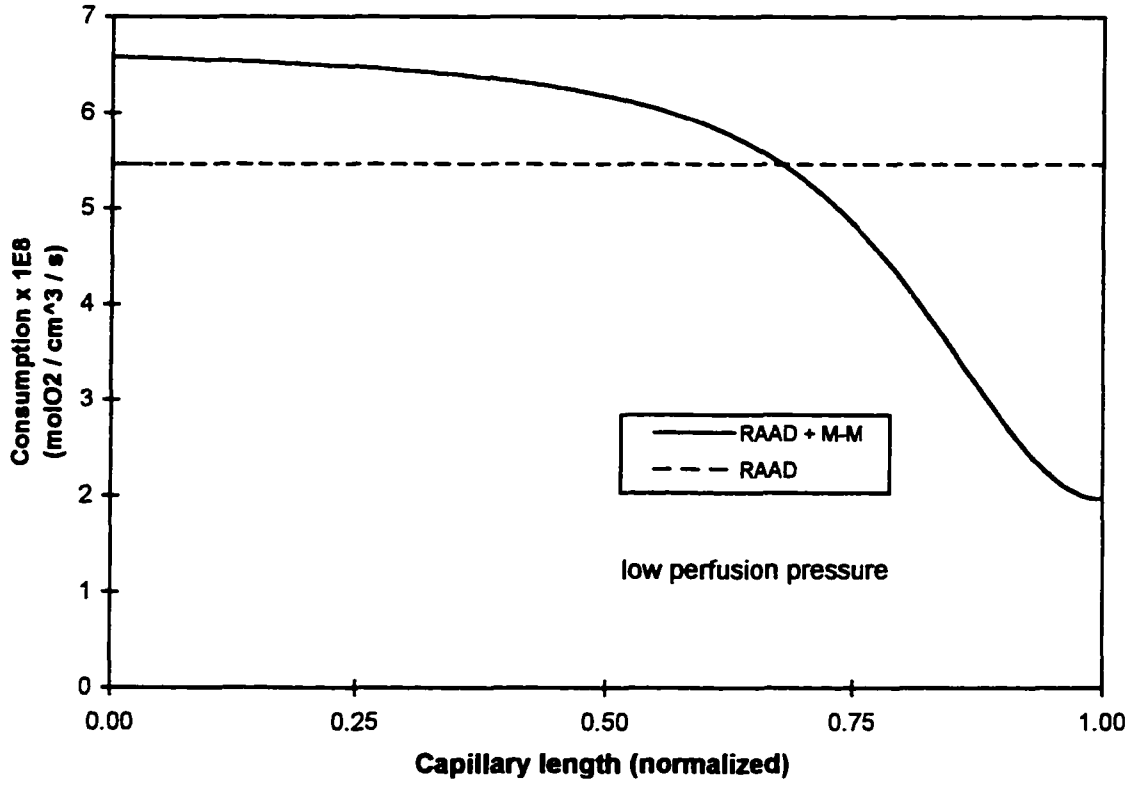

Figure 10: Axial profile of oxygen consumption. Profile of oxygen consumption for the RAAD and RAAD+M-M models at low perfusion pressure showing the pO_2 dependence of consumption for the RAAD model with Michaelis-Menten. The zero-order consumption of the RAAD model without M-M does not vary with pO_2.

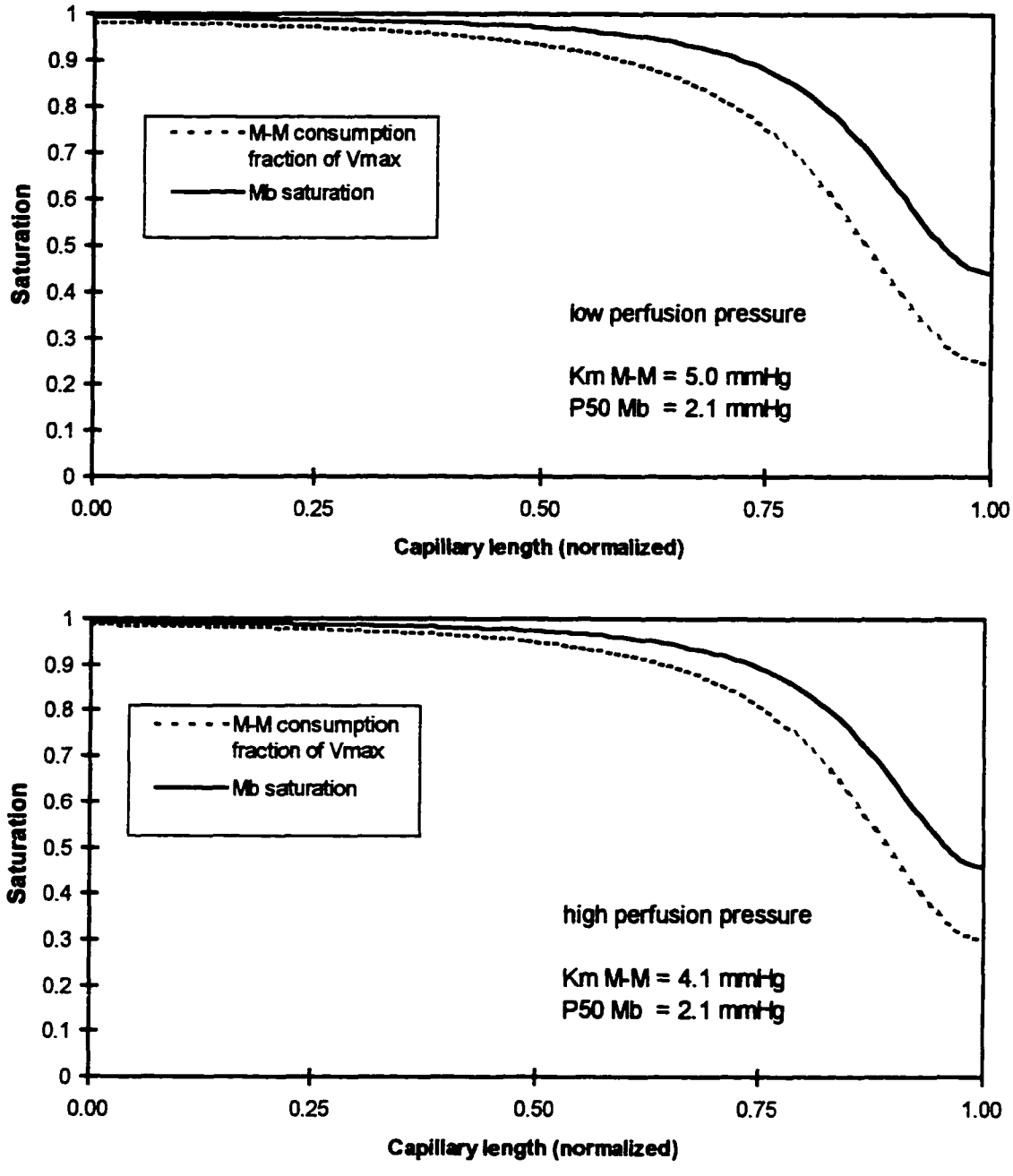

Figure 11: Saturation profiles of reactions. Saturation profiles of myoglobin and Michaelis-Menten consumption reactions in the RAAD+M-M+Mb model at high and low perfusion pressure. Mb remains above its P_{50} until the last 5% of the capillary, whereas M-M consumption is below 50% saturation the last 15% of the capillary length. Myoglobin saturation never drops below 44% for low and 46% for high perfusion pressures.

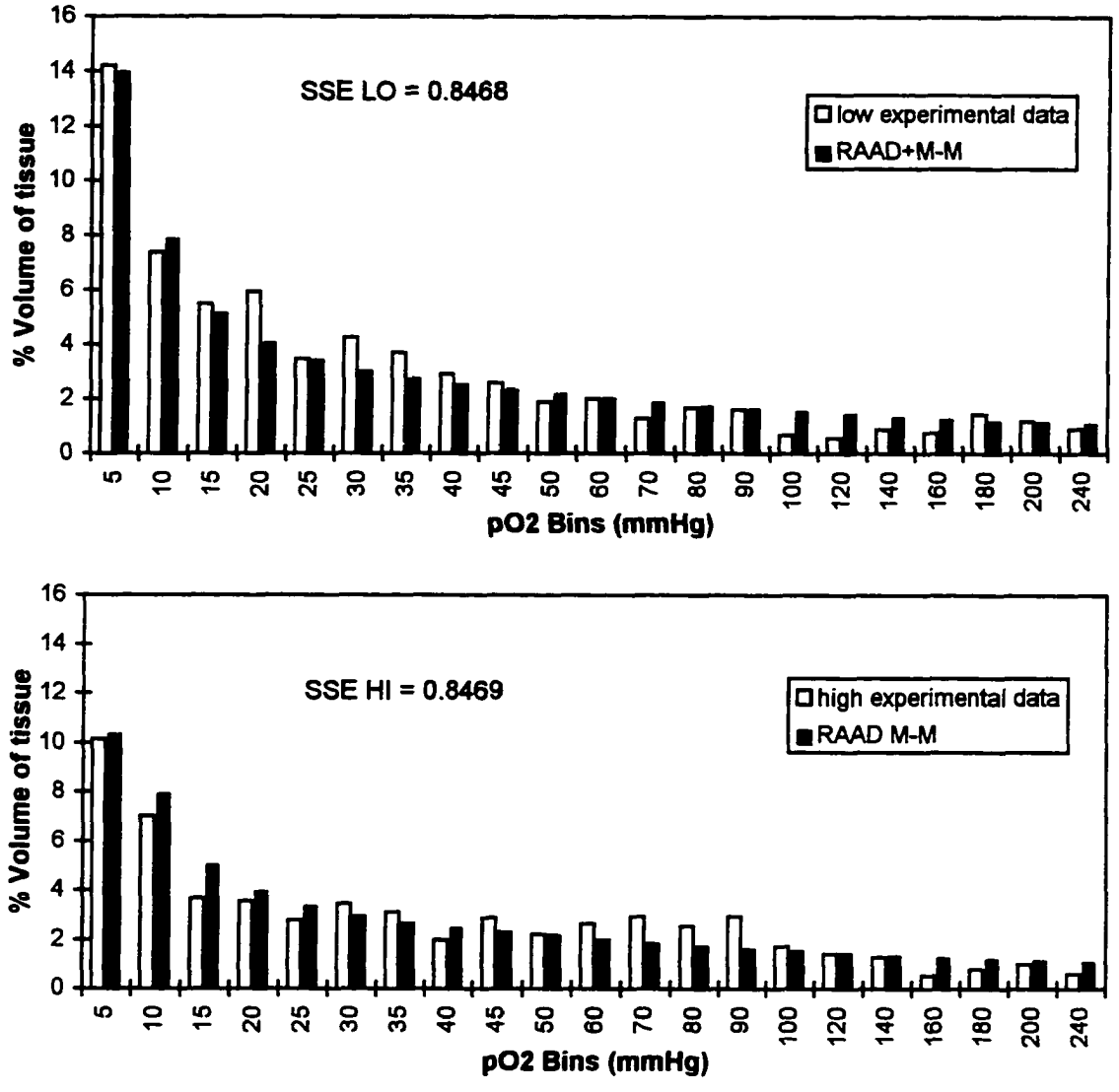

Figure 12: Model predicted histograms. Optimized pO_2 histogram fits for the RAAD + M-M solution, low and high perfusion pressures. The model successfully predicts the experimental pO_2 distributions, at both low (SSE_{LO} = 0.8468 x 10^4) and high perfusion pressure (SSE_{HI} = 0.8469 x 10^4), with SSE_{TOT} = 1.694 x 10^4. Results agree with prior simulations by Napper [Napper, Schubert, 1988].

Table 2: Comparison to prior modeling. RAAD + M-M simplex results are compared to Napper's simulations [Napper, 1985; Napper, Schubert, 1988]. Both models have similar histogram errors and optimized parameter values.

	NAPPER M-M MODEL		RAAD + M-M MODEL	
Perfusion pressure	LOW	HIGH	LOW	HIGH
model A-V difference (mmHg)	617.0	602.7	618.6	602.2
experimental A-V difference	620 ± 4	602 ± 5	620 ± 4	602 ± 5
K_m (mmHg)	4.99	3.97	4.98	3.97
$D_{Z,TIS}^*$ (times normal)	8.03		8.17	
$V_{max} \times 10^8$ (mol / cm^3·s)	6.75	6.72	6.72	6.72
Histogram error x 10^4	1.71		1.69	

* $D_{Z,TIS}$ (normal) = 1.65 x 10^{-5} cm^2 / s

Table 3: Simplex results. RAAD model simplex parameter optimization results are shown for each of the models simulated. The best fit to experimental data was given by the RAAD + M-M model, SSE = 1.694×10^4.

	MODEL							
	RAAD		RAAD + Mb		RAAD + M-M		RAAD + M-M + Mb	
Perfusion pressure	LOW	HIGH	LOW	HIGH	LOW	HIGH	LOW	HIGH
A-V difference (mmHg)	620.0	602.0	620.1	603.2	618.6	602.2	622.4	605.2
$D_{Z,TIS}$* (times normal)	12.63		12.80		8.17		8.29	
D_{Mb}** (times normal)	–		$1x10^{-7}$		–		$1x10^{-6}$	
K_m (mmHg)	–	–	–	–	4.98	3.97	5.00	3.99
$V_{max} \times 10^8$ (mol / s · cm^3)	–	–	–	–	6.72	6.72	6.72	6.71
Histogram error x 10^4	2.3938		2.4107		1.6938		1.7569	

* $D_{Z,TIS}$ (normal) = 1.65×10^{-5} cm^2 / s

** D_{Mb} (normal) = 2.2×10^{-7} cm^2/s

simulations. These parameter values represent the simplex that gave rise to the global minimum cost function and conformed to the mathematically imposed experimental constraints [Napper, 1985].

Relative differences between the various models are most visible in a plot of bin-by-bin comparison. Deviations between models are determined by calculating the difference bin-by-bin between the model predicted histograms for both low and high perfusion pressure. Deviations of the optimized RAAD+M-M model from the RAAD model are shown in Figure 13. Bin values represent deviations from the basic RAAD model because of inclusion of Michaelis-Menten kinetics. Changes to the RAAD+M-M solution after the addition of myoglobin are shown in Figure 14. Figure 15 shows a plot of the deviations of the optimized RAAD+Mb model relative to the RAAD model without myoglobin or Michaelis-Menten kinetics.

Additional simulations were performed holding the diffusion coefficient of myoglobin fixed, yet allowing the remaining parameters, including the diffusion coefficient of oxygen, to optimize. In this manner, D_{Mb} can be set to any desired value, and the effects on the pO_2 distribution can be observed without interference from the simplex routine attempting to determine an optimal D_{Mb}. Figures 16, 17, and 18 show how increasing the magnitude of D_{Mb} affects the pO_2 distribution predicted by the RAAD+Mb model for 1, 5, and 10 times D_{Mb}, respectively. The histograms plotted for the fixed myoglobin diffusivity simulations do not represent fully optimized solutions because the diffusion coefficient of myoglobin was not optimized to fit the experimental pO_2 data.

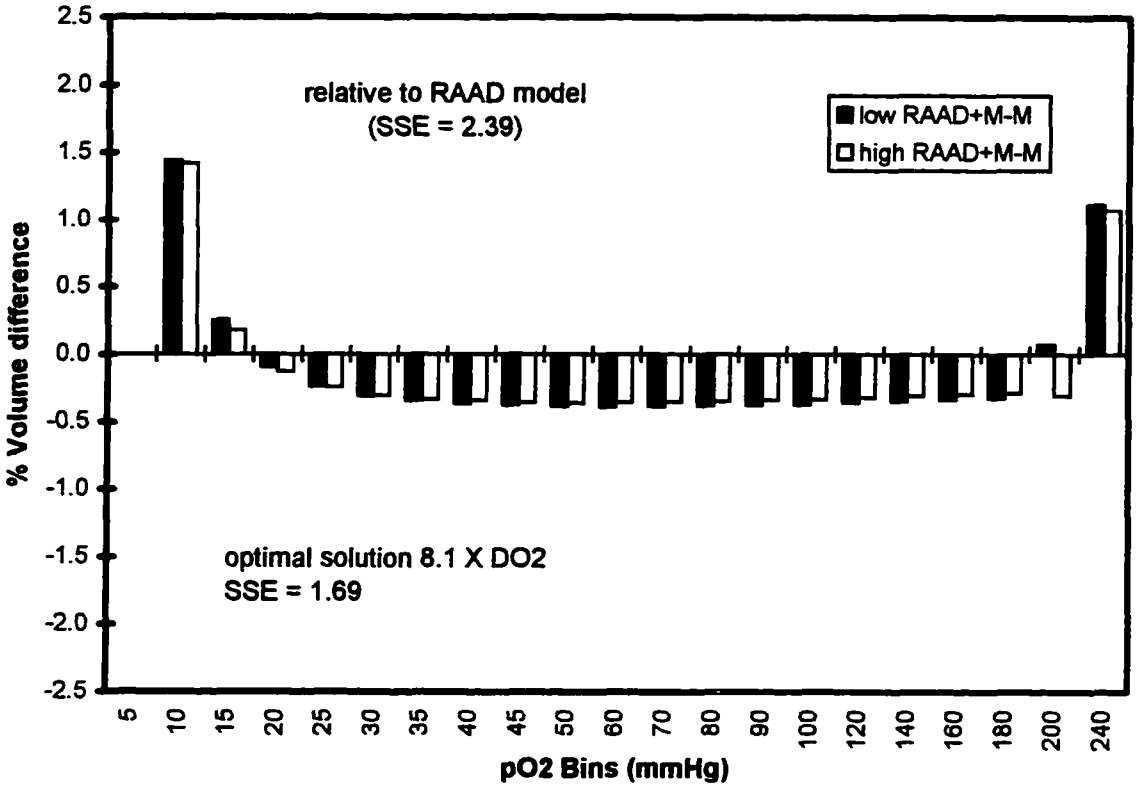

Figure 13: Relative histogram differences (RAAD+M-M vs. RAAD). Optimized solution of RAAD+M-M model as compared to the RAAD model for low and high perfusion pressures. Results plotted as the deviation bin-by-bin from the RAAD model with no M-M or Mb. Deviations represent changes to the RAAD model caused by the addition of M-M kinetics. The RAAD model has an SSE = 2.39×10^4. The RAAD + M-M model has an optimal solution of 8.1 times D_{O2} with an SSE = 1.69×10^4, providing a better fit to the experimental data than the RAAD model.

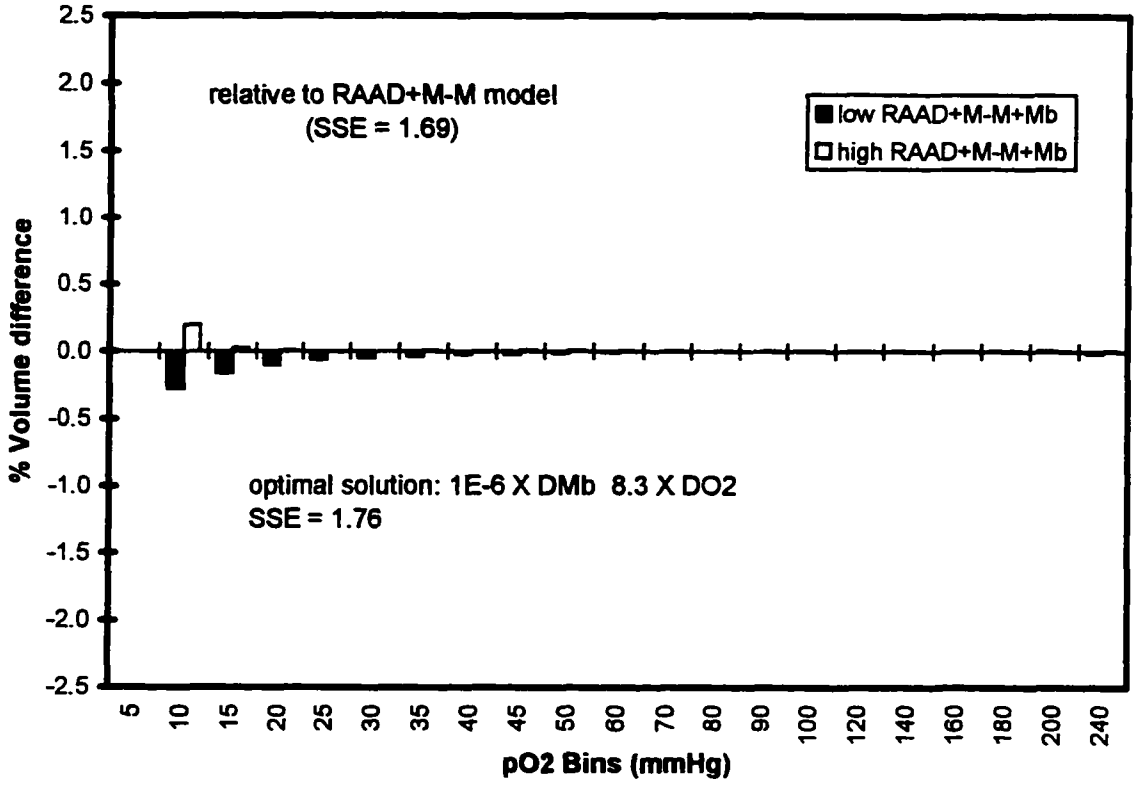

Figure 14: Relative histogram differences (RAAD+M-M+Mb vs. RAAD+M-M). Optimized solution of RAAD+M-M+Mb model as compared to the RAAD+M-M model for low and high perfusion pressures. Results plotted as the deviation bin-by-bin from the RAAD+M-M model with no Mb. Deviations represent changes to the RAAD+M-M model caused by the addition of Mb. The RAAD+M-M+Mb model has an optimal solution of 8.3 times D_{O2} with an SSE = 1.76×10^4. This data fit is no improvement over the RAAD+M-M model, SSE = 1.69×10^4. Simplex optimized D_{Mb} is near zero.

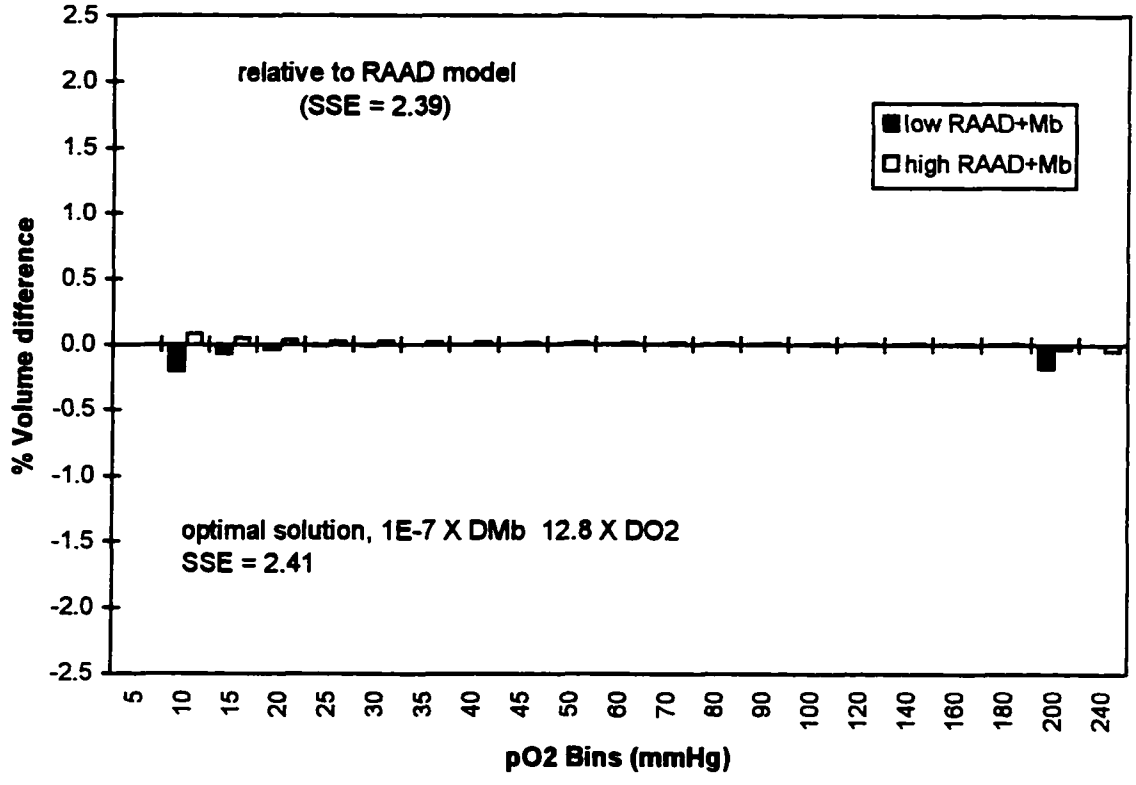

Figure 15: Relative histogram differences (RAAD+Mb vs. RAAD). Optimized solution of RAAD+Mb model as compared to the RAAD model for low and high perfusion pressures. Results plotted as the deviation bin-by-bin from the RAAD model with no Mb. Deviations represent changes to the RAAD model caused by the addition of Mb. The RAAD+Mb model has an optimal solution of 12.8 times D_{O2} with an SSE = 2.41 x 10^4. This data fit shows no improvement over the RAAD model, SSE = 2.39 x 10^4. Simplex optimized D_{Mb} is 1 x 10^{-7} times normal (≈ 0).

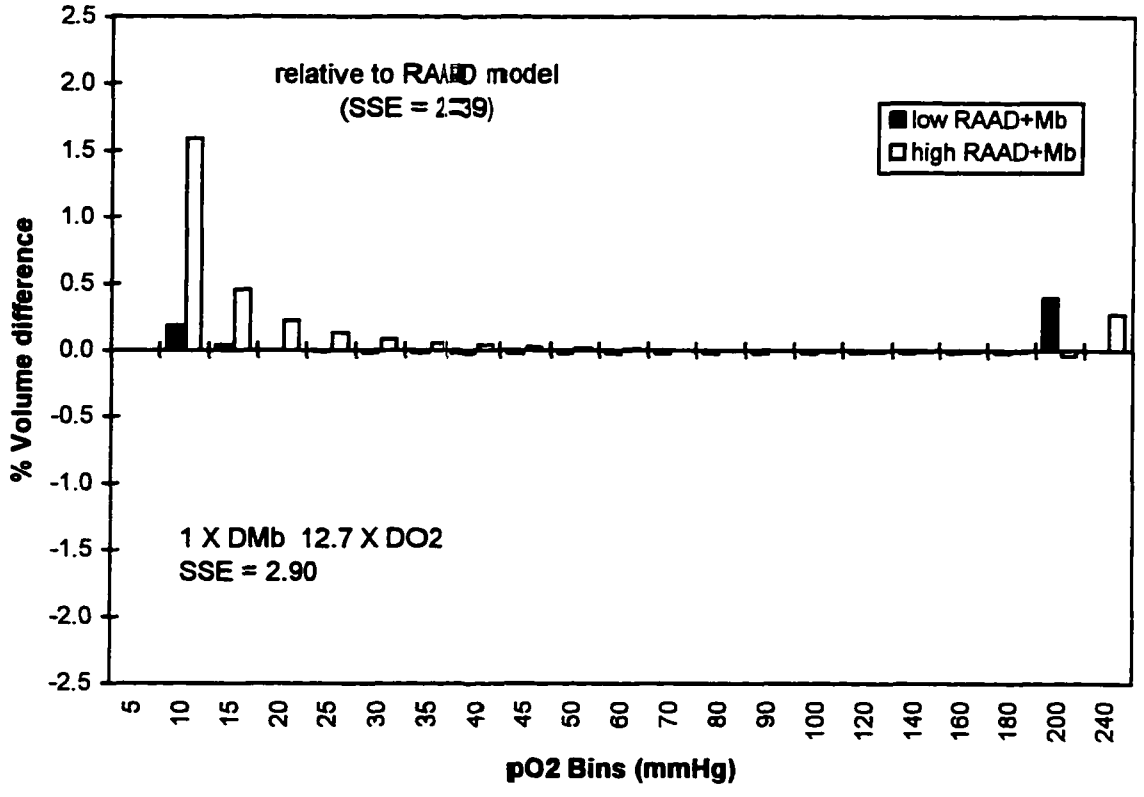

Figure 16: Relative histogram differences, 1 X D_{Mb} (RAAD+Mb vs. RAAD). Deviations of the RAAD+Mb model predicted histogram from that of the RAAD model. Diffusivity of myoglobin fixed at 1X normal. SSE shows no improvement over the fully optimized solution in Figure 15, SSE = 2.41 x 10^4. Myoglobin is shown to act primarily in the low pO_2 range.

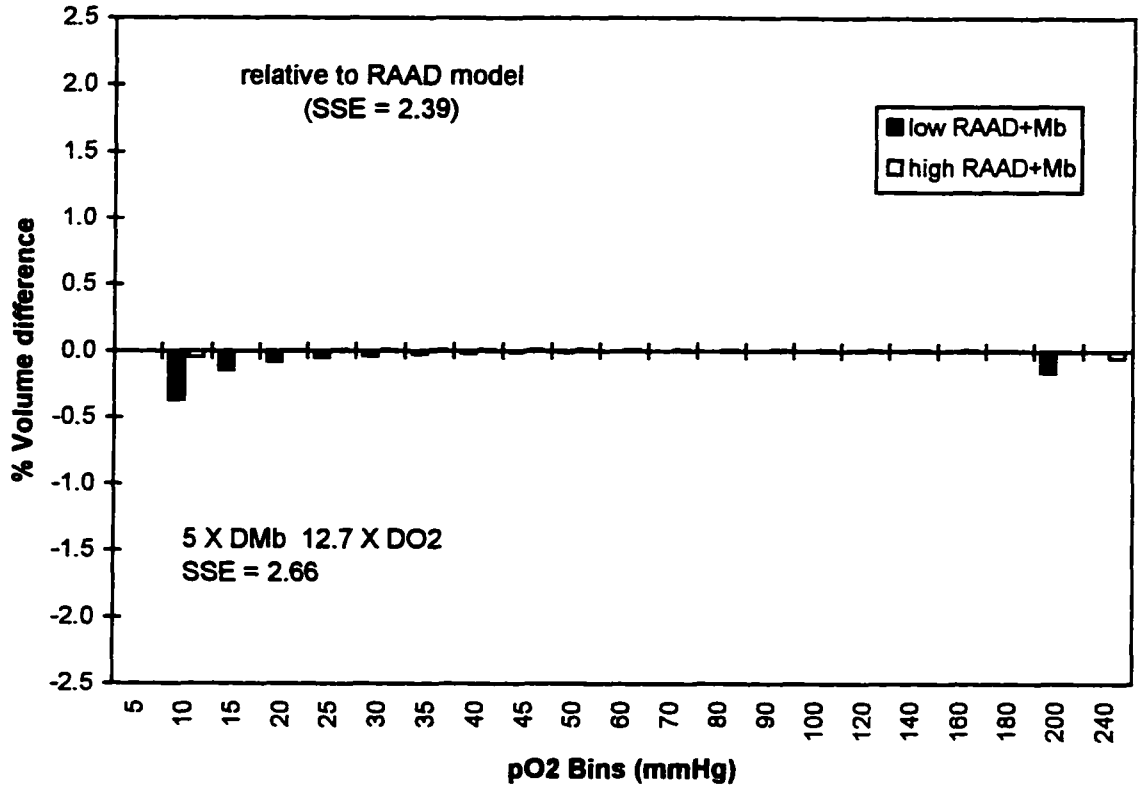

Figure 17: Relative histogram differences, 5 X D_{Mb} (RAAD+Mb vs. RAAD). Deviations of the RAAD+Mb model predicted histogram from that of the RAAD model. Diffusivity of myoglobin fixed at 5X normal. SSE (2.66×10^4) is improved when compared to the 1X D_{Mb} (2.90×10^4). SSE shows no improvement over the fully optimized solution in Figure 15, SSE = 2.41×10^4. Myoglobin is shown to have little effect on the model at 5X normal D_{Mb}. Further increases of D_{Mb} do not lead to improved SSE versus the fully optimized RAAD+Mb model (optimal $D_{Mb} \approx 0$).

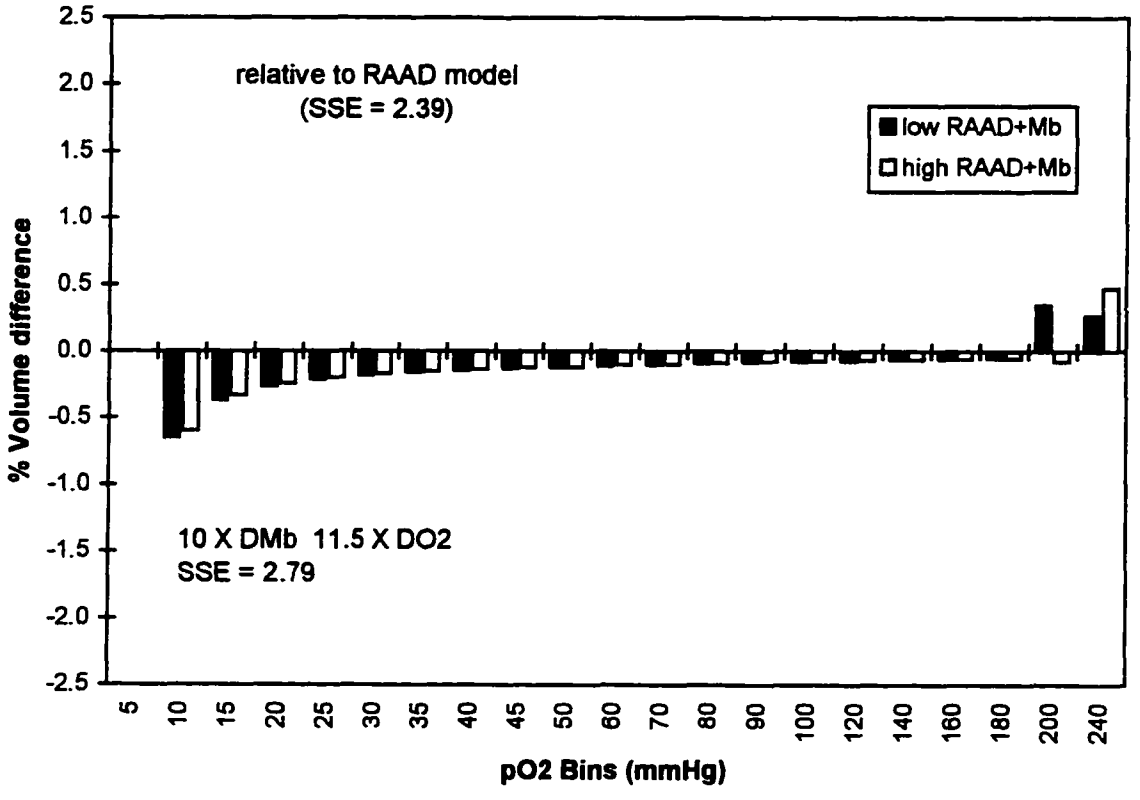

Figure 18: Relative histogram differences, 10 X D_{Mb} (RAAD+Mb vs. RAAD). Deviations of the RAAD+Mb model predicted histogram from that of the RAAD model. Diffusivity of myoglobin fixed at 10X normal. The higher SSE (2.79×10^4) states that the 10X normal solution does not fit the experimental data as well as the 5X D_{Mb} solution (2.66×10^4). Further increases of D_{Mb} do not lead to improved SSE versus the fully optimized RAAD+Mb model, 2.41×10^4.

Similar fixed D_{Mb} plots for the RAAD+M-M+Mb model are shown in Figures 19, 20, and 21 for D_{Mb} of 1, 5, and 30 times normal. Results for the fixed myoglobin diffusivity trials are summarized in Table 4. Figure 22 shows the relative contribution of myoglobin to total oxygen flux for the models with myoglobin.

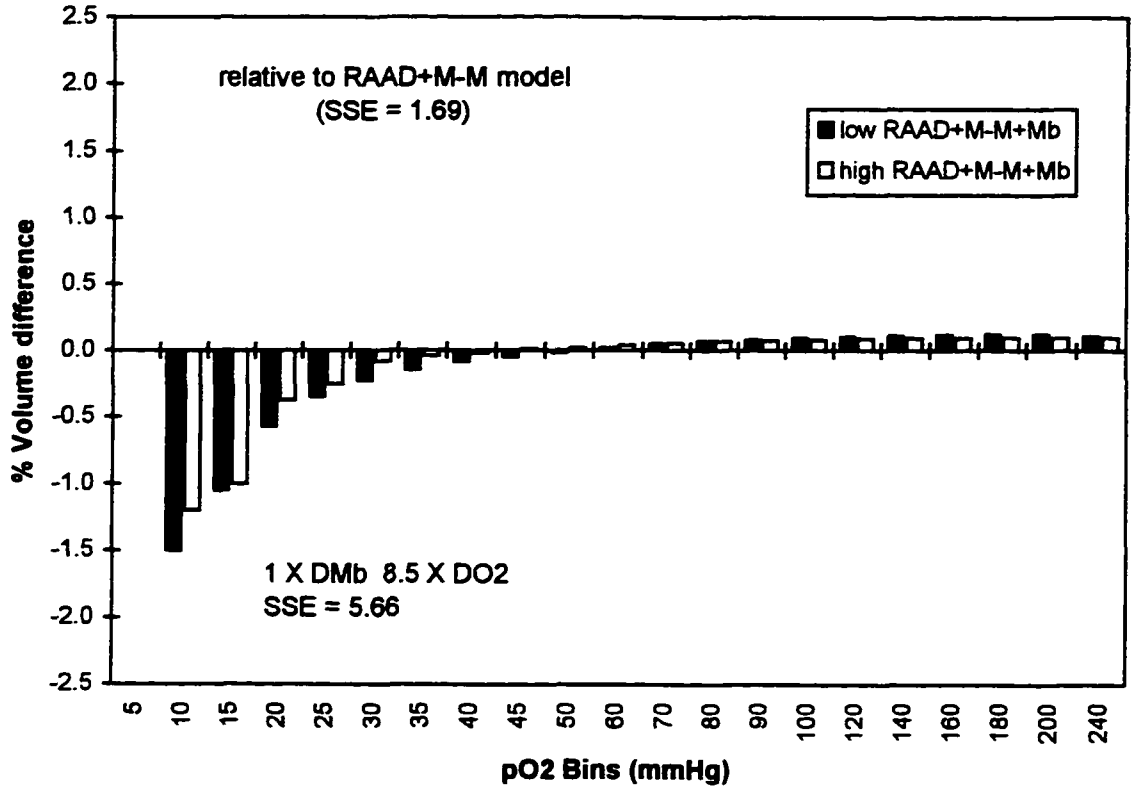

Figure 19: Relative histogram differences, 1 X D_{Mb} (RAAD+M-M+Mb vs. RAAD+M-M). Deviations of the RAAD+M-M+Mb model predicted histogram from that of the RAAD+M-M model. Diffusivity of myoglobin fixed at 1X normal. SSE (5.66×10^4) shows no improvement over the fully optimized solution in Figure 14, (1.76×10^4). As expected myoglobin acts primarily in the low pO_2 range.

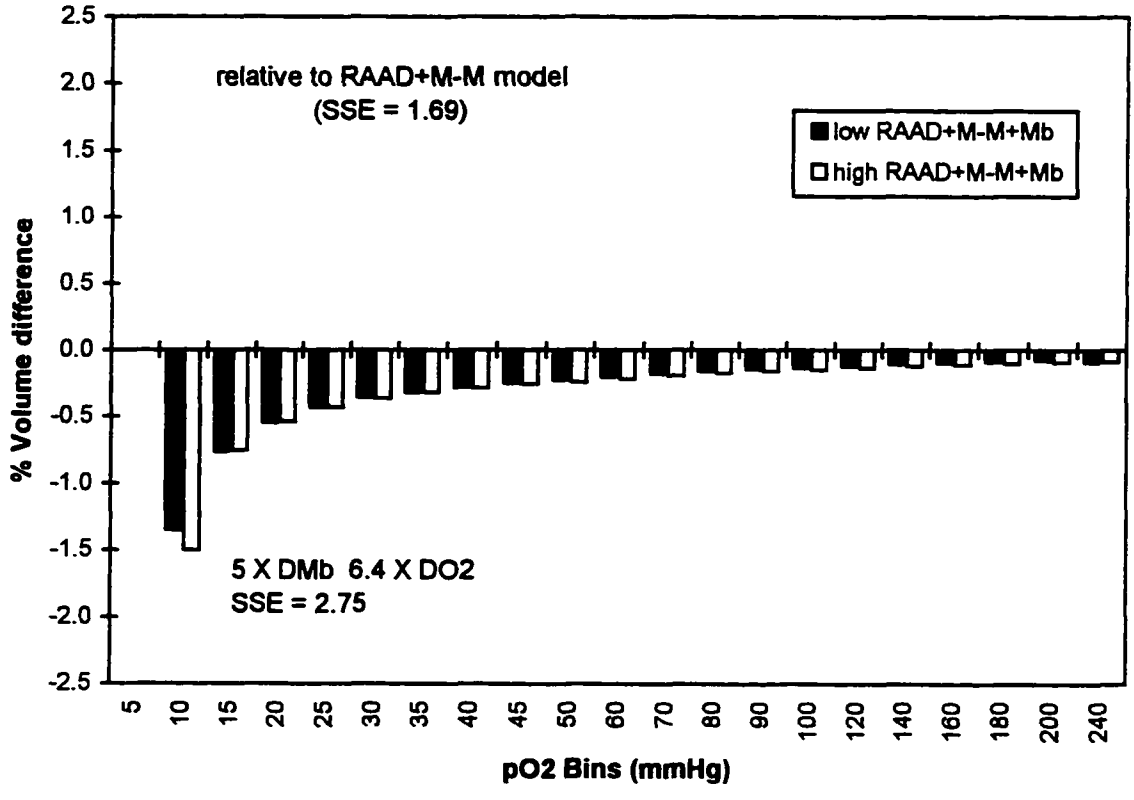

Figure 20: Relative histogram differences, 5 X D_{Mb} (RAAD+M-M+Mb vs. RAAD+M-M). Deviations of the RAAD+M-M+Mb model predicted histogram from that of the RAAD+M-M model. Diffusivity of myoglobin fixed at 5X normal. SSE is reduced (2.75×10^4) relative to the 1X D_{Mb} RAAD+M-M-Mb model (5.66×10^4), but shows no improvement over the fully optimized RAAD+M-M+Mb solution in Figure 14, (1.76×10^4). Further increases in D_{Mb} do not lead to SSE below that found by the simplex optimization of the RAAD+M-M+Mb solution, $D_{Mb} \approx 0$.

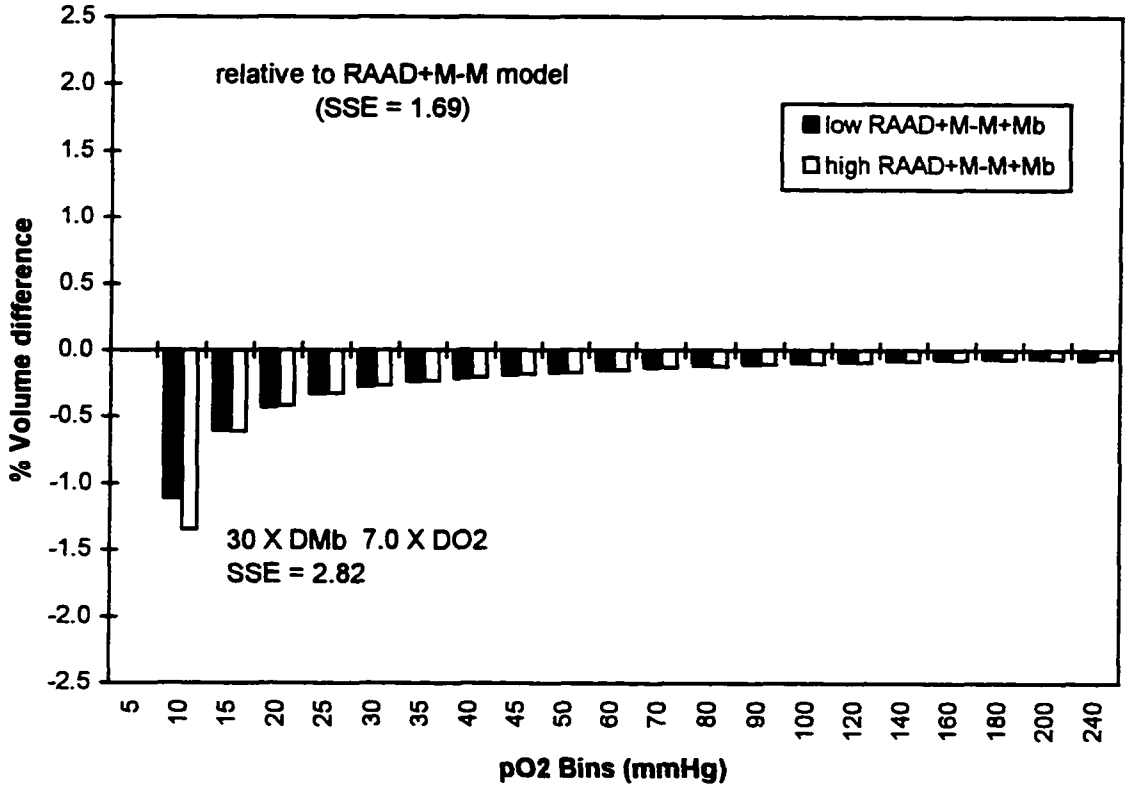

Figure 21: Relative histogram differences, 30 X D_{Mb} (RAAD+M-M+Mb vs. RAAD+M-M). Deviations of the RAAD+M-M+Mb model predicted histogram from that of the RAAD+M-M model. Diffusivity of myoglobin fixed at 30X normal. SSE is elevated (2.82×10^4) relative to the 1X and 5X D_{Mb} trials. Elevating D_{Mb} further leads to increased SSE.

Table 4: Simplex results for fixed values of the myoglobin diffusion coefficient. In these simulations, the diffusion coefficient of myoglobin (D_{Mb}) is fixed while the diffusion coefficient of oxygen ($D_{Z,TIS}$) is optimized by simplex. The error determined by simplex for the fully optimized models is not improved by fixing D_{Mb}. The solutions of both the RAAD+Mb and RAAD+M-M+Mb models have minimal SSE when D_{Mb} is near zero.

Fixed Mb Simulations (histogram error x 10^{-4})				
model	RAAD + 1x Mb**	RAAD + 5x Mb	RAAD + 10x Mb	RAAD + 20x Mb
SSE x 10^4	2.90	2.66	2.71	3.29
optimal $D_{Z,TIS}$* x normal	12.75	12.71	11.52	10.47
model	RAAD+M-M +1x Mb**	RAAD+M-M +5x Mb	RAAD+M-M +20x Mb	RAAD+M-M +30x Mb
SSE x 10^4	5.66	2.75	2.22	2.82
optimal $D_{Z,TIS}$* x normal	8.53	6.39	7.01	7.03

* $D_{Z,TIS}$ (normal) = 1.65 x 10^{-5} cm^2 / s ** 1x Mb means D_{Mb} = 2.2 x 10^{-7} cm^2 / s

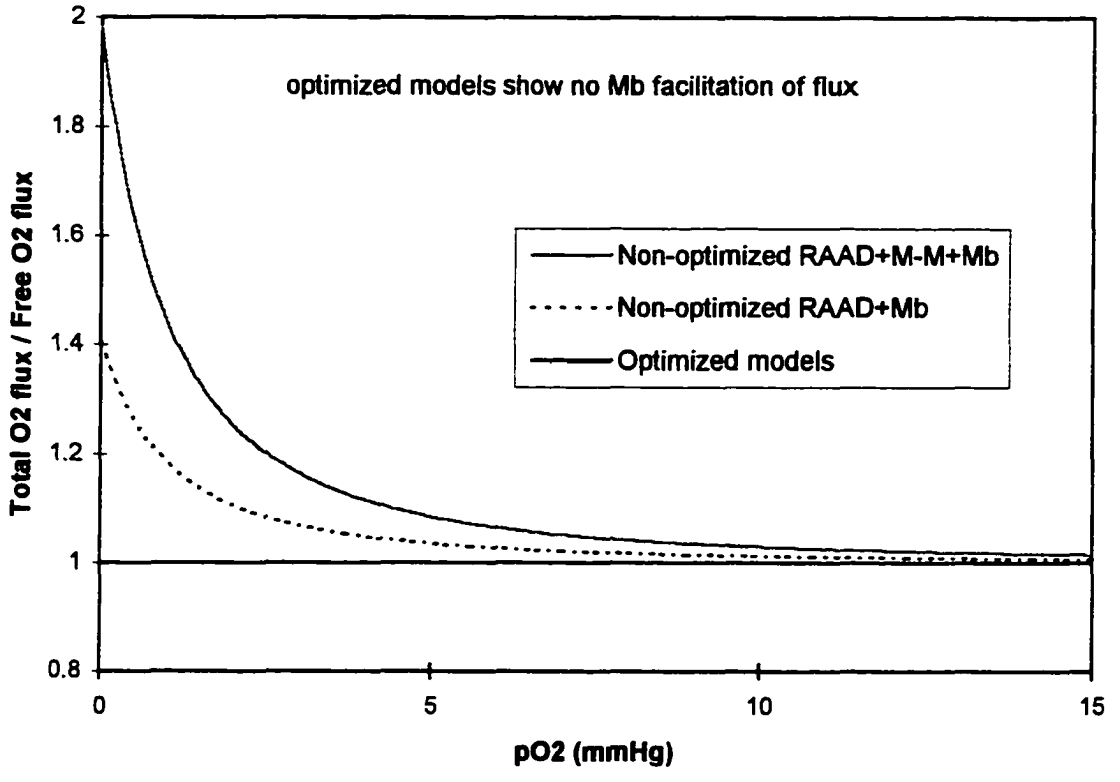

Figure 22: Plot of relative oxygen flux. For this plot the oxygen-myoglobin reaction is assumed at equilibrium. Total oxygen flux includes oxygen diffusion and myoglobin facilitation of oxygen diffusion. Free oxygen flux includes only oxygen diffusion and no myoglobin facilitation. A value of 1.0 for the ratio of total to free oxygen flux means that myoglobin contributes nothing to overall transport of oxygen [see Baylor and Pape, 1988]. Plots for the non-optimized solution show a maximum myoglobin facilitation of 98% and 41% at the lethal end of the tissue for the RAAD+Mb and RAAD+M-M+Mb models, respectively. Yet, plots of the optimized solutions show that myoglobin does not facilitate oxygen diffusion for either model (plots overlap).

CHAPTER 5

DISCUSSION

The RAAD model solutions were stiff at the inlet region of the capillary. This property is exhibited by the fact that about half (48% for RAAD, 40% for RAAD+Mb) of the total nodes in the solution occur in the first 10% of the capillary length. This result is not entirely surprising since others have observed ringing of the capillary solution [Fletcher, Schubert, 1987]. Noticeable features of the capillary and tissue profiles include the following:

1. little concentration gradient between the capillary and the tissue after z = 0.015 or 7.5 μm (Figure 9),
2. steep initial decline of pO_2 in the capillary (Figure 9, top),
3. capillary exit pO_2 near zero (Figure 9, top),
4. pO_2 dependence of O_2 consumption (Figure 10), and
5. high Mb saturation in the tissue (Figure 11).

The first three characteristics reflect that the modeled data were taken from an organ perfused with a hemoglobin-free linear perfusate, not blood, which was equilibrated with 95% oxygen and 5% carbon dioxide. The capillary pO_2 profile would look much different had the model included hemoglobin; in particular, the steep capillary gradients would be reduced. At the capillary inlet, the steep gradients for oxygen transport (>200 mmHg) cause a large amount of

oxygen to be drawn out of the capillary. The pO_2 gradient at a capillary position of 0.015, which corresponds to 7.5 μm past the inlet, is reduced to less than 1 mmHg. These effects are also attributed to the elevated axial transport in the tissue region. The addition of Michaelis-Menten kinetics on the RAAD model leads to a distinct pO_2 dependence for oxygen consumption rate (Figure 10). This rate should not be confused with whole-organ consumption. Tissue myoglobin saturation profiles (Figure 11) show that myoglobin exists near complete saturation with oxygen for about 95% of the capillary length. Myoglobin remains saturated because much of the tissue is at a pO_2 above the P_{50} of Mb, which is the oxygen partial pressure required for 50% saturation of myoglobin (2.07 mmHg) [Wittenberg, 1970; Wittenberg, Wittenberg, 1989]. Saturation never drops below 44% for low perfusion pressure and 46% for high. Saturation profiles for Michaelis-Menten kinetics show that oxygen consumption is near maximum for about 80% of the tissue region (Figure 11). Only in the last 15% of the tissue region does the pO_2 fall below the Michaelis-Menten kinetic constant, K_m. The relative values of P_{50} and K_m (4 to 5, vs. 2 mmHg) suggest that myoglobin will affect the pO_2 distribution over a smaller range. Radial profiles predicted by the RAAD model are not plotted because the tissue is considered space-averaged radially; once the axial pO_2 distribution is determined, the radial pO_2 values are given. A plot of pO_2 versus r, for any given axial position z, is a straight line. Further discussion of radial pO_2 profiles is given by Fletcher and Schubert [1987] and Zhang [1992].

Before evaluating the addition of myoglobin, the RAAD model solution with Michaelis-Menten was verified with a comparison to Napper's results, Table 2. The RAAD+M-M model solution gives nearly identical results; both predict a $D_{Z,TIS}$ of about 8

times normal with histogram errors near 1.70 x 10^4. The RAAD+M-M model shows a slightly lower histogram error (1.69 x 10^4), but predicts a higher $D_{Z,TIS}$ of 8.17 versus Napper's 8.03 times normal. Both models remain within the whole-organ A-V difference constraints. Optimized values for K_m are similar (Table 2). The fact that the RAAD model with Michaelis-Menten kinetics predicts the same results as Napper is offered as proof of mathematical procedures. This allows us to build upon Napper's previous modeling efforts.

Prior to the addition of myoglobin diffusion or Michaelis-Menten kinetics, the RAAD model (Table 3, column 1) required a 12.6 times normal $D_{Z,TIS}$ to predict histograms similar to the pO_2 data measurements of Schubert. This solution gave a histogram error of 2.39 x 10^4. Therefore, to match the experimental histograms, the model parameter value used for $D_{Z,TIS}$ must be increased to about 12 times the literature accepted value of 1.65 x 10^{-5} cm^2/s ($2/3 \cdot D_{water}$) [Homer et al., 1984]. Adding myoglobin to the RAAD model (Table 3, column 2) did not reduce the histogram error and therefore did not improve the model fit to data. The resulting error, 2.41 x 10^4, is slightly higher than the histogram error of the RAAD model, 2.39 x 10^4. The simplex parameter search determined an optimal D_{Mb} value of 1 x 10^{-7} times normal, effectively removing the influence of myoglobin from the simulation.

The addition of Michaelis-Menten to the RAAD model provided the greatest reduction of histogram error, 1.69 x 10^4, corresponding to a $D_{Z,TIS}$ of 8.17 times normal (Table 3, column 3). The RAAD+M-M model predicted histograms similar to the experimental data for both low and high perfusion pressures (Figure 12). The addition of myoglobin to the RAAD+M-M model (Table 3, column 4) did not lead to further

reduction of histogram error, 1.69 x 10^4. The simplex optimal D_{Mb} for the RAAD+M-M+Mb model was also near zero, 1 x 10^{-6} times normal. Simplex optimization of the RAAD models with myoglobin led to near zero values for diffusion coefficient of myoglobin as the routine searched to minimize the cost function predicted by the models. The assumption of non-equilibrium of oxygen-myoglobin reaction imparts D_{Mb} in the denominator of the equation describing MbO_2 diffusion in tissue. Because of this assumption, the simplex is unable to zero out the diffusion coefficient of myoglobin. It should be noted that solutions for the RAAD+Km model with D_{Mb} in the range of 1 x 10^{-3} to 1 x 10^{-7} times normal produced errors similar to the minimum error (within 0.06 x 10^4). Based upon this result, it appears that the simplex solutions predict a D_{Mb} close to, but not equal to, zero.

The effects of adding myoglobin and Michaelis-Menten kinetics to the RAAD model are not discernible through a comparison of axial pO_2 plots predicted by the various models. Yet, effects can be detected between models when comparing the relative changes in the predicted pO_2 histograms. The addition of Michaelis-Menten kinetics to the RAAD model shows distinct effects across the entire range of pO_2 from 5 to 240 mmHg (Figure 13). A similar plot for the addition of myoglobin to the RAAD+M-M model (Figure 14) shows only minor variations in the 5 to 20 mmHg pO_2 range. Similarly, the addition of myoglobin to the RAAD model does little to change the predicted histograms (Figure 15). Minor variations exist in the 5 to 15 mmHg range. The lack of variation between the models with and without myoglobin is not surprising considering that the optimal D_{Mb} was near zero. The greatest variation between models appeared with

the addition of Michaelis-Menten kinetics to the RAAD model (Figure 13) and corresponds to an improved data fit, 1.69×10^4 vs. 2.39×10^4 (Table 3, column 3).

Although the global minimum was found to exist with $D_{Mb} \approx 0$ for both the RAAD+Mb and RAAD+M-M+Mb models, several local minima resulted in non-zero values for D_{Mb}; however these solutions provided an inferior fit, in terms of SSE, to the experimental pO_2 distributions. These solutions are not reported here. However, hints of local minima can be seen in the fixed D_{Mb} results (Table 4).

Results of the fixed D_{Mb} trials show how the addition of myoglobin facilitation affects the histogram distributions of the RAAD and RAAD+M-M model. By fixing D_{Mb}, the relative effects of adding myoglobin to the RAAD models can be assessed without the simplex routine eliminating the contribution of myoglobin to oxygen transport by setting $D_{Mb} \approx 0$. From Table 4 (top), increasing D_{Mb} in the RAAD+Mb model leads to reduced values for the diffusion coefficient of oxygen, but this improvement is coupled with an increasing histogram error. Recall that the simplex optimized RAAD+Mb solution predicted a D_{O2} of 12.63 times normal and an SSE of 2.39×10^4. A value of 20 times D_{Mb} leads to a 17% reduction in D_{O2} (12.63 to 10.47 times normal). Unfortunately, this improvement also corresponds to an increase in SSE, 3.29×10^4. Deviations from the RAAD model are shown for the RAAD+Mb model with fixed D_{Mb} (Figures 16-18). A 1 times normal D_{Mb} leads to the greatest difference in predicted histograms. Table 4 (bottom) shows the effects of increasing D_{Mb} on the RAAD+M-M+Mb model. Increasing D_{Mb} leads to reduced D_{O2} but at the cost of increased histogram error. Recall the optimal RAAD+M-M+Mb solution of D_{O2} 8.17 times normal and an SSE of 1.69×10^4. The

greatest reduction of D_{O2} in the RAAD+M-M+Mb model is 14% (8.17 to 7.01 times normal) with an increase in SSE to 2.22×10^4. The RAAD+M-M and RAAD+M-M+Mb with fixed D_{Mb} are compared in Figures 19-20 for D_{Mb} of 1, 5, and 30 times normal. The greatest deviation occurs in the 5 to 20 mmHg range. Increasing D_{Mb} beyond 30 times normal in the RAAD+M-M+Mb model did not lead to further reduction of D_{O2}, but did lead to ever-increasing SSE. None of the fixed D_{Mb} trials for the RAAD models resulted in an SSE less than that determined by the simplex optimization routine. The local minimum for the RAAD+M-M+Mb model with D_{Mb} fixed at 20 times normal (Table 4, column 3) was confirmed to be merely a local minimum by restarting the simplex and allowing optimization of D_{Mb}. The fully optimized solution then converges to the global minimum (Table 3, column 4).

The effect of myoglobin on the total oxygen flux for the RAAD+Mb and RAAD+M-M+Mb models is shown for low pO_2 in Figure 22. Baylor and Pape [1988] use similar plots to evaluate myoglobin facilitation. They determined that about 2/3 (an additional 150%) of the total oxygen flux at the lethal end was due to myoglobin. For the non-optimized solutions of the RAAD+Mb and RAAD+M-M+Mb models, myoglobin facilitation is shown to provide about 1/3 (an additional 41%) and about 1/2 (an additional 98%) of the total oxygen flux at the lethal end, respectively. However, similar plots for the optimized solutions of the RAAD+Mb and RAAD+M-M+Mb models show no effective myoglobin facilitation. This result means that myoglobin does not increase the flux of oxygen in the tissue and does not facilitate oxygen diffusion.

The results of the simplex optimization suggest that the myoglobin does not significantly facilitate oxygen diffusion to tissue. Parameter optimizations determine a minimal D_{Mb} (≈ 0) for the optimized solutions of the RAAD+Mb and RAAD+M-M+Mb solutions (Table 3). Fixed D_{Mb} trials show that increasing D_{Mb} does not lead to an improved data fit for the RAAD+Mb or RAAD+Mb+M-M models (Table 4). Basically, the RAAD and RAAD+M-M models are better at fitting the pO_2 distribution without the inclusion of myoglobin (Table 3). Without question, the incorporation of Michaelis-Menten kinetics in the RAAD model improves the experimental data fit, leading to SSE reduction from 2.39×10^4 to 1.69×10^4 (Table 3). The addition of Michaelis-Menten kinetics is significant in reducing the need for an elevated tissue oxygen diffusion coefficient in the RAAD model, from 12.6 to 8.3 times normal (Table 3). The combined effects of myoglobin and Michaelis-Menten consumption do not provide a better fit to data (Table 3, column 4). Optimized values for $K_{m,LO}$ and $K_{m,HI}$ are not shown to change with the addition of myoglobin (Table 3, row 4, columns 3 and 4). This result suggests that exclusion of myoglobin from the RAAD+M-M model does not account for the somewhat high values of K_m determined by Napper [Napper, Schubert, 1988].

Based upon these simulations, myoglobin facilitated transport of oxygen does not account for the elevated diffusion found in modeling pO_2 data [Schubert, Fletcher, 1993]. Myoglobin appears to be rendered ineffective because of its relatively low value of P_{50}, 2.07 mmHg. At this value, myoglobin remains near complete saturation for most of the tissue region (Figure 11). The 50% saturation point for myoglobin corresponds to 95% of the capillary length (475 μm). In other words, only 5% of the tissue region exists at a pO_2

level low enough to cause significant unloading of oxygen from oxymyoglobin. Because myoglobin remains so highly saturated (≈ 50% at capillary exit) and does not appear to diffuse significantly, myoglobin's function may be limited to that of an oxygen reserve when the heart becomes very hypoxic. Others have also concluded that myoglobin diffusion is too low to significantly facilitate oxygen diffusion in muscle [Jaquez,1984; Gonzalez-Fernandez, Atta, 1982, 1986].

Because of the significant contribution of Michaelis-Menten consumption for reducing the error between model predictions and experimental data, Michaelis-Menten kinetics of oxygen consumption should be maintained in further numerical studies regarding the working heart. Further, as Napper and Schubert [1988] showed, Michaelis-Menten kinetics provides a basis for flow-dependent oxygen consumption, Gregg's phenomena, an interesting result consistent with experimental studies [McGoron, Nair, Schubert, 1996]. Based upon simulations performed in this study, it is recommended that myoglobin facilitation of oxygen diffusion be neglected from subsequent steady-state modeling studies of the isolated heart perfused with Krebs-Henseleit solution. Simulations performed using the RAAD model to assess myoglobin facilitation lead to the conclusion that myoglobin does not act as a significant facilitator of oxygen transport in cardiac tissue. These simulations do not dispute myoglobin's possible role as a short-term store for oxygen protecting the tissue from hypoxia during transient drops in pO_2 [Covell, Jaquez, 1987]. The transient role of myoglobin cannot be assessed with the steady-state RAAD tissue model.

Since myoglobin is ineffective for explaining the disparity between experimental pO_2 distributions and modeling results, other possibilities must be explored to explain why diffusion appears to be elevated in the working heart. Several researchers have suggested that working tissue appears stirred [Stainsby, 1973; Kreuzer, 1982; Jaquez, 1984; Schubert, Fletcher, 1993]. Schubert and Fletcher have proposed that working cardiac tissue may be stirred by the mechanisms responsible for contraction [Schubert, Fletcher, 1993]. This theory depicts the contractile elements in muscle as hinged stirring devices. Myosin and actin filaments involved in muscle contraction go through a process called cross-bridge cycling. The crystal structure of the myosin head has been determined in an effort to understand this mechanism further [Rayment, et al., 1993]. The proposed tissue stirring occurs when the myosin molecule moves along the actin filament (Figure 23). The myosin molecule has a hinged-head structure that "ratchets" along the actin filament during muscle contraction. It is this movement of the myosin head that may provide a convective source of transport in working tissue. Even during isovolumic contraction, the head of the myosin molecule "ratchets" in place without moving along the actin filament. Tissue stirring could explain the need for an elevated oxygen diffusion coefficient in the RAAD tissue model.

Baylor and Pape [1988] measured the diffusion coefficient of myoglobin in frog muscle during contraction. Also, Papadopoulos et al. [1995] measured the diffusion coefficient of myoglobin in rat skeletal muscle and tested the influence of muscle contraction. Baylor and Pape found no increased myoglobin diffusion through muscle contraction. Papadopoulos et al. found an increased diffusion coefficient of myoglobin in contracting muscle vs. resting muscle. The D_{Mb} increased from 1.25×10^{-7} to 1.33×10^{-7}

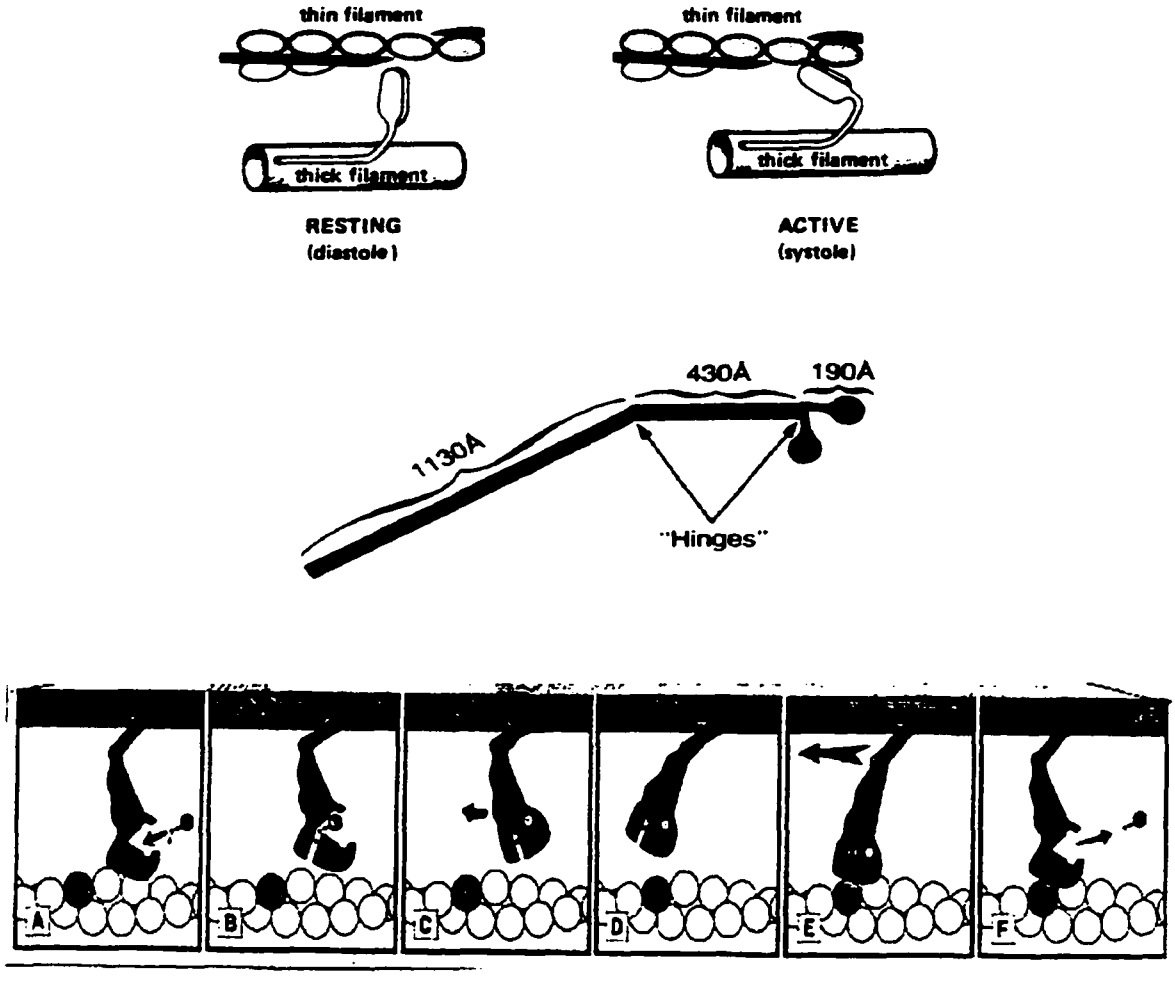

Figure 23: Myosin and actin interaction. Top: Highly schematic view of cross bridge cycling. This event may cause stirring of tissue as the actin and myosin bond, ratchet, and release [Katz, 1992]. Center: Location of two distinct hinge portions on the myosin molecular head. The crystalline structure of the myosin head has been determined. Also, the existence of flexible "hinge" regions on the myosin molecule has been proven [Rayment, et al., 1993]. Bottom: A better representation of myosin and actin interaction. (A-B) Myosin binds ATP and is released from the actin filament. (C-D) Myosin diffuses to the next active binding site on the actin filament. (E-F) Myosin binds to actin and hinges as ADP is released [Science, 1993].

cm^2/s, but the difference was not statistically significant. Papadopoulos et al. suggest that the myoglobin molecule is too large to be effectively stirred by the contractile proteins because of sterical hindrance. The diameter of myoglobin is 3.5 nm and is the same order of magnitude in size as the spacing between filaments [Papadopoulos, Jurgens, Gros, 1995]. Papadopoulos et al. state that the highly structured cytoskeletal system and contractile apparatus of the muscle cell cause inhibited diffusion of large molecules such as myoglobin. Because molecular oxygen is much smaller than myoglobin, this hindrance would not apply to the oxygen. No measurement has been made of species similar to oxygen diffusing through contracting tissue.

Popel et al. found a ten-fold discrepancy in oxygen flux between experimental spectrophotometric measurements and a mathematical model describing oxygen transport [1989]. Trying to explain this discrepancy several measurements of oxygen diffusion coefficient in living tissue have been made [Meng, Bentley, Pittman, 1992; Bentley, Meng, Pittman, 1993]. Bentley et al. [1993] found that in hamster striated muscle at 37 °C $D_{O2,TIS}$ was 2.4 times higher than previously reported values. Bentley's finding of elevated diffusion coefficient at higher temperature was not sufficient to fully explain the discrepancy between Popel's model and experimental data [Popel, Pittman, Ellsworth, 1989].

Wholpers et al. [1990] required the use of a short capillary length in their modeling of tracer washout curves in beating dog hearts to explain faster than normal transport. Although they acknowledged that the anatomical capillary length in a dog heart was 500 μm or greater, a capillary length of 200 μm was required in their simulation to match the

experimental data. Schubert and Fletcher [1993] discuss this finding, noting that parameters of the RAAD model suggest shortened capillaries as a possible alternative interpretation. However, capillaries are much longer than 200 μm in dog heart, and lengths this short are not consistent with dog physiology [Bassingthwaighte, Yipintsoi, Harvey, 1974]. Zhang [1992] shows through mathematical modeling that the RAAD model with capillary length reduced from 500 to 150-200 μm appears to fit experimental pO_2 data using a nominal value for oxygen diffusion coefficient. However, closer inspection reveals that there are observable differences in the model predicted histograms at higher pO_2 when using reduced capillary length. Schubert and Fletcher [1993] reject short capillary length as an explanation for faster than normal transport and suggest that elevated diffusion is more consistent with the known physiological mechanisms of muscle contraction. From these studies of oxygen transport in tissue, it becomes apparent that transport and delivery of oxygen in living, working tissue may be enhanced by mechanisms not yet known.

CHAPTER 6

CONCLUSIONS

The addition of myoglobin to the RAAD and RAAD+M-M model does not reduce the need for an elevated tissue oxygen diffusion coefficient required to obtain a reasonable match between modeled and experimental pO_2 distributions. Simplex parameter optimizations suggest that myoglobin does not diffuse significantly in tissue and does not act to facilitate oxygen diffusion in the steady-state. Fixed myoglobin diffusivity trials also suggest that inclusion of myoglobin in the RAAD model does nothing to improve the model's ability to predict experimental data or lower the apparent diffusion coefficient of oxygen in tissue, $D_{Z,TIS}$. The addition of Michaelis-Menten kinetics to the RAAD model led to an improved fit of the pO_2 data as it had in previous work. No further improvement was found by the combined addition of Michaelis-Menten and myoglobin to the model. Based upon these findings, it is suggested that myoglobin be excluded from further steady-state modeling efforts involving the saline perfused isolated heart preparation. Myoglobin facilitated diffusion of oxygen does not account for the disparity between the RAAD or the RAAD+M-M model and isolated heart pO_2 data which causes the need for an elevated tissue oxygen diffusion coefficient in the model. The simulations performed do not identify a cause for the elevated diffusion, but tissue stirring by contractile elements seems

possible. A measurement determining the transport of a diffusible species similar to oxygen in working heart tissue is needed to rectify this modeling perplexity.

CHAPTER 7

RECOMMENDATIONS

To provide clear evidence of elevated diffusion in working muscle, experiments must be performed that will reveal the mechanisms responsible for the appearance of elevated diffusion. Measurement of a diffusible species similar in transport properties to oxygen should be made in working heart muscle. The rat papillary muscle would be a viable preparation for assessing elevated diffusion. The muscle must be small enough in cross-section to ensure oxygenation. One method for ensuring oxygenation is isolating the muscle preparation in a chamber where the concentration of oxygen in the gas surrounding the muscle is controlled and adjusted for experimentation. Because the muscle consumes more oxygen during contraction than at rest, the pO_2 deep in tissue may approach zero as the muscle contracts. A hypoxic core could alter the surrounding tissue and the rate of pH sensitive enzymes involved in metabolism. A full discussion of this phenomenon is contained in McGoron [1991]. Efforts should be made to avoid measurements in or near the hypoxic region. Modeling shows that even the use of 95% O_2 and 5% CO_2 will not prevent the formation of a hypoxic core in working papillary muscle of 1 mm diameter [Schubert, personal communication]. However, the outer 100 μm remain a viable region to study oxygen diffusion in working heart muscle. Because of

its flammability, working with high oxygen concentration may present hazardous conditions and will require heightened consideration for safety.

The current RAAD tissue model should be extended to include hemoglobin in the capillary regions. The RAAD model with hemoglobin could no longer be compared to the isolated heart experimental pO_2 data because the heart was perfused with a cell-free, high pO_2, perfusate that did not contain hemoglobin. However, the theoretical evaluation of this addition would answer questions regarding the effects of hemoglobin on the model-predicted pO_2 distribution. Results could lead to better understanding of the oxygen transport situation in the isolated heart preparation and the modeling assumptions associated with this preparation. The strong axial diffusion found in modeling the saline perfused heart may not exist in a heart perfused with a hemoglobin containing perfusate such as blood. Enhanced diffusion would still be present, but tissue gradients may be reduced because of hemoglobin in the capillary. In the blood perfused heart, dissolved oxygen accounts for only a small amount (less then 5%) of the oxygen in blood [Guyton, Hall, 1994]. The majority of the oxygen in blood is bound to hemoglobin. However, in saline perfusate there is no hemoglobin, and all of the oxygen exists in dissolved form. Therefore, to deliver the same amount of oxygen to tissue, the capillary inlet concentration of oxygen must be much higher for saline perfusion than for blood perfusion. The capillary pO_2 profile (Figure 9) clearly shows that the inlet pO_2, 620.3 mmHg, is far above the physiological value of 100 mmHg. Also, the capillary exit pO_2 is near zero which is much lower than 40 mmHg found in blood perfused heart. The inclusion of hemoglobin should reduce the steep axial gradients at the capillary inlet. The effect on the tissue

region is unknown, but the need and/or importance of an elevated axial diffusion coefficient of oxygen may be reduced with hemoglobin in the capillary.

Multi-component transport as it relates to the possibility of interacting fluxes should be investigated [Kreuzer, 1982; Taylor, Krishna, 1993]. The possibility exists that transport in cardiac muscle cannot be described simply as binary diffusion. In the heart, rapid transport of ions is common during the cardiac cycle. Calcium ion fluxes within the muscle fiber may interact with the flux of oxygen providing enhanced transport [Kreuzer, 1982]. During excitation and contraction of the muscle fiber, calcium is released from the sarcoplasmic reticulum in large amounts and rapidly diffuses to the contractile elements within the muscle [Katz, 1992]. During relaxation, calcium is actively transported from the intracellular fluid (cytosol) to both the extracellular fluid and the sarcoplasmic reticulum. This extensive movement of calcium ions may pull oxygen molecules more quickly through the working heart tissue.

Higher-order models of oxygen consumption should be considered [personal communication, Dr. F. Jones]. Buerk and Saidel [1978] used zero-order, first-order, and Michaelis-Menten kinetics of oxygen consumption to model metabolism in brain and liver slices. They found that the Michaelis-Menten kinetic model provided the best data fit. Napper [1985] also found an improved data fit when he added Michaelis-Menten to the RAAD model which previously used zero-order kinetics of oxygen consumption. Adding a multi-step kinetic model, multiple K_m, for oxygen transport to the RAAD model may provide an even better fit to the experimental pO_2 data, thereby explaining some of the elevated axial diffusion coefficient.

It is recommended that further numerical modeling studies involving the PASVA routine make use of a PC compiler and not the IBM VM mainframe. Mainframe trials requiring over 30 minutes of processing time are limited to a schedule of 11 p.m. to 7 a.m. One problem is that the current PASVA and simplex code are programmed in IBM VS FORTRAN. This version of FORTRAN is a hybrid of FORTRAN 77 and FORTRAN 90. The FORTRAN VS code is not directly portable to FORTRAN 77 compilers. Based upon numerous inquiries to the comp.lang.fortran newsgroup, the Watcom compiler is recommended [Powersoft]. This compiler is not to be confused with the "learning tool" FORTRAN compiler Watfor. Several programmers surveyed suggested that Microsoft Powerstation does not readily compile FORTRAN VS code. They recommended Watcom as the best compiler for using FORTRAN VS mainframe code on an IBM PC platform.

APPENDIX A

PARAMETER LIST

ATP	=	adenosine triphosphate
A-V	=	Arterio-venous
AV_{diff}	=	A-V difference, mmHg (see Appendix D)
C_{Mb}	=	concentration of myoglobin
$C_{MbO2,TIS}$	=	concentration of oxymyoglobin in tissue
C_o	=	normalizing concentration, varies, mol / cm^3
$C_{O2,\,CAP}$	=	capillary oxygen concentration
$\overline{C}_{O2,\,CAP}$	=	normalized capillary oxygen concentration $C_{O2,\,CAP} / C_o$
$C_{Mb,TOT}$	=	total tissue concentration of myoglobin, 1.0×10^{-6} mol / cm^3 [Fletcher, 1980; Wittenberg, Wittenberg, 1990]
$C_{O2,\,TIS}$	=	tissue oxygen concentration
$\overline{C}_{O2,\,TIS}$	=	normalized tissue oxygen concentration $C_{O2,\,TIS} / C_o$
CONSERR	=	difference between experimental and model A-V difference (see Appendix D)
D_{Mb}	=	Mb tissue diffusion coefficient D_{MbO2}
D_{MbO2}	=	MbO_2 tissue diffusion coefficient, 2.2×10^{-7} cm^2 / s [Papadopoulos, Jurgens, Gros, 1995]
$D_{MbO2,TIS}$	=	D_{MbO2}
$D_{Z,\,TIS}$	=	axial diffusion coefficient of oxygen in tissue, $2/3 \times D_{water}$ (1.65×10^{-5} cm^2 / s) [Homer et al., 1984]
$D_{O2,TIS}$	=	$D_{Z,TIS}$
D_{water}	=	diffusion coefficient of oxygen in water

D_r = radial diffusion coefficient of oxygen in tissue
1/2 x $D_{Z,TIS}$ [Schubert, Fletcher, 1993]

DELEPS = parameter used in PASVA to advance EPSNU

d = differential operator

EPSNU = parameter used in PASVA for continuation

Flowrate = flow rate of perfusate (see Table 1)

HI = denotes high perfusion pressure

HISERR = histogram error, sum of SSE_{LO} and SSE_{HI}

HISDIFF = histogram error, $(SSE_{LO} - SSE_{HI})^2$

$HIST_{DATA,LO}$ = experimental data histogram for low perfusion pressure

$HIST_{MODEL,LO}$ = model histogram for low perfusion pressure

k''' = O_2 metabolic rate in tissue, mol / s·cm^3
perfusion dependent (see Appendix D)

k'''_{model} = O_2 metabolic rate in tissue calculated from model, mol / s·cm^3
(see Appendix D)

k_1 = oxygen-myoglobin on rate,
2.4 x 10^{10} cm^3 / mol·s [Wittenberg, 1970; Fletcher, 1980]

k_2 = oxygen-myoglobin off rate,
65 s^{-1} [Wittenberg, 1970; Fletcher, 1980]

K_m = Michaelis-Menten kinetic constant, mmHg

K = RAAD model parameter defined in Equation (6) for first-order O_2 consumption or Equation (18) for M-M consumption

L = capillary length, also Krogh cylinder length
0.05 cm [Napper, Schubert, 1988]

LO = denotes low perfusion pressure

Mb = myoglobin

MbO_2 = oxymyoglobin

M-M = Michaelis-Menten

N = number of parameters to be optimized

$NData_{LO}$ = number of data points for low perfusion pressure

$N_{O2,CAP}$ = capillary oxygen flux

$N_{O2,TIS}$ = tissue oxygen flux

$N_{O2,Rc}$ = oxygen flux leaving capillary at $r = r_{CAP}$

O_2 = oxygen

P = capillary mass transport coefficient (see Appendix C and D) chosen to match radial Krogh extraction, cm / s

pO_2 = partial pressure of oxygen, mmHg, similar to concentration (e.g., C_{O2} = solubility x pO_2)

PP = perfusion pressure

P_{50} = pO_2 required for 50% saturation of myoglobin

PASVA = finite-difference routine used to solve RAAD model

RAAD = Radially-Averaged, Axially-Distributed

r = radial position, cm

r_{CAP} = capillary radius, 2.5×10^{-4} cm [Napper, Schubert, 1988]

r_{TIS} = Krogh tissue cylinder radius (see Appendix D) perfusion dependent, cm

R_C = r_{CAP}

SSE = sum-of-squares error, measure of model fit to data set

SSE_{LO} = sum-of-squares error for low perfusion pressure

SSE_{HI} = sum-of-squares error for high perfusion pressure

V_{max} = maximal tissue oxygen consumption, mol / $s \cdot cm^3$

VAR_{LO} = estimate of variance for low perfusion data, Equation (22)

Y = fraction of Mb saturated with oxygen, Equation (19) for oxygen-myoglobin reaction at equilibrium

Z, z = axial position, cm

$\overline{Z}$ = normalized axial position Z / Z_o

Z_o = normalizing length, capillary length 0.5 cm

α	=	RAAD model parameter defined in Equation (5)
β	=	RAAD model parameter defined in Equation (11)
μ_{CAP}	=	capillary density, capillaries / cm^3
v_{CAP}	=	perfusate velocity in capillary (see Appendix D) perfusion dependent, cm / s
Ω_1	=	RAAD model parameter defined in Equation (7)
Ω_2	=	RAAD model parameter defined in Equation (9)
$\omega_1, \omega_2, \omega_3$	=	weights for cost function, 1.0
π	=	3.14159265259
ρ	=	oxygen-myoglobin reaction rate, mol / s·cm^3, Equation (2)

Note: Solubility of oxygen in tissue used in simulations was 1.31147×10^{-9} mol / mmHg·cm^3 corrected for temperature at 32.5 °C [Napper, Schubert, 1988].

Schuder et al. using subunit-exchange chromatography determined a myoglobin concentration in cat ventricle tissue of 177 μmol/kg (0.2 mol/cm^3) [Schuder et al., 1978]. This value was not used in modeling of the isolated cat heart because the sample size was too small to cancel out the large variations of C_{Mb} that exists among animals [J.B. Wittenberg, personal communication].

APPENDIX B

FULL DERIVATION OF RAAD MODEL

B.1 RAAD Model Assumptions

1. Steady state
2. Straight, parallel, concurrent, homogeneously distributed capillaries (Krogh cylinders)*
3. Constant perfusate velocity in capillary
4. Slight solubility of oxygen in perfusate
5. Radially uniform capillary
6. Zero-order oxygen consumption in the tissue region, model is also solved with Michaelis-Menten kinetics
7. Homogeneous oxygen consumption in the tissue region
8. Radially uniform tissue (radially space-averaged)
9. Axial diffusion in tissue
10. Equal solubility in tissue and perfusate

* See Kreuzer [1982] for an extended discussion of the Krogh cylinder model assumptions.

B.2 RAAD Model Derivation

The RAAD model is derived following the shell-balance method discussed in Bird, Stewart, and Lightfoot, Chapter 17 [1960].

B.2.1 Derivation of RAAD Capillary Region

An oxygen mass balance on the differential shell describing the capillary region, Figure 24, with the assumption of steady state, yields

$$\{Total\ Flux\}_{IN} - \{Total\ Flux\}_{OUT} = 0 \tag{B1}$$

$$\{Total\ Flux\}_{IN} = \pi r_{CAP}^2 N_{O_2,CAP}\Big|_{Z=Z} \tag{B2}$$

$$\{Total\ Flux\}_{OUT} = \pi r_{CAP}^2 N_{O_2,CAP}\Big|_{Z=Z+\Delta Z} + 2\pi r_{CAP}\Delta Z N_{O_2,Rc}\Big|_{r=Rc} \tag{B3}$$

Axial flux in the capillary is modeled as convection only; therefore,

$$N_{O_2,CAP} = C_{O_2,CAP} v_{CAP} \tag{B4}$$

Equation (B4) incorporates the assumption that oxygen is slightly soluble in the perfusate.

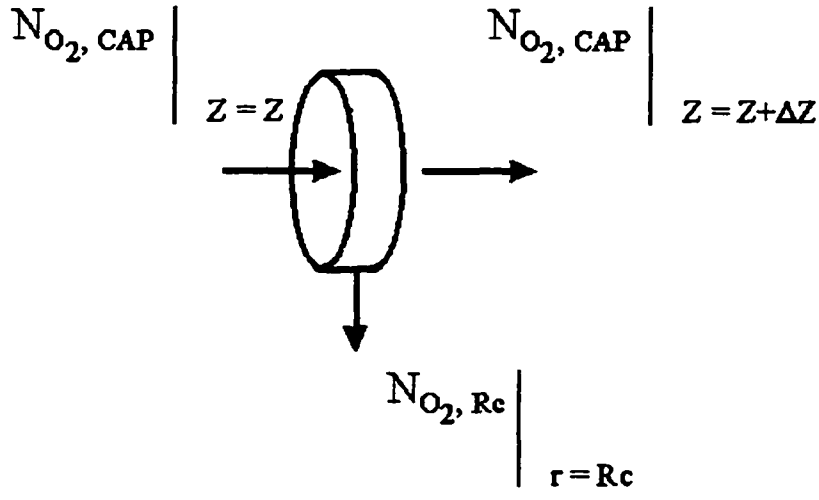

Figure 24: Differential shell describing the capillary region. The shell has a radius of r = Rc and a differential thickness of ΔZ. The capillary is axially distributed and radially averaged. A space averaged flux, $N_{O2,RC}$, exits the capillary radially at Rc.

Flux leaving the capillary radially is represented as a mass transfer coefficient times a concentration gradient:

$$N_{O_2,Rc} = P \cdot \left(C_{O_2,CAP} - C_{O_2,TIS} \right) \tag{B5}$$

The value chosen for P is discussed in Appendix C. Dividing the species mass balance by $\pi\, r^2_{CAP}\, \Delta Z$ and taking the limit as $\Delta Z \rightarrow 0$ yields the differential equation describing the capillary region:

$$\frac{dN_{O_2,CAP}}{dZ} = \frac{2P}{r_{CAP}} (C_{O_2,TIS} - C_{O_2,CAP}) \tag{B6}$$

Substituting Equation (B4) into (B6) and dividing by v_{CAP}, the equation describing the capillary region in terms of concentration is

$$\frac{dC_{O_2,CAP}}{dZ} = \frac{2P}{v_{CAP}\, r_{CAP}} (C_{O_2,TIS} - C_{O_2,CAP}) \tag{B7}$$

The equation can then be normalized by dividing the dependent variables by appropriately chosen normalizing coefficients, C_o and Z_o [Myers, 1987]:

$$\frac{C_o Z_o \cdot dC_{O_2,CAP}}{C_o Z_o \cdot dZ} = \frac{2P}{v_{CAP}\, r_{CAP}} (C_{O_2,TIS} - C_{O_2,CAP}) \cdot \frac{C_o}{C_o} \tag{B8}$$

The resulting normalized equation is

$$\frac{d\overline{C}_{O_2,CAP}}{d\overline{Z}} = \frac{2PZ_o}{v_{CAP}\, r_{CAP}}(\overline{C}_{O_2,TIS} - \overline{C}_{O_2,CAP}) \qquad \text{(B9)}$$

B.2.2 Derivation of RAAD Tissue Region

The equations for the tissue region are developed by the same methods used for the capillary region. An oxygen mass balance on the differential shell describing the tissue region, Figure 25, with the assumption of steady state, yields

$$\{Total\ Flux\}_{IN} - \{Total\ Flux\}_{OUT} + \{Total\ production\} = 0 \qquad \text{(B10)}$$

$$\{Total\ Flux\}_{IN} = \pi\left(r_{TIS}^2 - r_{CAP}^2\right)N_{O_2,TIS}\Big|_{Z=Z} + 2\pi r_{CAP}\,\Delta Z\, N_{O_2,Rc}\Big|_{r=Rc} \qquad \text{(B11)}$$

$$\{Total\ Flux\}_{OUT} = \pi\left(r_{TIS}^2 - r_{CAP}^2\right)N_{O_2,TIS}\Big|_{Z=Z+\Delta Z} \qquad \text{(B12)}$$

$$\{Total\ production\} = -\pi\left(r_{TIS}^2 - r_{CAP}^2\right)$$
$$\{Total\ production\} = -\pi\left(r_{TIS}^2 - r_{CAP}^2\right)\Delta Z\cdot(k'''+\rho) \qquad \text{(B13)}$$

where k''' represents homogeneous oxygen consumption and ρ is the reaction rate of myoglobin-oxygen reaction as given by

$$\rho = C_{Mb,TOT}\left[k_1 C_{O2,TISS}(1-Y) - k_2 Y\right] \qquad \text{(B14)}$$

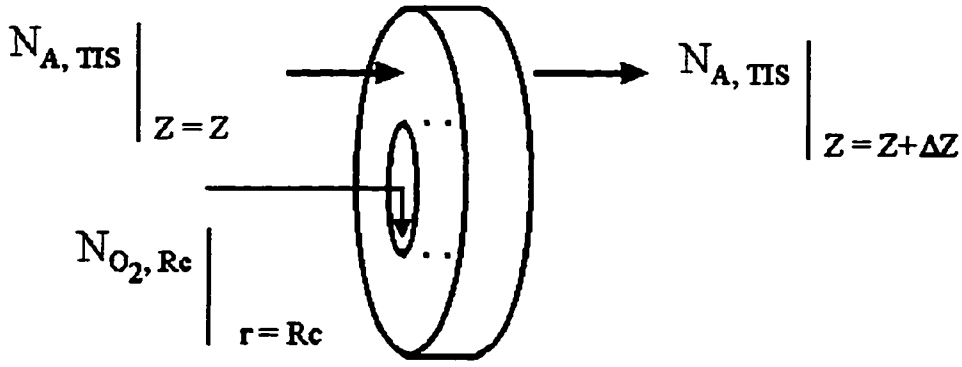

Figure 25: Differential shell describing the tissue region. The tissue is axially distributed and radially averaged. The shell has an inner radius of r = Rc, an outer radius of r = Rt, and a differential thickness of ΔZ. The space averaged flux exiting the capillary, enters the tissue region at r = R_C. No flux leaves the surface at r = Rt in agreement with the assumption of non-interacting Krogh-like tissue cylinders.

In the case of Michaelis-Menten kinetics of oxygen consumption, k''' is replaced by

$$\frac{V_{MAX} C_{O2,TIS}}{\left[C_{O2,TIS} + K_m\right]} \tag{B15}$$

Axial flux in the tissue region is modeled as simple diffusion; therefore,

$$N_{O_2,TIS} = -D_{O_2,TIS} \frac{d C_{O_2,TIS}}{d Z} \tag{B16}$$

Equation (B16) implies that oxygen is slightly soluble in the tissue. Flux entering the tissue radially is represented as a mass transfer coefficient times a concentration gradient, Equation (B5).

Dividing the species mass balance by π (r^2_{TIS} - r^2_{CAP}) ΔZ and taking the limit as $\Delta Z \rightarrow 0$ yields the differential equation for the tissue region:

$$\frac{d N_{O_2,TIS}}{d Z} = \frac{2 r_{CAP} P}{(r_{TIS}^2 - r_{CAP}^2)} (C_{O_2,TIS} - C_{O_2,CAP}) - k''' - \rho \tag{B17}$$

Substituting Equation (B16) into (B17) and dividing by - $D_{O2,TIS}$, the equation describing the tissue region in terms of concentration is

$$\frac{d^2 C_{O_2,TIS}}{d Z^2} = \frac{-2 r_{CAP} P}{D_{O_2,TIS}(r_{TIS}^2 - r_{CAP}^2)} (C_{O_2,TIS} - C_{O_2,CAP}) + \frac{k'''}{D_{O_2,TIS}} + \frac{\rho}{D_{O_2,TIS}} \tag{B18}$$

The equation can be normalized in the same manner as the capillary equation, resulting in

$$\frac{d^2\overline{C}_{O_2,TIS}}{d\overline{Z}^2}=\frac{-2r_{CAP}PZ_o^2}{D_{O_2,TIS}(r_{TIS}^2-r_{CAP}^2)}(\overline{C}_{O_2,TIS}-\overline{C}_{O_2,CAP})+\frac{Z_o^2}{D_{O_2,TIS}C_o}(k'''+\rho) \qquad \text{(B19)}$$

The differential equation describing myoglobin transport is derived through a species mass balance on MbO_2. The equations are the same as the equations for oxygen in tissue with the exception that there is no k''' and there is a sign difference on the myoglobin reaction term because, as the reaction term is written, oxygen is "consumed" by the myoglobin reaction to form MbO_2. This appears as a consumption term in the oxygen balance and as a production term in the MbO_2 balance. Following the same mass balance procedure, the equation describing MbO_2 transport in tissue is

$$\frac{d^2C_{MbO_2,TIS}}{dZ^2}=-\frac{\rho}{D_{MbO_2,TIS}} \qquad \text{(B20)}$$

The total amount of myoglobin in tissue is fixed, $C_{Mb,TOT}$. The relationship between myoglobin saturation and oxymyoglobin saturation is $C_{MbO2} = C_{Mb,TOT}$ x Y, where Y is the fraction of myoglobin saturated with oxygen. With this, Equation (B20) can be rewritten:

$$C_{Mb,TOT}\frac{d^2Y}{dZ^2}=-\frac{\rho}{D_{MbO2,TIS}} \qquad \text{(B21)}$$

The equation describing oxymyoglobin transport is then normalized to

$$\frac{d^2Y}{d\bar{Z}^2} = -\frac{\rho Z_o^2}{D_{MbO2,TIS} C_{Mb,TOT}} \tag{B22}$$

APPENDIX C

DERIVATION OF SPACE-AVERAGED PERMEABILITY

The RAAD model incorporates a mass transfer coefficient or permeability, P, times a concentration gradient to represent radial transport of oxygen. The value of P is determined such that in the absence of axial diffusion, the RAAD model produces radial fluxes equivalent to the Krogh model. To do this, the Krogh model is space-averaged radially to determine an averaged radial flux. This flux is set equal to the expression for the capillary flux in the RAAD model, and P is determined.

The Krogh-Erlang solution for radial diffusion in tissue with zero-order oxygen consumption is

$$C_{O_2,TIS} - C_{O_2,CAP} = \frac{k'''}{2D_r}\left[\frac{1}{2}(r^2 - r_{CAP}^2) - r_{TIS}^2 \ln\left(\frac{r}{r_{CAP}}\right)\right] \qquad \text{(C1)}$$

The tissue equation for the RAAD model with no axial diffusion and zero-order oxygen consumption is

$$C_{O_2,TIS} - C_{O_2,CAP} = \frac{-k'''}{2r_{CAP}P}\left(r_{TIS}^2 - r_{CAP}^2\right) \qquad \text{(C2)}$$

The Krogh model, Equation (C1), is space-averaged over the tissue compartment and set equal to the RAAD model expression for radial flux:

$$-\frac{k'''}{2r_{CAP}P}\left(r_{TIS}^2 - r_{CAP}^2\right) = \frac{\dfrac{k'''}{2D_r}\displaystyle\int_{r\,CAP}^{r\,TIS}\left[\frac{1}{2}(r^2 - r_{CAP}^2) - r_{TIS}^2 \ln\left(\frac{r}{r_{CAP}}\right)\right]dr}{\displaystyle\int_{r\,CAP}^{r\,TIS} r\,dr} \qquad \text{(C3)}$$

The resulting value for the space-averaged permeability is

$$P = \frac{-D_r\left(r_{TIS}^2 - r_{CAP}^2\right)\Big/ r_{CAP}}{\frac{1}{2}\left(r_{TIS}^2 - r_{CAP}^2\right) + \frac{1}{4}\left(r_{TIS}^2 + r_{CAP}^2\right) + r_{TIS}^4 \ln\left(\frac{r_{CAP}}{r_{TIS}}\right)\Big/\left(r_{TIS}^2 - r_{CAP}^2\right)} \qquad \text{(C4)}$$

APPENDIX D

WHOLE-ORGAN MODELING CONSTRAINTS

Whole-organ constraints are applied to the RAAD tissue model in an effort to maintain consistency between model and experiment. Table 1 lists experimentally determined parameters from the isolated cat heart experiment at low and high perfusion pressure. These experimental parameters are used to calculate model parameters for simulation. Capillary velocity, v_{CAP}, is a function of perfusion pressure and is determined from experimental flow rate by assuming equal distribution of flow into each capillary and plug flow,

$$v_{CAP} = \frac{Flow\ rate \cdot L}{\pi\ r_{CAP}^2 \cdot \mu_{CAP}} \tag{D1}$$

where L is the Krogh cylinder length (0.05 cm) and μ_{CAP} is capillary density (capillaries/cm^2). The Krogh tissue radius, r_{TIS}, is dependent on the capillary density which is assumed to change with low and high perfusion pressure. Krogh tissue radius is determined by

$$r_{TIS}^2 = \frac{\left(1 + \pi\ r_{CAP}^2 \cdot \mu_{CAP}\right)}{\mu_{CAP}} \tag{D2}$$

Equation (D2) is determined as the metabolizing area represented by a cross-section of the RAAD model (see Schubert, 1976 for details). This area does not include the capillary region. Additionally, the space-averaged permeability, P, is dependent on r_{TIS} and therefore changes with perfusion pressure (see Appendix C).

The whole-organ consumption for the isolated heart preparation was determined from extraction (A-V difference) measurements at low and high perfusion pressure. An extra constraint on the RAAD model is that the consumption predicted by the model must match the whole-organ consumption. For the homogeneous consumption case, the model consumption is simply set to the experimentally determined values for whole-organ consumption (after various modifications) [Schubert, 1976]; but, in the case of Michaelis-Menten kinetics, the overall consumption cannot be set in the model. For comparison, the predicted A-V difference from the model can be used to calculate an overall consumption, from

$$k'''_{model} = \frac{AV\,diff \cdot v_{CAP} r_{CAP}^2}{L\left(r_{TIS}^2 - r_{CAP}^2\right)} \qquad \text{(D3)}$$

The A-V difference predicted by the RAAD model is constrained to match the experimentally determined extraction. In this way, the model is guaranteed to maintain physiological consistency regarding oxygen consumption by predicting values equal to that of the whole-organ data. This consumption matching method is used to adjust the capillary inlet pO_2 boundary condition. Adjustments are made until the model converges

to an acceptable A-V difference (95% confidence, as described by Schubert, Whalen, and Nair [1978]) which corresponds to ± 4 mmHg and ± 5 mmHg for low and high perfusion pressure, respectively. The same procedure was used by Napper and Schubert [1988].

REFERENCES

American Heart Association, Heart and Stroke Facts: 1996 Statistical Supplement, printed from http://ovchin.uc.edu/htdocs/heart/Heart_Disease.html, 1996.

Araki, R., M. Tamura, and I. Yamazaki, "The Effect of Intracellular Oxygen Concentration on Lactate Release, Pyridine Nucleotide Reduction, and Respiration Rate in the Rat Cardiac Tissue," Circ. Res., 53: 448-455, 1983.

Bailey, J.R., D.H. Sephton, and W.R. Driedzic, "Oxygen Uptake by Isolated Perfused Fish Hearts with Differing Myoglobin Concentrations Under Hypoxic Conditions," J. Mol. Cell. Cardiol., 22: 1125-1134, 1990.

Bassingthwaighte, J.B., T. Yipintsoi, and R.B. Harvey, "Microvasculature of the Dog Left Ventricular Myocardium," Microvas. Res., 7: 229, 1974.

Baylor, S.M., and P.C. Pape, "Measurement of Myoglobin Diffusivity in the Myoplasm of Frog Skeletal Muscle Fibres," J. Phys., 406: 247-275, 1988.

Bentley, T.B., H. Meng, and R.N. Pittman, "Temperature Dependence of Oxygen Diffusion and Consumption in Mammalian Striated Muscle," Am. J. Physiol., 264: H1825-H1830, 1993.

Bird, R.B., W.E. Stewart, and E.N. Lightfoot, Transport Phenomena, John Wiley and Sons, New York, 1960.

Bloch, I., "Model of Oxygen Transport to Tissue," Bull. Math. Biophys., 5: 1-20, 1943.

Blum, J. J., "Concentration Profiles in and Around Capillaries," Am. J. Physiol., 198: 991-998, 1960.

Buerk, D.G., and G.M. Saidel, "Local Kinetics of Oxygen metabolism in Brain and Liver Tissues," Microvasc. Res., 16: 391-405, 1978.

Chance B., A. Mayevsky, C. Goodwin, and L. Mela, "Factors In Oxygen Delivery to Tissue," Microvasc. Res., 8: 276-282, 1974.

Covell, D.G., and J.A. Jacquez, "Does Myoglobin Contribute Significantly to Diffusion of Oxygen in Red Skeletal Muscle?," Am. J. Physiol., 252: R341-R347, 1987.

Duling, B.R., "Oxygen, Metabolism, and Microcirculatory Control," Microcirculation, 3: 401-429, 1978.

Federspiel, W.J., "A Model Study of Intracellular Oxygen Gradients in a Myoglobin-Containing Skeletal Muscle Fiber," Biophys. J., 49: 857-868, 1986.

Fletcher, J.E., "Facilitated Oxygen Diffusion in Muscle Tissues," Biophys. J., 29: 437-458, 1980.

Fletcher, J.E., and R.W. Schubert, "On the Computation of Substrate Levels in Perfused Tissues," Math. BioSci., 62: 75-106, 1982.

Fletcher, J.E., and R.W. Schubert, "Axial Diffusion and Wall Permeability Effects in Perfused Capillary-Tissue Structures," BioSystems, 20: 153-174, 1987.

Gardner, J.D., and R.W. Schubert, "Evaluation of Myoglobin in the Presence of Axial Diffusion," Oxygen Transport to Tissue, Plenum Press, New York, 1995 (accepted).

Gayeski, T.E.J., R.J. Connett, and C.R. Honig, "Minimum Intracellular pO2 for Maximum Cytochrome Turnover in Red Muscle In Situ," Am. J. Physiol., 252: H906-H915, 1987.

Gayeski, T.E.J., and C.R. Honig, "Intracellular pO2 in Individual Cardiac Myocytes in Dogs, Cats, Rabbits, Ferrets, and Rats," Am. J. Physiol., 260: H522-H531, 1991.

Gonzalez-Fernandez, J.M., and S.E. Atta, "Facilitated Transport of Oxygen in the Presence of Membranes in the Diffusion Path," Biophys. J., 38: 133-141, 1982.

Gonzalez-Fernandez, J.M., and S.E. Atta, "Comparative Facilitated Transport of Oxygen," Am. J. Physiol., 251: R1-R12, 1986.

Groebe, K., "A Versatile Model of Steady State O2 Supply to Tissue," Biophys. J., 57: 485-498, 1990.

Groebe, K., "An Easy-to-Use Model for O2 Supply to Red Muscle. Validity of Assumptions, Sensitivity to Errors in Data," Biophys. J., 68: 1246-1269, 1995.

Groebe, K., and G. Thews, "Calculated Intra- and Extracellular PO_2 Gradients in Heavily Working Red Muscle," Am. J. Physiol., 259: H84-H92, 1990. a

Groebe, K., and G. Thews, "Role of Geometry and Anisotropic Diffusion for Modelling pO2 Profiles in Working Red Muscle," Respir. Phys., 79: 255-278, 1990. b

Guyton, A.C., and J.E. Hall, Textbook of Medical Physiology, 9th ed., W.B. Saunders, Philadelphia, 1994.

Hoffman, J.D., Numerical Methods for Engineers and Scientists, McGraw-Hill, Inc., New York, 1992.

Homer, L.D., J.B. Shelton, C.H. Dorsey, and T.J. Williams, "Anisotropic Diffusion of Oxygen in Slices of Rat Muscle," Am. J. Physiol., 246: R107-R113, 1984.

Hoofd, L., "Calculation of Oxygen Pressures in Tissue with Anisotropic Capillary Orientation. II. Coupling of Two-Dimensional Planes," Math. Biosci., 129: 25-39, 1995.

Hsu, R., and T.W. Secomb, "A Green's Function Method for Analysis of Oxygen Delivery to Tissue by Microvascular Networks," Math. Biosci., 96: 61-78, 1989.

Jaquez, J.A., "The Physiological Role of Myoglobin: More Than a Problem in Reaction-Diffusion Kinetics," Math. Biosci. 68: 57-97, 1984.

Jones, D.P., and F.G. Kennedy, "Analysis of Intracellular Oxygenation of Isolated Adult Cardiac Myocytes," Am. J. Physiol., 250: C384-C390, 1986.

Jurgens, K.D., T. Peters, and G. Gros, "Diffusivity of Myoglobin in Intact Skeletal Muscle Cells," Proc. Natl. Acad. Sci. Physiology, 91: 3829-3833, 1994.

Katz, A.M., Physiology of the Heart, 2d ed., Raven Press, New York, 1992.

Kreuzer, F., "Facilitated Diffusion of Oxygen and its Possible Significance: A Review," Resp. Physiol., 9: 1-30, 1970.

Kreuzer, F., "Oxygen Supply to Tissues: The Krogh Unit and its Assumptions," Experientia, 38: 1415-1426, 1982.

Kreuzer, F., and L. Hoofd, "Facilitated Diffusion of O_2 and CO_2," Handbook of Physiology, Farhi, L.E. and S.M. Tenney eds., American Physiological Society, Washington, D.C., 4: 89-141, 1982.

Kreutzer, U., and T. Jue, "Critical Intracellular O_2 in Myocardium as Determined by ^1H Nuclear Magnetic Resonance Signal of Myoglobin," Am. J. Physiol., 268: H1675-H1681, 1995.

Krogh, A., "The Number and Distribution of Capillaries in Muscles with Calculations of the Oxygen Pressure Head Necessary for Supplying the Tissue," J. Physiol., 52: 409-415, 1919.

Lenhoff, A.M., and E.N. Lightfoot, "The Effects of Axial Diffusion and Permeability Barriers on the Transient Response of Tissue Cylinders," J. Theor. Biol., 97: 663-677, 1982.

Leninger-Follert, E., and D.W. Lubbers, "Determination of Local Myoglobin Concentration in the Guinea Pig Heart," Pflugers Arch., 341: 271-280, 1973.

Lentini, M., and V. Pereyra, "An Adaptive Finite Difference Solver for Nonlinear Two-Point Boundary Problems with Mild Boundary Layers," SIAM J. Num. Anal., 14: 91-111, 1979.

Levitt, D.G., "Theoretical Model of Capillary Exchange Incorporating Interactions Between Capillaries," Am. J. Physiol., 220: 250-255, 1971.

Loiselle, D.S., "The Effect of Myoglobin-Facilitated Oxygen Transport on the Basal Metabolism of Papillary Muscle," Biophys. J., 51: 905-913, 1987.

McGoron, A.J., Reversibility of Oxygen Demand by Rat Brain Slices Exposed To Hypoxia Demonstrated by a Variable Michaelis-Menten Model of Oxygen Metabolism, Ph.D. Dissertation, Louisiana Tech University, 1991.

McGoron, A., P. Nair, and R.W. Schubert, "Michaelis-Menten Kinetics Model of Oxygen Consumption by Rat Brain Slices Following Hypoxia," Ann. Biomed. Eng., (accepted), 1996.

Meng, H., T.B. Bentley, and R.N. Pittman, "Oxygen Diffusion in Hamster Striated Muscle: Comparison of In Vitro and Near In Vivo Conditions," Am. J. Physiol., 263: H35-H39, 1992.

Meng, H., T.B. Bentley, and R.N. Pittman, "Myoglobin Content of Hamster Skeletal Muscles," J. Appl. Physiol., 74: 2194-2197, 1993.

Myers, G.E, Analytical Methods In Conduction Heat Transfer, Genium Publishing Corp., Schenectady, NY, 1987.

Napper, S.A., A Mathematical Model of Oxygen Transport in Isolated Heart, Ph.D. Dissertation, Louisiana Tech University, 1985.

Napper, S.A., and R.W. Schubert, "Mathematical Evidence for Flow-Induced Changes in Myocardial Oxygen Consumption," Ann.Biomed. Eng., 16, 349-365, 1988.

Nicol, R., P. Smith, P.R. Raggatt, "The Use of the Simplex Method for the Optimization of Non-Linear Function on a Laboratory Microcomputer," Comput. Biol. Med., 16(2): 145-152, 1985.

Papadopoulos, S., K.D. Jurgens, and G. Gros, "Diffusion of Myoglobin in Skeletal Muscle Cells - Dependence on Fibre Type, Contraction, and Temperature," Pflugers Arch - Eur. J. Physiol., 430: 519-525, 1995.

Pittman, R.N., "Influence of Microvascular Architecture on Oxygen Exchange in Skeletal Muscle," Microcirc., 2: 1-18, 1995.

Popel, A.S., "Theory of Oxygen Transport to Tissue," Critical Reviews in Biomedical Engineering, 17: 257-321, 1989.

Popel, A.S., Pittman, R.N., and M.L. Ellsworth, "Rate of Oxygen Loss from Arterioles is an Order of Magnitude Higher than Expected," Am. J. Physiol., 256: H921-H924, 1989.

Powersoft, WWW address: http://www.powersoft.com/, phone number: (508) 287-1500.

Press, W.H., S.A. Teukolsky, W.T. Vetterling, B.P. Flannery, Numerical Recipes in C, 2d ed. Cambridge University Press, 1992.

Rayment, I., H.M. Holden, M. Whittaker, C.B. Yohn, M. Lorenz, K.C. Holmes, and R.A. Milligan, "Structure of the Actin-myosin Complex and its Implications for Muscle Contraction," Science, 261: 58, 1993.

Reneau, D. D., D.F. Bruley, and M.H. Knisely, "A Digital Simulation of Transient Oxygen Transport in Capillary Tissue Systems (Cerebral Grey Matter)," AIChE J., 15(6): 916-925, 1969.

Salathe, E.P., and C. Chen, "The Role of Myoglobin in Retarding Oxygen Depletion in Skeletal Muscle," Math. Biosci., 116: 1-20, 1993.

Schneiderman, G., T.K. Goldstick, "Oxygen Fields Induced by Recessed and Needle Oxygen Microelectrodes in Homogenous Media," Oxygen Transport to Tissue - II, Grote, J., and D.D. Reneau eds., Plenum Publishing, New York, 1975.

Schubert, R.W., A Physiological and Mathematical Study of Oxygen Distribution in the Autoregulating Isolated Heart, Ph.D. Dissertation, Case Western Reserve University, 1976.

Schubert, R.W., J.E. Fletcher, and D.D. Reneau, "An Analytical Model for Axial Diffusion in the Krogh Cylinder," Oxygen Transport To Tissue - VI, Bruley, D.F., H.I. Bicher, and D.D. Reneau, eds., Plenum Press, New York, 433-442, 1985.

Schubert, R.W., and J.E. Fletcher, "Rethinking Oxygen Transport to Tissue: Model and Experiment Compared," Comments on Theoretical Biology, 3: 23-42, 1993.

Schubert, R.W., and W.J. Whalen, "A Mass Transport Model for Predicting O_2 Distribution in the Autoregulating Myocardium," Microvas. Res., 11(1): 127, 1976.

Schubert, R.W., W.J. Whalen, and P. Nair, "Myocardial PO_2 Distribution: Relationship to Coronary Autoregulation," Am. J. Physiol., 234: H361-H370, 1978.

Schubert, R.W., and X. Zhang, "Dependence of Oxygen Distribution on Transport Assumptions," FASEB J., 6 (4-1): A1518, 1992.

Schubert, R.W., and X. Zhang, "The Krogh Cylinder Revisited: Axial Transport," Oxygen Transport to Tissue, Plenum Press, New York, 1995 (accepted).

Schuder, S., J.B. Wittenberg, B. Haseltine, and B.A. Wittenberg, "Spectrophotometric Determination of Myoglobin in Cardiac and Skeletal Muscle: Separation from Hemoglobin by Subunit-Exchange Chromatography," Analytical Biochem., 92: 473-481, 1979.

Science, "Crystal Structure of the Myosin Head Turbocharges Molecular-Motor Research," 261: 50-65, 1993.

Secomb, T.W., R. Hsu, and M.W. Dewhirst, "Models for Oxygen Exchange Between Microvascular Networks and Surrounding Tissue," Advances in Biological Heat and Mass Transfer, 231: 121-127, 1992.

Secomb, T.W., R. Hsu, M.W. Dewhirst, B. Klitzman, and J.F. Gross, "Analysis of Oxygen Transport to Tumor Tissue by Microvascular Networks," Int. J. Radiation Oncology Biol. Phys., 25: 481-489, 1993.

Snedecor, G.W., and W.G. Cochran, Statistical Methods, 8th ed., Iowa State University Press, Ames, 1989.

Stainsby, W.N., "Local Control of Regional Blood Flow," Ann. Rev. Physiol., 35: 151-168, 1973.

Taylor, R., and R. Krishna, Multicomponent Mass Transfer, John Wiley and Sons, Inc., New York, 1993.

Vanderkooi, J.M., M. Erecinska, and I.A. Silver, "Oxygen in Mammalian Tissue: Methods of Measurement and Affinities of Various Reactions," Am. J. Physiol., 260: C1131-C1150, 1991.

Whalen, W.J., "Intracellular pO_2 in Heart and Skeletal Muscle," Physiologist, 14: 69-82, 1971.

Whalen, W.J., P. Nair, and D.G. Buerk, "Oxygen Tension in the Beating Cat Heart In Situ.," Oxygen Supply, ed. Kessler, et al., Urban and Schwarzenberg, Berlin, 1973.

Whalen, W.J., J. Riley, and P. Nair, "A Microelectrode for Measuring Intracellular pO_2," J. Appl. Physiol., 23(5): 798-801, 1967.

Wholpers, H.G., A. Hoeft, H. Korb, P.R. Lichtlen, and G. Hellige, "Transport of Inert Gases in Mammalian Myocardium: Comparison with a Convection-Diffusion Model," Am. J. Physiol., 259: H167-H173, 1990.

Wittenberg, B.A., and J. B. Wittenberg, "Myoglobin-Mediated Oxygen Delivery to Mitochondria of Isolated Cardiac Myocytes," Proc. Natl. Acad. Sci., 84: 7503-7507, 1987.

Wittenberg, B.A., and J.B. Wittenberg, "Transport of Oxygen in Muscle," Annu. Rev. Physiol., 51: 857-878, 1989.

Wittenberg, J.B., "Myoglobin-Facilitated Oxygen Diffusion: Role of Myoglobin in Oxygen Entry Into Muscle," Physiol. Rev., 50: 559-636, 1970.

Wittenberg, J.B., and B.A. Wittenberg, "Mechanisms of Cytoplasmic Hemoglobin and Myoglobin Function," Annu. Rev. Biophys. Biophys. Chem., 19: 217-241, 1990.

Zhang, X., Theoretical Oxygen Distribution in Tissue: Effects of Radial Transport Assumptions, M.S. Thesis, Louisiana Tech University, 1992.

Zitko, V., "Simplex Optimization," Access, Sept/Oct: 6-11 1986.